Blekinge Institute of Technology
Research Report No 2004:04

Convergence and Complexity Analysis of Delayless Subband Adaptive Filters

J. M. de Haan

Department of Signal Processing
Blekinge Institute of Technology

Convergence and Complexity Analysis of Delayless Subband Adaptive Filters

J. M. de Haan

Department of Signal Processing
Blekinge Institute of Technology
Ronneby, Sweden

Abstract

Subband adaptive filters have been proposed to circumvent the drawbacks of slow convergence and high computational complexity associated with time domain adaptive filters. Subband processing introduces transmission delays and signal degradations due to aliasing effects. In order to overcome the transmission delays, delayless adaptive filtering has been introduced where the coefficient adaptation is performed in the subband domain while signal filtering is performed in fullband. In this paper convergence behavior and computational complexity of two different types of delayless adaptive filters are considered. Both open loop and closed loop configurations are studied. The theoretical results are compared with simulations of algorithms in a system identification scenario.

Chapter 1

Introduction

Frequency domain adaptive filters [1, 2, 3], subband adaptive filters [4, 5, 6], and hybrid systems [7] have been introduced to reduce computational costs and to increase convergence speed inherent from high order adaptive filters. These approaches however, may introduce transmission delay in the signal path. This is an undesired effect, especially in telecommunication applications [8] such as channel equalization [9] and acoustic echo cancellation [10].

Delayless subband adaptive filters are introduced to circumvent the drawback of transmission delay, at the expense of some computational complexity [11]. Such subband adaptive filters do not introduce delay in the signal path, although delay may still be present in the algorithm path. Since the filtering is done in time-domain, rather than in subband domain, there is no aliasing/imaging distortion present in the output signal. Inband aliasing effects may still impair the performance of the adaptive algorithm, thus the filter weights may only be suboptimal. The first approach of delayless subband adaptive filtering [11] comprises a transformation to obtain fullband filter coefficients from filter coefficients, which are adapted in the subband domain. The first approach comprises a transform employing the discrete fourier transform (DFT) [11]. After the initial paper, several new filter bank and transform configurations have been proposed, such as an improved scheme using the DFT, and a synthesis filter bank approach [12]. Another scheme has been proposed, with tree structured filter banks and Hadamard transforms [13] and a scheme based on uniform DFT filter bank design [14]. New delayless subband adaptive filters have also been introduced, see for example [15], which originates from the subband adaptive filtering concept, and [16], which originates from the frequency domain adaptive filtering concept.

In this study, the convergence behavior delayless adaptive filters is studied. Both open loop and closed loop configurations are analyzed. It is shown that in the open loop configuration, the subband-to-fullband transform affects the performance in terms of mean square error but does not affect the convergence behavior. For the closed loop configuration, the subband-to-fullband transform plays an important role in the convergence behavior. Based on the results for the closed loop case, the transform with the optimal convergence performance is derived.

Further, a novel delayless subband adaptive filter is presented, which comprises a combination of new techniques for subband adaptive filtering [6] with the delayless fullband filtering approach [11]. The new approach has the following properties:

- The fullband coefficients in the delayless subband adaptive filter are directly updated without the use of a subband-to-fullband coefficient transform and hence

the number of coefficients for the delayless subband adaptive filter is the same as for a fullband adaptive filter.

- Both open loop and closed loop delayless adaptive filters attain the Wiener solution, and have the same convergence performance.
- Efficient block transform based techniques can be used to implement the filtering process efficiently.

The convergence analysis presented in this paper is based on the simple convergence analysis of the LMS adaptive filter, which relates the convergence speed to the eigenvalues of the input correlation matrix. The reason for this is two-fold. The first reason is that the results can easily be compared to the results for the LMS adaptive filters and related algorithms. The second reason is that the simple convergence analysis has proven itself to be a good tool to predict convergence behavior. It is important to point out that the detailed convergence analysis of the LMS algorithm has been a difficult mathematical task for the past decades [17], and it has also been shown that the eigenvalue spread sometimes can be a misleading quantity when judging convergence rates [18]. The analysis results in this study, using the suggested technique, show very good correspondence to simulation results and can thus be good tools to predict convergence behavior.

In Chapter 2, the open loop and closed loop configurations of the conventional delayless subband adaptive filter are described. A convergence analysis of both configurations is given. In Chapter 3, the optimal subband-to-fullband transformation is derived for the closed loop configuration, based on the results from the convergence analysis in Chapter 2. In Chapter 4, the delayless adaptive filter with adaptive polyphase filters is described. A convergence analysis is given for the open loop and closed loop configurations. A convergence speed comparison is given in Chapter 5. Chapter 6 presents complexity issues and finally, Chapter 7 concludes the paper.

Chapter 2

Delayless Subband Adaptive Filtering with Subband-to-Fullband Transform

2.1 Description of the Subband Adaptive Filter

A general description of the delayless subband adaptive filter, initially proposed in [11], is presented in this section. The general structure is described including the open loop and closed loop configurations.

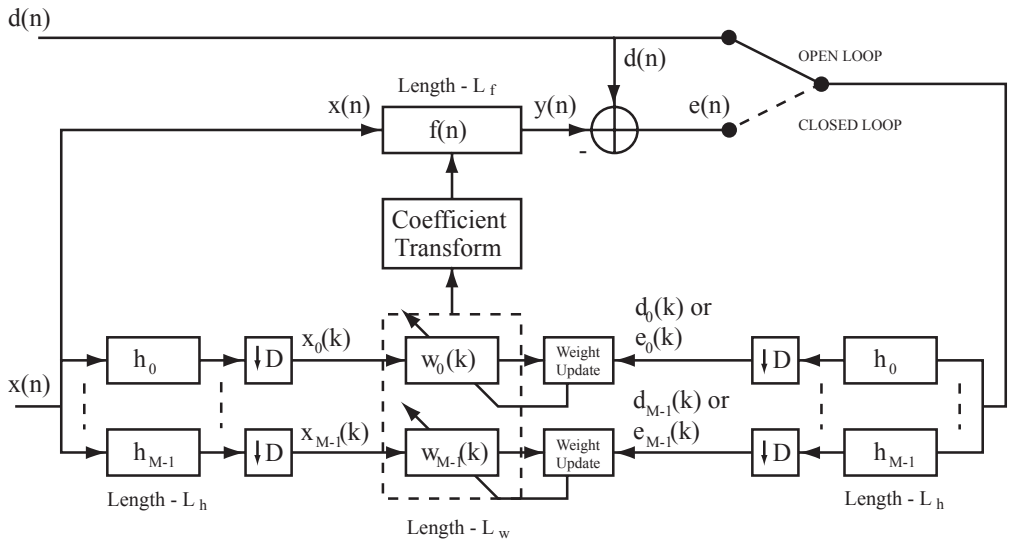

Figure 2.1: *Original approach of delayless subband adaptive filters with open loop and closed loop configurations.*

As adaptive filters in general, delayless subband adaptive filters consist of two main parts, a filtering operation and a coefficient adaptation operation. The filtering operation is performed by a fullband filter in the time-domain, see Fig. 2.1. In a practical implementation, a long fullband filter has high computational complexity. In some cases it may be preferable to implement the fullband filter partially in the frequency domain. This is addressed in Chapter 5.

The filter coefficients of filters operating in the subband domain are adapted and transformed to fullband coefficients using a subband-to-fullband transform. The advantage of adapting filter coefficients in the subband domain is two-fold. It can be computationally more efficient and the convergence speed can be increased. The use of com-

putationally efficient implementations may reduce the complexity even further.

Consider the input signal $x(n)$ and the desired signal $d(n)$ where n is the full rate time index. The output signal $y(n)$ is obtained by filtering $x(n)$ with the fullband coefficients $\mathbf{f}(k)$

$$y(n) = \mathbf{f}^T \left(\lfloor \tfrac{n}{D} \rfloor \right) \mathbf{x}(n), \tag{2.1}$$

where $\mathbf{f}(k) = [f_0(k), \ldots, f_{L_f-1}(k)]^T$ is a vector containing fullband filter coefficients at time instant k. The variable k denotes the subband signal time index which is related to the full rate time index n according to $k = \lfloor \frac{n}{D} \rfloor$ where $\lfloor \cdot \rfloor$ denotes round-off towards the closest integer towards minus infinity. Vector $\mathbf{x}(n) = [x(n), \ldots, x(n - L_f + 1)]^T$ is the input signal vector. The fullband filter length is denoted by L_f. A fullband error signal $e(n)$ is obtained as

$$e(n) = d(n) - y(n). \tag{2.2}$$

Consider a filter bank with M subbands, causal FIR analysis filters $h_m(n)$ of length L_h, and decimators with decimation rate D. The input signal $x(n)$ is decomposed into subband signals $x_m(k)$ according to

$$x_m(k) = \mathbf{h}_m^T \mathbf{x}(kD), \qquad m = 0, \ldots, M-1, \tag{2.3}$$

where $\mathbf{h}_m = [h_{m,0}, \ldots, h_{m,L_h-1}]^T$ and $\mathbf{x}(kD)$ is an input signal vector of corresponding length.

The delayless subband adaptive filter has two operation configurations, *open loop* and *closed loop*. In the open loop configuration, the desired signal is decomposed into subband signals as

$$d_m(k) = \mathbf{h}_m^T \mathbf{d}(kD), \tag{2.4}$$

and subband error signals $e_m(k)$ are obtained as

$$e_m(k) = d_m(k) - y_m(k) = d_m(k) - \mathbf{w}_m^T(k)\mathbf{x}_m(k). \tag{2.5}$$

where $\mathbf{w}_m(k) = [w_{m,0}(k), \ldots, w_{m,L_w-1}(k)]^T$ is a vector containing the adaptive filter coefficients at time instant k, and $\mathbf{x}_m(k) = [x_m(k), \ldots, x_m(k - L_w + 1)]^T$ is an input subband signal vector. The length of the adaptive filters L_w is related to the fullband filter length L_f and the decimation rate D as $L_w = L_f/D$.

In the closed loop configuration, the subband error signals are obtained by decomposing the fullband error signal into subband error signals

$$e_m(k) = \mathbf{h}_m^T \mathbf{e}(kD). \tag{2.6}$$

In both configurations, a Normalized Least Mean Square (NLMS) algorithm is used in the subbands. Other adaptive algorithms can also be used, such as Recursive Least

Squares (RLS), or Affine Projection Algorithm (APA) [17]. The subband NLMS coefficient adaption equation is

$$\mathbf{w}_m(k+1) = \mathbf{w}_m(k) + \mu_m(k) e_m(k) \mathbf{x}_m^*(k). \tag{2.7}$$

The time-varying subband step size μ_m is calculated as

$$\mu_m(k) = \mu / \hat{P}_m(k), \tag{2.8}$$

where μ is a global step size and $P_m(k)$ is the short time subband power estimate of the m-th subband signal $x_m(k)$

$$\hat{P}_m(k) = \frac{\mathbf{x}_m^H(k)\mathbf{x}_m(k)}{L_w}. \tag{2.9}$$

The fullband coefficients are obtained from the subband coefficients by means of a linear coefficient transform

$$\mathbf{f}(k) = \mathbf{T}\mathbf{w}(k), \tag{2.10}$$

where $\mathbf{w}(k) = [\mathbf{w}_0^T(k), \ldots, \mathbf{w}_{M-1}^T(k)]^T$ is a concatenated adaptive filter coefficient vector at time instant k, and matrix $\mathbf{T}$ is the subband-to-fullband transform.

The open loop configuration is summarized by the equations

for all n :

$$y(n) = \mathbf{f}\left(\lfloor \tfrac{n}{D} \rfloor\right)^T \mathbf{x}(n) \tag{2.11}$$

for all $k = \lfloor \frac{n}{D} \rfloor$:

$$\begin{aligned}
x_m(k) &= \mathbf{h}_m^T \mathbf{x}(kD) && (2.12)\\
d_m(k) &= \mathbf{h}_m^T \mathbf{d}(kD) && (2.13)\\
y_m(k) &= \mathbf{w}_m^T(k)\mathbf{x}_m(k) && (2.14)\\
e_m(k) &= d_m(k) - y_m(k) && (2.15)\\
\hat{P}_m(k) &= \mathbf{x}_m^H(k)\mathbf{x}_m(k)/L_w && (2.16)\\
\mu_m(k) &= \mu/\hat{P}_m(k) && (2.17)\\
\mathbf{w}_m(k+1) &= \mathbf{w}_m(k) + \mu_m(k) e_m(k) \mathbf{x}_m^*(k) && (2.18)\\
\mathbf{f}(k+1) &= \mathbf{T}\mathbf{w}(k+1) && (2.19)
\end{aligned}$$

The closed loop configuration is summarized by the equations

for all n :

$$\begin{aligned} y(n) &= \mathbf{f}\left(\lfloor \tfrac{n}{D} \rfloor\right)^T \mathbf{x}(n) && (2.20)\\ e(n) &= d(n) - y(n) && (2.21) \end{aligned}$$

for all $k = \lfloor \frac{n}{D} \rfloor$:

$$\begin{aligned} x_m(k) &= \mathbf{h}_m^T \mathbf{x}(kD) && (2.22)\\ e_m(k) &= \mathbf{h}_m^T \mathbf{e}(kD) && (2.23)\\ \hat{P}_m(k) &= \mathbf{x}_m^H(k)\mathbf{x}_m(k)/L_w && (2.24)\\ \mu_m(k) &= \mu/\hat{P}_m(k) && (2.25)\\ \mathbf{w}_m(k+1) &= \mathbf{w}_m(k) + \mu_m(k) e_m(k) \mathbf{x}_m^*(k) && (2.26)\\ \mathbf{f}(k+1) &= \mathbf{T}\mathbf{w}(k+1) && (2.27) \end{aligned}$$

In the next sections an overview of different existing subband-to-fullband transforms in combination with filter banks for the subband signal decompositions is presented.

2.2 Filter Bank and Transform Configurations

2.2.1 Uniform DFT Filter Banks

A uniform DFT Filter Bank consists of M analysis filters $H_m(z)$, see Fig. 2.2, which are modulated from a prototype filter $H(z)$ according to

$$H_m(z) = H(zW_M^m), \tag{2.28}$$

where $W_M = e^{-j2\pi/M}$. Let $A_l(z)$, $l = 0, \ldots, M-1$, denote the polyphase components of the prototype filter $H(z)$

$$H(z) = \sum_{l=0}^{M-1} z^{-l} A_l(z^M). \tag{2.29}$$

Accordingly, the polyphase decomposition of all analysis filters is given by

$$H_m(z) = \sum_{l=0}^{M-1} z^{-l} A_l(z^M) W_M^{-ml}. \tag{2.30}$$

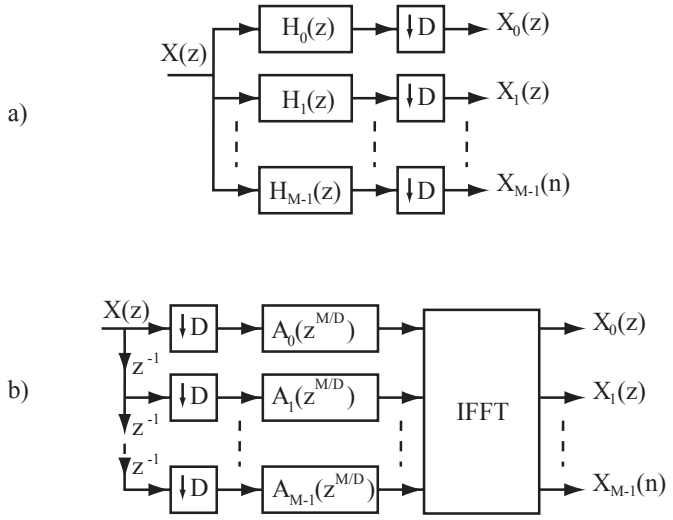

Figure 2.2: **a)** *Direct Form and* **b)** *equivalent Polyphase Form of an Analysis Uniform-DFT Filter Bank.*

The filter bank can be implemented efficiently according to the polyphase decomposition, consisting of a delayline, polyphase filters and an IFFT operation, see Fig. 2.2. An important efficiency gain is obtained when the decimators and the polyphase components trade place, and $A_l(z^M)$ is replaced by $A_l(z^{M/D})$, according to the noble identity [19]. The efficiency gain comes from the fact that only the samples in the decimated subband signals are computed, which is not the case in the direct form where many samples are discarded by the decimators.

DFT-1 Subband-to-Fullband Transform

In the original approach of delayless subband adaptive filtering by Morgan and Thi [11], a scheme is proposed with oversampled uniform DFT filter banks. The decimation factor in this approach is set to $D = M/2$. In the subband-to-fullband transform each subband coefficient vector is first transformed using a DFT with length L_w, then the frequency bins are stacked into one large vector and this vector is finally transformed to the fullband filter coefficients by an inverse DFT, see Fig. 2.3

A matrix expression for this transform is

$$\mathbf{T} = \mathbf{T}_1^{-1}\mathbf{S}\ \mathrm{diag}[\mathbf{T}_2, \ldots, \mathbf{T}_2] \tag{2.31}$$

where $\mathbf{T}_2$ is an $L_w \times L_w$ DFT matrix, $\mathbf{T}_1^{-1}$ is an $L_f \times L_f$ inverse DFT matrix, $\mathbf{S}$ is an $L_f \times ML_w$ stacking matrix, and diag$[\cdots]$ denotes block diagonal matrix. The stacking

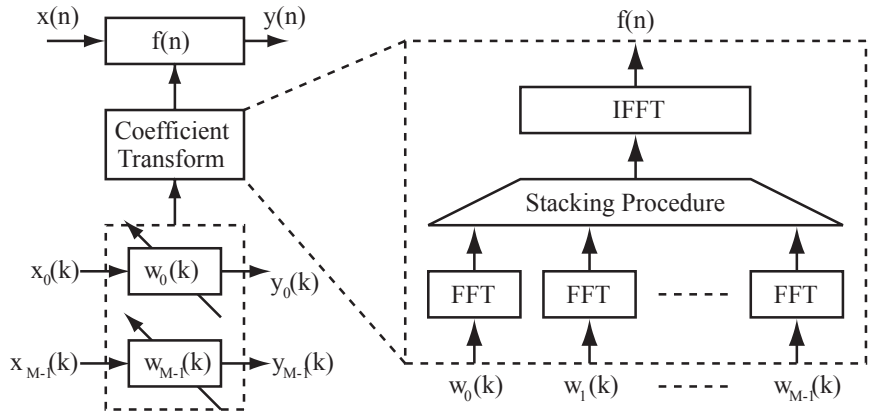

Figure 2.3: *DFT-1 Transform.*

matrix $\mathbf{S}$ can be expressed using identity- and zero matrix sub-blocks according to

$$\mathbf{S} = \begin{bmatrix} \mathbf{I} & \mathbf{0} & \mathbf{0} & \mathbf{0} & & & & & & & & & & & & \\ & & & & \mathbf{0} & \mathbf{I} & \mathbf{0} & \mathbf{0} & & & & & & & & \\ & & & & \mathbf{0} & \mathbf{0} & \mathbf{I} & \mathbf{0} & & & & & & & & \\ & & & & & & & & \mathbf{0} & \mathbf{0} & \mathbf{0} & \mathbf{I} & & & & \\ & & & & & & & & \mathbf{I} & \mathbf{0} & \mathbf{0} & \mathbf{0} & & & & \\ & & & & & & & & & & & & \ddots & & & \\ & & & & & & & & & & & & & \mathbf{0} & \mathbf{I} & \mathbf{0} & \mathbf{0} \\ & & & & & & & & & & & & & \mathbf{0} & \mathbf{0} & \mathbf{I} & \mathbf{0} \\ & & & & & & & & & & & & & & & & \\ & & & & & & & & & & & & & & & & \mathbf{0} & \mathbf{0} & \mathbf{0} & \mathbf{I} \\ & & & & & & & & & & & & & & & & \mathbf{I} & \mathbf{0} & \mathbf{0} & \mathbf{0} \\ \mathbf{0} & \mathbf{0} & \mathbf{0} & \mathbf{I} & & & & & & & & & & & & \end{bmatrix}, \tag{2.32}$$

where $\mathbf{I}$ is a $L_w/4 \times L_w/4$ identity matrix and $\mathbf{0}$ is a $L_w/4 \times L_w/4$ zero matrix. Not shown sub-block entries are equal to the zero matrix $\mathbf{0}$.

DFT-2 subband-to-fullband Transform

An improved scheme of the delayless subband adaptive filter approach was proposed by Huo et. al. [12], where all subband coefficient vectors are first zero-padded with L_w zeros. Internally, the scheme is essentially the same as the DFT-1 scheme but the fullband coefficients are the first L coefficients obtained from the inverse DFT, see Fig. 2.4. In [12], it has been shown that the transform improves the steady state error level in the open loop configuration and the convergence speed in both the open loop and the closed loop configurations.

A matrix expression of the subband-to-fullband transformation is given by

$$\mathbf{T} = \mathbf{Q}\mathbf{T}_1^{-1}\mathbf{S}\ \mathrm{diag}[\mathbf{T}_2\mathbf{P}, \ldots, \mathbf{T}_2\mathbf{P}] \tag{2.33}$$

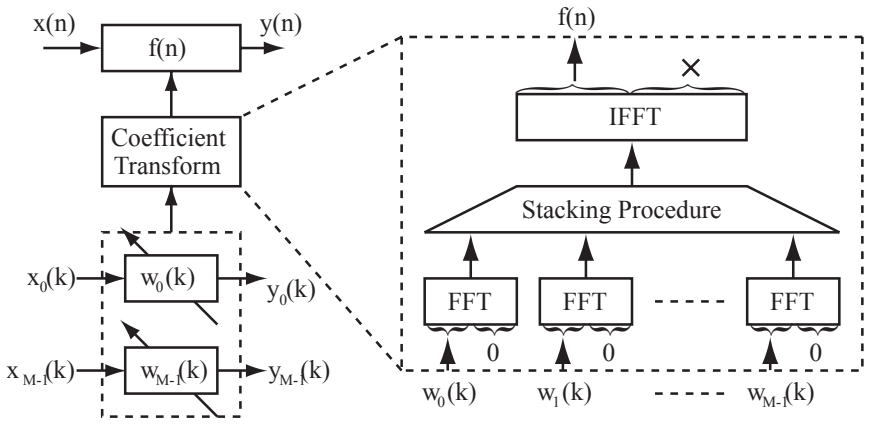

Figure 2.4: *DFT-2 Transform.*

where

$$\mathbf{P} = \begin{bmatrix} \mathbf{I}_{L_w} \\ \mathbf{0}_{L_w} \end{bmatrix}, \quad \mathbf{Q} = \begin{bmatrix} \mathbf{I}_{L_f} & \mathbf{0}_{L_f} \end{bmatrix} \tag{2.34}$$

Compared to the DFT-1 transform all matrices in Eq. (2.33), $\mathbf{T}_2, \mathbf{T}_1^{-1}$,and the sub-block matrices $\mathbf{I}$ and $\mathbf{0}$ in the stacking matrix $\mathbf{S}$ are doubled in size. The indices on the identity matrices $\mathbf{I}$ and the zero matrices $\mathbf{0}$ in Eq. (2.34) denote their size.

2.2.2 Tree-Structured Uniform Filter Banks

In a tree-structured uniform filter bank, the input signal $x(n)$ is filtered with a lowpass and highpass filter and critically decimated, i.e. with a decimation rate of $D = 2$. The subband signals are successively splitted into a low and high frequency subband signal, using a lowpass filter $H_L(z)$ and a highpass filter $H_H(z)$, see Fig 2.5. The structure is developed for uniform filter banks where the number of subbands is a power of two. The filter bank structure is closely related to octave filter banks, but in octave filter banks only the lowpass branches are successively splitted [20].

Hadamard subband-to-fullband Transform

Delayless subband adaptive filters with critically sampled filter banks ($D = M$) have been proposed by Hirayama et. al. [21, 13], where it is shown that under certain conditions, the use of tree structured filter banks in the closed-loop configuration leads to a very efficient subband-to-fullband coefficient transformation employing Hadamard transforms. A Hadamard matrix $\mathcal{H}$ is a $M \times M$ square matrix with elements 1 and -1 such that

$$\mathcal{H}_M^H \mathcal{H}_M = M\mathbf{I} \tag{2.35}$$

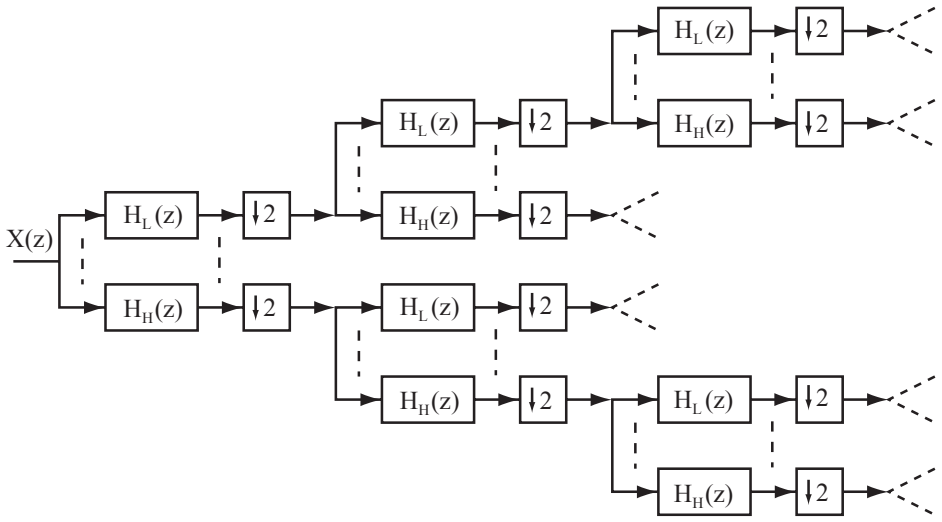

Figure 2.5: *Tree-structured Uniform Filter Bank.*

In the case of Hadamard matrices where M is a power of 2, a recursive definition is given by

$$\mathcal{H}_{2m} = \begin{bmatrix} \mathcal{H}_m & \mathcal{H}_m \\ \mathcal{H}_m & -\mathcal{H}_m \end{bmatrix}, \quad m = 0, 1, 2, \ldots \tag{2.36}$$

assuming that $\mathcal{H}_1 = 1$. The advantage of Hadamard transforms is that there are no multiplications in the transform. The transform includes only summations and sign alterations.

The coefficient transform $\mathbf{T}$ is defined, such that block partitions of the fullband filter, with block-length M, are transformed with a $M \times M$ Hadamard matrix from the adaptive filter coefficients according to [13]

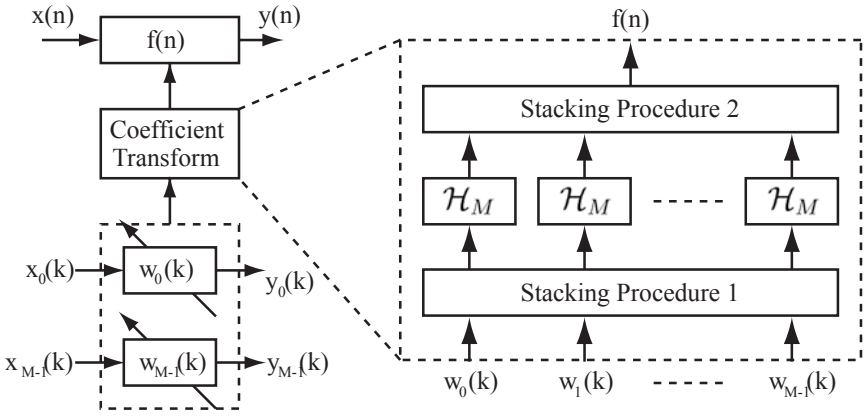

Figure 2.6: *subband-to-fullband Transform using Hadamard Transforms.*

$$\begin{bmatrix} f_{Mi} \\ f_{Mi+1} \\ \vdots \\ f_{Mi+M-1} \end{bmatrix} = \frac{1}{M}\mathcal{H}_M \begin{bmatrix} w_{0,i} \\ w_{1,i} \\ \vdots \\ w_{M-1,i} \end{bmatrix}, \quad i = 0, \ldots, L_f/M - 1 \tag{2.37}$$

Hence, first all filter coefficients with the same coefficient index are collected from the adaptive filters in the subband domain, and combined into L_w separate vectors (stacking procedure 1, see Fig. 2.6). Then, the Hadamard transform is applied on each vector. The resulting vectors are block partitions of the fullband filter, and the fullband filter is thus obtained simply by stacking these vectors (stacking procedure 2, see Fig. 2.6).

2.2.3 Analysis Filter Bank Design

In this section an analysis filter bank design procedure for the delayless subband adaptive filter is described. Lossless power complementary filter banks with minimum phase property is designed. The reason for the use of this design method is that the design procedure is applicable for both uniform-DFT (M-channel filter bank design) and tree structured filter banks (two-channel filter bank design).

The power complementary constraint for an M-channel analysis filter bank is given by

$$\sum_{m=0}^{M-1} \left|H_m(e^{j\omega})\right|^2 = 1, \tag{2.38}$$

where the analysis filters $H_m(z)$ are derived from a lowpass prototype analysis filter $H(z)$ with real coefficients according to $H_m(z) = H(zW_M^m)$. With the spectral factorization $Q(z) = H(z)H(z^{-1})$, where $Q(e^{j\omega})$ is a real-valued frequency function and $Q(e^{j\omega}) \geq 0$ [22], the power complementary constraint can be rewritten as

$$\sum_{m=0}^{M-1} Q(e^{j\omega}W_M^m) = 1. \tag{2.39}$$

The transfer function $Q(z)$ is a zero phase FIR filter with coefficients q_i

$$Q(z) = \sum_{i=-L+1}^{L-1} q_i z^{-i}. \tag{2.40}$$

The power complementary constraint can be transformed to the time-domain according to

$$\sum_{m=0}^{M-1} q_i W_M^{-mi} = \delta_i, \tag{2.41}$$

where $\delta_i = 1$ for $i = 0$ and zero otherwise. Since

$$\sum_{m=0}^{M-1} W_M^{-mi} = \begin{cases} M & \text{for } i = 0, \pm M, \pm 2M, \ldots \\ 0 & \text{otherwise} \end{cases} \tag{2.42}$$

the power complementary constraint becomes

$$q_i = M\delta_i, \text{ for } i = 0, \pm M, \pm 2M, \ldots \tag{2.43}$$

Since q_i is symmetric about $i = 0$, i.e. $q_i = q_{-i}$, the z-transform can be rewritten as

$$Q(z) = q_0 + \sum_{i=1}^{\infty} q_i\{z^i + z^{-i}\} = q_0 + 2\sum_{i=1}^{\infty} q_i \text{Re}\{z^i\} = \boldsymbol{\phi}^T(z)\mathbf{q}. \tag{2.44}$$

Defining a stopband $\Omega = [\omega_s, \pi]$, the energy in the stopband can be minimized subject to the power complementary constraint. This design problem can be formulated as a quadratic program according to

$$\begin{cases} \min\limits_{\mathbf{q}} \int_{\Omega} |Q(e^{j\omega})|^2 d\omega \\ q_i = M\delta_i, \text{ for } i = 0, \pm M, \pm 2M, \ldots \end{cases} \tag{2.45}$$

which can be rewritten as

$$\begin{cases} \min\limits_{\mathbf{q}} \mathbf{q}^T\mathbf{A}\mathbf{q} \\ \mathbf{B}\mathbf{q} = \mathbf{c}/M \end{cases} \tag{2.46}$$

where $\mathbf{B}$ is a diagonal matrix with ones on the main diagonal at each M-th entry and zeros otherwise, $\mathbf{c}$ is a vector with a one at the first entry and zeros otherwise, and

$$\mathbf{A} = \int_{\Omega} \boldsymbol{\phi}(e^{j\omega})\boldsymbol{\phi}^T(e^{j\omega}) d\omega \tag{2.47}$$

with $\phi_0(e^{j\omega}) = 1$ and $\phi_i(e^{j\omega}) = 2\cos(\omega i)$ for $i > 0$. The minimum phase analysis prototype filter $H(z)$ is obtained by taking the roots of $Q(z)$ which are inside the unit circle. Roots on the unit circle are taken only once [22],

$$H(z) = (1 - z^{-1}z_1)\cdots(1 - z^{-1}z_{L-1})\sqrt{\frac{|q_{L-1}|}{|z_1 \cdots z_{L-1}|}}. \tag{2.48}$$

A prototype filter design example is given in Fig. 2.7. A prototype filter was designed for a $M = 4$ subband uniform-DFT filter bank with decimation rate $D = 2$ and filter length $L = 16$. The stopband parameters is set to $\omega_s = \pi/D$.

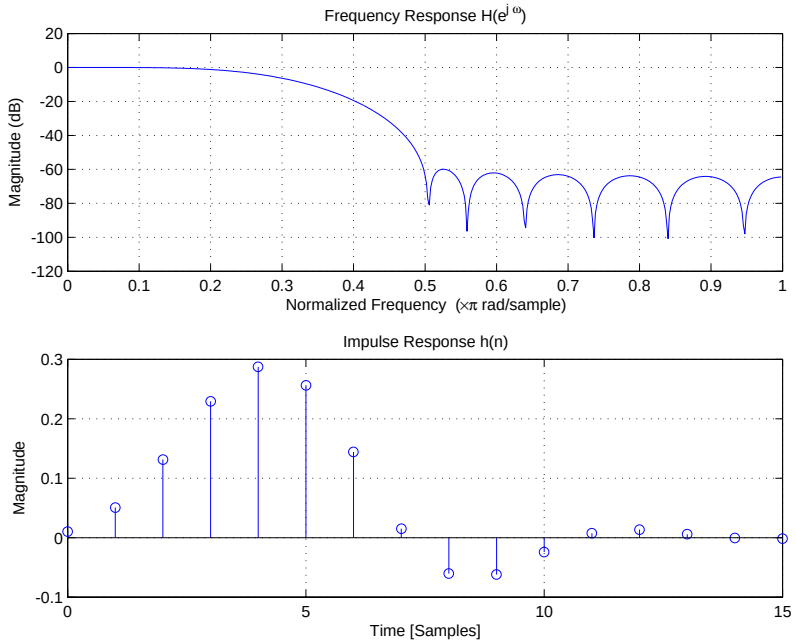

Figure 2.7: *Magnitude and impulse response of a length $L = 16$ prototype analysis filter $H(z)$ for an analysis filter bank with $M = 4$ subbands and power complementary minimum phase analysis filters. The stopband parameters is set to $\omega_s = \pi/D$, with a decimation rate of $D = 2$.*

2.3 Convergence Analysis

In this section a convergence analysis is given comparable to a well known analysis of the LMS adaptive filter [17], see the Appendix for the convergence analysis of the LMS. The analysis is used to study the convergence of the filter coefficients in the mean, and relates convergence speed to the eigenvalues of the input correlation matrix [23].

For both the open and closed loop configurations, the fullband filter coefficient update equation can be written as

$$\mathbf{f}(k+1) = \mathbf{f}(k) - \tfrac{1}{2}\mu\mathbf{T}\mathbf{P}^{-1}(k)\boldsymbol{\nabla}(k), \tag{2.49}$$

where μ is the global step-size and $\mathbf{P}(k)$ is a diagonal matrix with subband signal power estimates

$$\mathbf{P}(k) = \begin{bmatrix} \hat{P}_0(k)\mathbf{I} & & 0 \\ & \ddots & \\ 0 & & \hat{P}_{M-1}(k)\mathbf{I} \end{bmatrix}, \tag{2.50}$$

where $\mathbf{I}$ is the unit matrix. The gradient vector $\boldsymbol{\nabla}(k)$ is composed of subband gradient vectors

$$\boldsymbol{\nabla}(k) = -2\left[e_0(k)\mathbf{x}_0^H(k), \ldots, e_{M-1}(k)\mathbf{x}_{M-1}^H(k)\right]^T. \tag{2.51}$$

The convergence in the mean can be studied by taking the expected value of the full-band filter coefficient update equation

$$E\{\mathbf{f}(k+1)\} = E\{\mathbf{f}(k)\} - \tfrac{1}{2}\mu\mathbf{T}\mathbf{P}^{-1}E\{\boldsymbol{\nabla}(k)\} \tag{2.52}$$

where $E\{\cdot\}$ denotes ensemble average and the input is assumed to be stationary $P_m(k) = P_m = E\{|x_m(k)|^2\}$. Let $\overline{\mathbf{f}}(k) = E\{\mathbf{f}(k)\}$ and $\overline{\boldsymbol{\nabla}}(k) = E\{\boldsymbol{\nabla}(k)\}$. The mean gradient vector is given by

$$\overline{\boldsymbol{\nabla}}(k) = -2\left[E\{e_0(k)\mathbf{x}_0^H(k)\}, \ldots, E\{e_{M-1}(k)\mathbf{x}_{M-1}^H(k)\}\right]^T. \tag{2.53}$$

2.3.1 Convergence Analysis of the Open Loop Configuration

In the open loop configuration, the subband error signals are calculated in the subband domain $e_m(k) = d_m(k) - y_m(k)$, as defined in Eq. (2.5). Hence, the mean gradient vector $\overline{\boldsymbol{\nabla}}(k)$ can be expressed as

$$\overline{\boldsymbol{\nabla}}(k) = -2\begin{bmatrix} E\{d_0(k)\mathbf{x}_0^*(k)\} - E\{\mathbf{w}_0^T(k)\mathbf{x}_0(k)\mathbf{x}_0^*(k)\} \\ \vdots \\ E\{d_{M-1}(k)\mathbf{x}_{M-1}^*(k)\} - E\{\mathbf{w}_{M-1}^T(k)\mathbf{x}_{M-1}(k)\mathbf{x}_{M-1}^*(k)\} \end{bmatrix} \tag{2.54}$$

Assuming that the adaptive filter coefficients $\mathbf{w}_m(k)$ are independent of the subband signals $x_m(k)$, Eq. (2.54) can be rewritten as

$$\overline{\boldsymbol{\nabla}}(k) = -2\begin{bmatrix} \mathbf{r}_0 \\ \vdots \\ \mathbf{r}_{M-1} \end{bmatrix} + 2\begin{bmatrix} \mathbf{R}_0\overline{\mathbf{w}}_0(k) \\ \vdots \\ \mathbf{R}_{M-1}\overline{\mathbf{w}}_{M-1}(k) \end{bmatrix}, \tag{2.55}$$

where $\overline{\mathbf{w}}_m(k) = E\{\mathbf{w}_m(k)\}$, and $\mathbf{r}_m$ is a subband signal cross-correlation vector, defined as

$$\mathbf{r}_m = E\{\mathbf{x}_m^*(k)d_m(k)\} = \mathbf{H}_m^H E\{\mathbf{x}^*(k)\mathbf{d}^T(k)\}\mathbf{h}_m = \mathbf{H}_m^H\mathbf{R}_{dx}\mathbf{h}_m, \tag{2.56}$$

and $\mathbf{R}_m$ is a subband signal correlation matrix is defined as

$$\mathbf{R}_m = E\{\mathbf{x}_m^*(k)\mathbf{x}_m^T(k)\} = \mathbf{H}_m^H E\{\mathbf{x}^*(k)\mathbf{x}^T(k)\}\mathbf{H}_m = \mathbf{H}_m^H\mathbf{R}_{xx}\mathbf{H}_m, \tag{2.57}$$

where $\mathbf{H}_m$ is a convolution matrix with analysis filters in the columns.

$$\mathbf{H}_m = \begin{bmatrix} \mathbf{h}_m & & 0 \\ & \ddots & \\ 0 & & \mathbf{h}_m \end{bmatrix}. \tag{2.58}$$

In each column of $\mathbf{H}_m$, the analysis filter column vector $\mathbf{h}_m$ is shifted downwards by D positions, relative to the previous column.

Eq. (2.55) can be rewritten as

$$\overline{\boldsymbol{\nabla}}(k) = -2 \begin{bmatrix} \mathbf{r}_0 \\ \vdots \\ \mathbf{r}_{M-1} \end{bmatrix} + 2 \begin{bmatrix} \mathbf{R}_0 & & 0 \\ & \ddots & \\ 0 & & \mathbf{R}_{M-1} \end{bmatrix} \begin{bmatrix} \overline{\mathbf{w}}_0(k) \\ \vdots \\ \overline{\mathbf{w}}_{M-1}(k) \end{bmatrix}. \tag{2.59}$$

A composite block diagonal correlation matrix $\mathbf{R}$ is defined as

$$\mathbf{R} = \begin{bmatrix} \mathbf{R}_0 & & 0 \\ & \ddots & \\ 0 & & \mathbf{R}_{M-1} \end{bmatrix}, \tag{2.60}$$

and a composite cross-correlation vector $\mathbf{r}$ is defined as

$$\mathbf{r} = \left[\mathbf{r}_0^T, \ldots, \mathbf{r}_{M-1}^T\right]^T. \tag{2.61}$$

The mean gradient vector now can be expressed as

$$\overline{\boldsymbol{\nabla}}(k) = -2\mathbf{r} + 2\mathbf{R}\overline{\mathbf{w}}(k), \tag{2.62}$$

where $\overline{\mathbf{w}}(k) = [\overline{\mathbf{w}}_0^T(k), \ldots, \overline{\mathbf{w}}_{M-1}^T(k)]^T$. Assuming that the adaptive filter converges in the mean, then

$$\lim_{k\to\infty} \overline{\boldsymbol{\nabla}}(k) = \mathbf{0}, \tag{2.63}$$

which leads to the system of equations

$$\mathbf{R}\mathbf{w}_{\text{conv}} = \mathbf{r}, \tag{2.64}$$

where $\mathbf{w}_{\text{conv}}$ denotes the converged subband coefficient vector. The solution to Eq. (2.64) is given by

$$\mathbf{w}_{\text{conv}} = \mathbf{R}^{-1}\mathbf{r}, \tag{2.65}$$

and the corresponding fullband filter coefficients are given by $\mathbf{f}_{\text{conv}} = \mathbf{T}\mathbf{w}_{\text{conv}}$. Note that the optimal solution of the open loop delayless subband adaptive filter $\mathbf{f}_{\text{conv}} = \mathbf{T}\mathbf{R}^{-1}\mathbf{r}$ generally does not lead to the optimal Wiener solution $\mathbf{f}_{\text{Wiener}} = \mathbf{R}_{xx}^{-1}\mathbf{r}_{dx}$, see Appendix A.

Since $\mathbf{R}$ is decomposed of sub-block hermitian correlation matrices, $\mathbf{R}_m = \mathbf{R}_m^H$, the solution $\mathbf{w}_{\text{conv}}$ is composed of the individual Wiener solutions in the subbands $\mathbf{w}_{m,\text{Wiener}} = \mathbf{R}_m^{-1}\mathbf{r}_m$. The update equation of the composite filter coefficient vector of the adaptive filters in the subbands is given by

$$\mathbf{w}(k+1) = \mathbf{w}(k) - \tfrac{1}{2}\mu\mathbf{P}^{-1}(k)\boldsymbol{\nabla}(k). \tag{2.66}$$

Taking the expected value of Eq. (2.66), assuming stationary input and inserting Eq. (2.62), the filter vector update equation for $\overline{\mathbf{w}}(k)$ is given by

$$\overline{\mathbf{w}}(k+1) = \left(\mathbf{I} - \mu\mathbf{P}^{-1}\mathbf{R}\right)\overline{\mathbf{w}}(k) + \mu\mathbf{P}^{-1}\mathbf{r} \tag{2.67}$$

The coefficient error vector $\Delta\overline{\mathbf{w}}(k)$ is defined as

$$\Delta\overline{\mathbf{w}}(k) = \overline{\mathbf{w}}(k) - \mathbf{w}_{\text{conv}} \tag{2.68}$$

Inserting Eq. (2.67) into Eq. (2.68) and replacing $\mathbf{r}$ by $\mathbf{R}\mathbf{w}_{\text{conv}}$ yields

$$\begin{aligned}
\Delta\overline{\mathbf{w}}(k) &= \left(\mathbf{I} - \mu\mathbf{P}^{-1}\mathbf{R}\right)\overline{\mathbf{w}}(k-1) + \mu\mathbf{P}^{-1}\mathbf{R}\mathbf{w}_{\text{conv}} - \mathbf{w}_{\text{conv}} && (2.69)\\
&= \left(\mathbf{I} - \mu\mathbf{P}^{-1}\mathbf{R}\right)\left(\overline{\mathbf{w}}(k-1) - \mathbf{w}_{\text{conv}}\right) && (2.70)\\
&= \left(\mathbf{I} - \mu\mathbf{P}^{-1}\mathbf{R}\right)\Delta\overline{\mathbf{w}}(k-1) && (2.71)
\end{aligned}$$

The fullband coefficient error vector is simply obtained by multiplying with the transformation matrix, i.e. $\Delta\overline{\mathbf{f}}(k) = \overline{\mathbf{f}}(k) - \mathbf{f}_{\text{conv}} = \mathbf{T}\Delta\overline{\mathbf{w}}(k)$.

The $ML_w \times ML_w$ correlation matrix $\mathbf{R}$ can be decomposed using the eigenvalue decomposition for hermitian matrices $\mathbf{R} = \mathbf{V}\mathbf{\Lambda}\mathbf{V}^H$, where $\mathbf{V}$ is an orthogonal eigenvector matrix and $\mathbf{\Lambda}$ is a diagonal matrix with eigenvalues λ_i, $i = 0, \ldots, ML_w - 1$ [24]. Similarly, the sub-block correlation matrices $\mathbf{R}_m$ can be decomposed using the eigenvalue decompositions $\mathbf{R}_m = \mathbf{V}_m\mathbf{\Lambda}_m\mathbf{V}_m^H$, with eigenvalues $\lambda_{m,i}$. Combining all eigenvalues from all $\mathbf{\Lambda}_m$ gives all eigenvalues in $\mathbf{\Lambda}$.

The update equation for the coefficient error vector $\Delta\overline{\mathbf{w}}(k)$ can be rewritten using the eigenvalue decomposition

$$\begin{aligned}
\Delta\overline{\mathbf{w}}(k+1) &= \left(\mathbf{V}\mathbf{V}^H - \mu\mathbf{P}^{-1}\mathbf{V}\mathbf{\Lambda}\mathbf{V}^H\right)\Delta\overline{\mathbf{w}}(k) && (2.72)\\
&= \mathbf{V}\left(\mathbf{I} - \mu\mathbf{P}^{-1}\mathbf{\Lambda}\right)\mathbf{V}^H\Delta\overline{\mathbf{w}}(k) && (2.73)
\end{aligned}$$

A modal coefficient error vector is defined as $\Delta\overline{\mathbf{w}}'(k) = \mathbf{V}^H\Delta\overline{\mathbf{w}}(k)$, and based on start vector $\mathbf{w}(0)$ with modal error vector $\Delta\mathbf{w}'(0)$, the update equation is given by

$$\Delta\overline{\mathbf{w}}'(k) = \left(\mathbf{I} - \mu\mathbf{P}^{-1}\mathbf{\Lambda}\right)^k\Delta\mathbf{w}'(0), \quad k \geq 0. \tag{2.74}$$

Since $(\mathbf{I} - \mu\mathbf{P}^{-1}\mathbf{\Lambda})$ is a diagonal matrix, the modal coefficient errors become independent

$$\Delta\overline{w_i}'(k) = (1 - \mu\lambda_i/P_m)^k\Delta w_i'(0), \quad k \geq 0. \tag{2.75}$$

Hence, the adaptive filter converges in the mean if

$$0 < \mu < \frac{2}{\max\limits_{m,i}\left(\lambda_{m,i}/P_m\right)}. \tag{2.76}$$

An important and useful measure of performance is the behavior of the fullband mean square error as a function of time. The definition of fullband mean square error (MSE) is given by

$$J(n) = E\{|e(n)|^2\} \tag{2.77}$$

where $e(n) = d(n) - y(n)$ and $y(n) = \mathbf{f}^T\left(\lfloor \frac{n}{D} \rfloor\right)\mathbf{x}(n)$. For a coefficient vector $\mathbf{f}\left(\lfloor \frac{n}{D} \rfloor\right)$ at time instant n, the mean square error is

$$\begin{aligned} J(n) &= E\left\{\left|d(n) - \mathbf{f}^T\left(\lfloor \tfrac{n}{D} \rfloor\right)\mathbf{x}(n)\right|^2\right\} && (2.78)\\ &= \sigma_d^2 - \mathbf{f}^H\left(\lfloor \tfrac{n}{D} \rfloor\right)\mathbf{r}_{xd} - \mathbf{r}_{xd}^H\mathbf{f}\left(\lfloor \tfrac{n}{D} \rfloor\right) + \mathbf{f}^H\left(\lfloor \tfrac{n}{D} \rfloor\right)\mathbf{R}_{xx}\mathbf{f}\left(\lfloor \tfrac{n}{D} \rfloor\right), && (2.79) \end{aligned}$$

where $\sigma_d^2 = E\left\{|d(n)|^2\right\}$, $\mathbf{r}_{xd} = E\left\{\mathbf{x}^*(n)d(n)\right\}$, and $\mathbf{R}_{xx} = E\left\{\mathbf{x}^*(n)\mathbf{x}^T(n)\right\}$. In the case where $\mathbf{f}$ is the converged coefficient vector $\mathbf{f}_{\text{conv}}$, the Minimum Mean Square Error (MMSE) is given by

$$J_{\text{min}} = \sigma_d^2 - \mathbf{f}_{\text{conv}}^H\mathbf{r}_{xd} - \mathbf{r}_{xd}^H\mathbf{f}_{\text{conv}} + \mathbf{f}_{\text{conv}}^H\mathbf{R}_{xx}\mathbf{f}_{\text{conv}}, \tag{2.80}$$

which is in general not equal to the MMSE of the Wiener solution. A major drawback of the open loop configuration is that the algorithm generally does not reach the same MMSE. The performance in terms of the MMSE depends the choice of filter banks and subband-to-fullband transform.

The eigenvalue spread, and thereby the convergence speed, greatly depends on three factors: the input signal correlation, the analysis filters and the decimation rate. In a practical situation with a decaying input correlation function, a higher decimation rate will give more uncorrelated subband input signal samples. The length of the analysis filters also affects the subband input correlation. Hence, the open loop configuration may in certain situations converge at a slower speed than the fullband counterpart, for example when the input is uncorrelated but the analysis filters cause correlated input samples to the adaptive filters in the subbands.

2.3.2 Convergence Analysis of the Closed Loop Configuration

In the closed loop configuration, the subband error signals are obtained from the fullband error signal according to Eq. (2.6). Hence, the mean gradient can be written as

$$\overline{\boldsymbol{\nabla}}(k) = -2\begin{bmatrix} \mathbf{h}_0^T E\{\mathbf{e}(kD)\mathbf{x}_0^*(k)\} \\ \vdots \\ \mathbf{h}_{M-1}^T E\{\mathbf{e}(kD)\mathbf{x}_{M-1}^*(k)\} \end{bmatrix}. \tag{2.81}$$

Inserting the fullband error signal vector $\mathbf{e}(n) = \mathbf{d}(n) - \mathbf{y}(n)$ gives

$$\overline{\boldsymbol{\nabla}}(k) = -2\begin{bmatrix} \mathbf{h}_0^T E\{\mathbf{d}(kD)\mathbf{x}_0^*(k)\} - \mathbf{h}_0^T E\{\mathbf{y}(kD)\mathbf{x}_0^*(k)\} \\ \vdots \\ \mathbf{h}_{M-1}^T E\{\mathbf{d}(kD)\mathbf{x}_{M-1}^*(k) - \mathbf{h}_{M-1}^T E\{\mathbf{y}(kD)\mathbf{x}_{M-1}^*(k)\} \end{bmatrix}. \tag{2.82}$$

The output signal vector $\mathbf{y}(n)$ can be expressed in terms of the fullband filter coefficients as

$$\mathbf{y}(kD) = \mathbf{F}^T(k)\mathbf{x}(kD), \tag{2.83}$$

where $\mathbf{F}(k)$ is a convolution matrix with fullband filter coefficients at time instant k

$$\mathbf{F}(k) = \begin{bmatrix} \mathbf{f}(k) & & 0 \\ & \ddots & \\ 0 & & \mathbf{f}(k) \end{bmatrix}. \tag{2.84}$$

Observe that Eq. (2.83) is only true when the coefficients in $\mathbf{f}(k)$ are constant over time. For convenience it is assumed that the coefficients adapt slowly enough for Eq. (2.83) to be approximately true. The vector products $\mathbf{h}_m^T\mathbf{y}(kD)$ in Eq. (2.82) can be rewritten using the fullband filter coefficient matrix $\mathbf{F}(k)$

$$\mathbf{h}_m^T\mathbf{y}(kD) = \mathbf{h}_m^T\mathbf{F}^T(k)\mathbf{x}(kD) \tag{2.85}$$

Changing the order of filtering yields

$$\mathbf{h}_m^T\mathbf{y}(kD) = \mathbf{f}^T(k)\tilde{\mathbf{H}}_m^T\mathbf{x}(kD), \tag{2.86}$$

where $\tilde{\mathbf{H}}_m$ is a conventional (non-decimated) convolution matrix with analysis filter coefficients. The product $\tilde{\mathbf{H}}_m^T\mathbf{x}(kD)$ is a non-decimated subband signal vector. Hence

$$\mathbf{h}_m^T\mathbf{y}(kD) = \mathbf{f}^T(k)\tilde{\mathbf{x}}_m(kD), \tag{2.87}$$

where vector $\tilde{\mathbf{x}}_m(n)$ contains non-decimated subband signal samples, i.e. $\tilde{\mathbf{x}}_m(n) = [\tilde{x}_m(n), \ldots, \tilde{x}_m(n-L_f+1)]^T$, where $\tilde{x}_m(n)$ is the m-th non-decimated subband input signal. The desired signal $d(n)$ filtered with the analysis filters yields the subband desired signals $d_m(k)$

$$\mathbf{h}_m^T\mathbf{d}(kD) = d_m(k), \tag{2.88}$$

Inserting Eqs. (2.87) and (2.88) into Eq. (2.82), and using the independence assumption yields

$$\overline{\boldsymbol{\nabla}}(k) = -2\begin{bmatrix} E\{d_0(k)\mathbf{x}_0^*(k)\} \\ \vdots \\ E\{d_{M-1}(k)\mathbf{x}_{M-1}^*(k)\} \end{bmatrix} + 2\begin{bmatrix} E\{\mathbf{x}_0^*(k)\tilde{\mathbf{x}}_0^T(kD)\}\overline{\mathbf{f}}(k) \\ \vdots \\ E\{\mathbf{x}_{M-1}^*(k)\tilde{\mathbf{x}}_{M-1}^T(kD)\}\overline{\mathbf{f}}(k) \end{bmatrix} \tag{2.89}$$

Non-quadratic correlation matrices $\tilde{\mathbf{R}}_m$ with size $L_w \times L_f$ are defined as

$$\tilde{\mathbf{R}}_m = E\{\mathbf{x}_m^*(k)\tilde{\mathbf{x}}_m^T(kD)\} = \mathbf{H}_m^H E\{\mathbf{x}^*(k)\tilde{\mathbf{x}}^T(kD)\}\tilde{\mathbf{H}}_m = \mathbf{H}_m^H\mathbf{R}_{xx}\tilde{\mathbf{H}}_m. \tag{2.90}$$

Inserting Eq. (2.90) into Eq. (2.89) and using the correlation vector $\mathbf{r}_m$ defined in Eq. (2.56) yields

$$\overline{\boldsymbol{\nabla}}(k) = -2\begin{bmatrix} \mathbf{r}_0 \\ \vdots \\ \mathbf{r}_{M-1} \end{bmatrix} + 2\begin{bmatrix} \tilde{\mathbf{R}}_0 \\ \vdots \\ \tilde{\mathbf{R}}_{M-1} \end{bmatrix}\overline{\mathbf{f}}(k), \tag{2.91}$$

which can be simplified to

$$\overline{\boldsymbol{\nabla}}(k) = -2\mathbf{r} + 2\tilde{\mathbf{R}}\overline{\mathbf{f}}(k). \tag{2.92}$$

Assuming that the adaptive filter converges in the mean, then

$$\lim_{k\to\infty} \overline{\boldsymbol{\nabla}}(k) = \mathbf{0} \tag{2.93}$$

which leads to the system of equations

$$\tilde{\mathbf{R}}\mathbf{f} = \mathbf{r}. \tag{2.94}$$

Since $\tilde{\mathbf{R}}$ is a non-quadratic matrix, the system is overdetermined. The coefficient transformation matrix $\mathbf{T}$ and the subband power matrix $\mathbf{P}$ can be included in Eq. (2.92) to form a "transformed gradient" according to

$$\mathbf{T}\mathbf{P}^{-1}\overline{\boldsymbol{\nabla}}(k) = -2\mathbf{T}\mathbf{P}^{-1}\mathbf{r} + 2\mathbf{T}\mathbf{P}^{-1}\tilde{\mathbf{R}}\overline{\mathbf{f}}(k), \tag{2.95}$$

see Eq. (2.52). By setting Eq. (2.95) to zero, $\mathbf{T}\mathbf{P}^{-1}\overline{\boldsymbol{\nabla}}(k) = \mathbf{0}$, the following system of equations is obtained

$$\mathbf{T}\mathbf{P}^{-1}\tilde{\mathbf{R}}\mathbf{f}_{\text{conv}} = \mathbf{T}\mathbf{P}^{-1}\mathbf{r}, \tag{2.96}$$

where $\mathbf{T}\mathbf{P}^{-1}\tilde{\mathbf{R}}$ is a quadratic matrix. Let $\mathbf{Q} = \mathbf{T}\mathbf{P}^{-1}\tilde{\mathbf{R}}$. A unique solution $\mathbf{f}_{\text{conv}}$ exists when $\mathbf{Q}$ is non-singular. By inserting Eq. (2.95) into Eq. (2.52), the coefficient update in the mean can be expressed as

$$\begin{aligned}
\overline{\mathbf{f}}(k+1) &= \overline{\mathbf{f}}(k) + \mu\left(\mathbf{T}\mathbf{P}^{-1}\mathbf{r} - \mathbf{T}\mathbf{P}^{-1}\tilde{\mathbf{R}}\overline{\mathbf{f}}(k)\right) && (2.97)\\
&= \left(\mathbf{I} - \mu\mathbf{T}\mathbf{P}^{-1}\tilde{\mathbf{R}}\right)\overline{\mathbf{f}}(k) + \mu\mathbf{T}\mathbf{P}^{-1}\tilde{\mathbf{R}}\mathbf{f}_{\text{conv}} && (2.98)\\
&= \left(\mathbf{I} - \mu\mathbf{Q}\right)\overline{\mathbf{f}}(k) + \mu\mathbf{Q}\mathbf{f}_{\text{conv}} && (2.99)
\end{aligned}$$

Subtracting $\mathbf{f}_{\text{conv}}$ from $\overline{\mathbf{f}}(k)$ gives the coefficient error vector

$$\Delta\overline{\mathbf{f}}(k) = \overline{\mathbf{f}}(k) - \mathbf{f}_{\text{conv}} \tag{2.100}$$

Inserting Eq. (2.99) into Eq. (2.100) yields

$$\begin{aligned}
\Delta\overline{\mathbf{f}}(k+1) &= \left(\mathbf{I} - \mu\mathbf{Q}\right)\overline{\mathbf{f}}(k) + \mu\mathbf{Q}\mathbf{f}_{\text{conv}} - \mathbf{f}_{\text{conv}} && (2.101)\\
&= \left(\mathbf{I} - \mu\mathbf{Q}\right)\left(\overline{\mathbf{f}}(k) - \mathbf{f}_{\text{conv}}\right) && (2.102)\\
&= \left(\mathbf{I} - \mu\mathbf{Q}\right)\Delta\overline{\mathbf{f}}(k) && (2.103)
\end{aligned}$$

Matrix $\mathbf{Q}$ cannot be factorized using the eigenvalue decomposition for hermitian matrices (the spectral theorem $\mathbf{Q} = \mathbf{V}\boldsymbol{\Lambda}\mathbf{V}^H$), since the matrix is generally not hermitian and the eigenvalues of $\mathbf{Q}$ are generally complex valued. However, the eigenvalue decomposition for any square matrix, $\mathbf{Q} = \mathbf{V}\boldsymbol{\Lambda}\mathbf{V}^{-1}$, can still be used.

The coefficient error vector update equation can be rewritten as

$$\begin{aligned} \Delta\overline{\mathbf{f}}(k+1) &= \left(\mathbf{V}\mathbf{V}^{-1} - \mu\mathbf{V}\mathbf{\Lambda}\mathbf{V}^{-1}\right)\Delta\overline{\mathbf{f}}(k) && (2.104) \\ &= \mathbf{V}\left(\mathbf{I} - \mu\mathbf{\Lambda}\right)\mathbf{V}^{-1}\Delta\overline{\mathbf{f}}(k) && (2.105) \end{aligned}$$

The modal coefficient error vector is defined as

$$\Delta\overline{\mathbf{f}}'(k) = \mathbf{V}^{-1}\Delta\overline{\mathbf{f}}(k). \tag{2.106}$$

Combining Eqs. (2.105) and (2.106) yields

$$\Delta\overline{\mathbf{f}}'(k+1) = (\mathbf{I} - \mu\mathbf{\Lambda})\Delta\overline{\mathbf{f}}'(k). \tag{2.107}$$

If the adaptive filter is initialized with coefficients $\mathbf{f}(0)$, then $\Delta\mathbf{f}(0) = \mathbf{f}(0) - \mathbf{f}_{\text{conv}}$ and $\Delta\mathbf{f}'(0) = \mathbf{V}^{-1}\Delta\mathbf{f}(0)$. Hence

$$\Delta\overline{\mathbf{f}}'(k) = (\mathbf{I} - \mu\mathbf{\Lambda})^k\Delta\mathbf{f}'(0). \tag{2.108}$$

Since $(\mathbf{I} - \mu\mathbf{\Lambda})$ is a diagonal matrix, the elements in $\Delta\overline{\mathbf{f}}'(k)$ may be expressed as

$$\Delta\overline{f_i}'(k) = (1 - \mu\lambda_i)^k\Delta f_i'(0), \quad i = 0, \ldots, L_f - 1 \tag{2.109}$$

In order for $\mathbf{f}(k)$ to converge to $\mathbf{f}_{\text{conv}}$, it is necessary that the coefficient error vector $\Delta\mathbf{f}(k)$ converges to zero, and therefore that $\Delta\mathbf{f}'(k)$ converges to zero. This will occur for any $\Delta\mathbf{f}'(0)$ if and only if

$$|1 - \mu\lambda_i| < 1, \quad n = 0, \ldots, L_f - 1 \tag{2.110}$$

Since $|1 + \mu|\lambda_i|| \leq |1 + \mu\lambda_i|$ a tighter bound is obtained, which places the following restriction on the step size

$$0 < \mu < \frac{2}{|\lambda_{\text{max}}|}, \tag{2.111}$$

which is comparable to the bound in the fullband LMS with real eigenvalues.

The fullband mean square error is given by

$$J(k) = E\{|e(n)|^2\} \tag{2.112}$$

and the minimum MSE (MMSE) is given by

$$J_{\text{min}} = \sigma_d^2 - \mathbf{f}_{\text{conv}}^H\mathbf{r}_{xd} - \mathbf{r}_{xd}^H\mathbf{f}_{\text{conv}} + \mathbf{f}_{\text{conv}}^H\mathbf{R}_{xx}\mathbf{f}_{\text{conv}}. \tag{2.113}$$

An advantage of the closed loop configuration is that the algorithm can reach the same minimum MSE as the fullband counterpart. The convergence analysis show that the convergence speed is mainly dependent on how the subband-to-fullband transform matches the correlation matrix $\mathbf{R}$. Another important advantage is that the closed loop configuration is less computationally complex since it does not require filtering operations in the subband domain, which are required in the open loop configuration.

2.4 Simulation Results

2.4.1 Open Loop Delayless Subband Adaptive Filter

In this section the convergence properties of an open loop delayless subband adaptive filter in a system identification scenario is studied. The theoretical results are compared with Monte Carlo simulations of the algorithm. The open loop delayless subband adaptive filter has $L_f = 8$ fullband coefficients. Uniform-DFT analysis filter banks are used with $M = 4$ subbands, decimation rate $D = 2$ and filter length $L = 2M = 8$. The prototype filter is designed using the method described in Chapter 2.2.3. The coefficient transform is DFT-2. The step size is set at $\mu = 0.05 \cdot 2/\lambda_{\text{max}}$.

The input signal $x(n)$ is an AR-1 process with a pole at $z = 0.9$. The unknown system $s(n)$ is a length L_f FIR filter with randomly generated coefficients, see Fig. 2.8. The system noise power level is -80 dB .

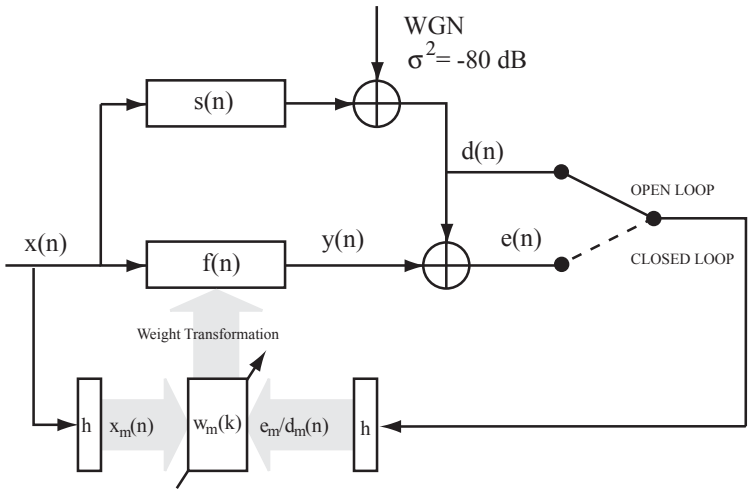

Figure 2.8: *System identification scenario.*

Fig. 2.9 shows the evolution of the MSE as a function of time. The MSE evolution is shown theoretically according to the coefficient update in the mean Eq. (2.99) and by averaging of multiple simulations with the adaptive algorithm according to Eq. (2.7). It can be seen that the simulation results correspond to the theoretical results. The following consecutive figures, Figs. 2.10, 2.11 and 2.12 show the evolution of the coefficients, the coefficient errors and the modal coefficient errors. Clearly from Fig. 2.11 it can be seen that the coefficient errors decay to zero. However, in Fig. 2.12 it can be seen that modes decay with different speeds depending on the eigenvalue-spread.

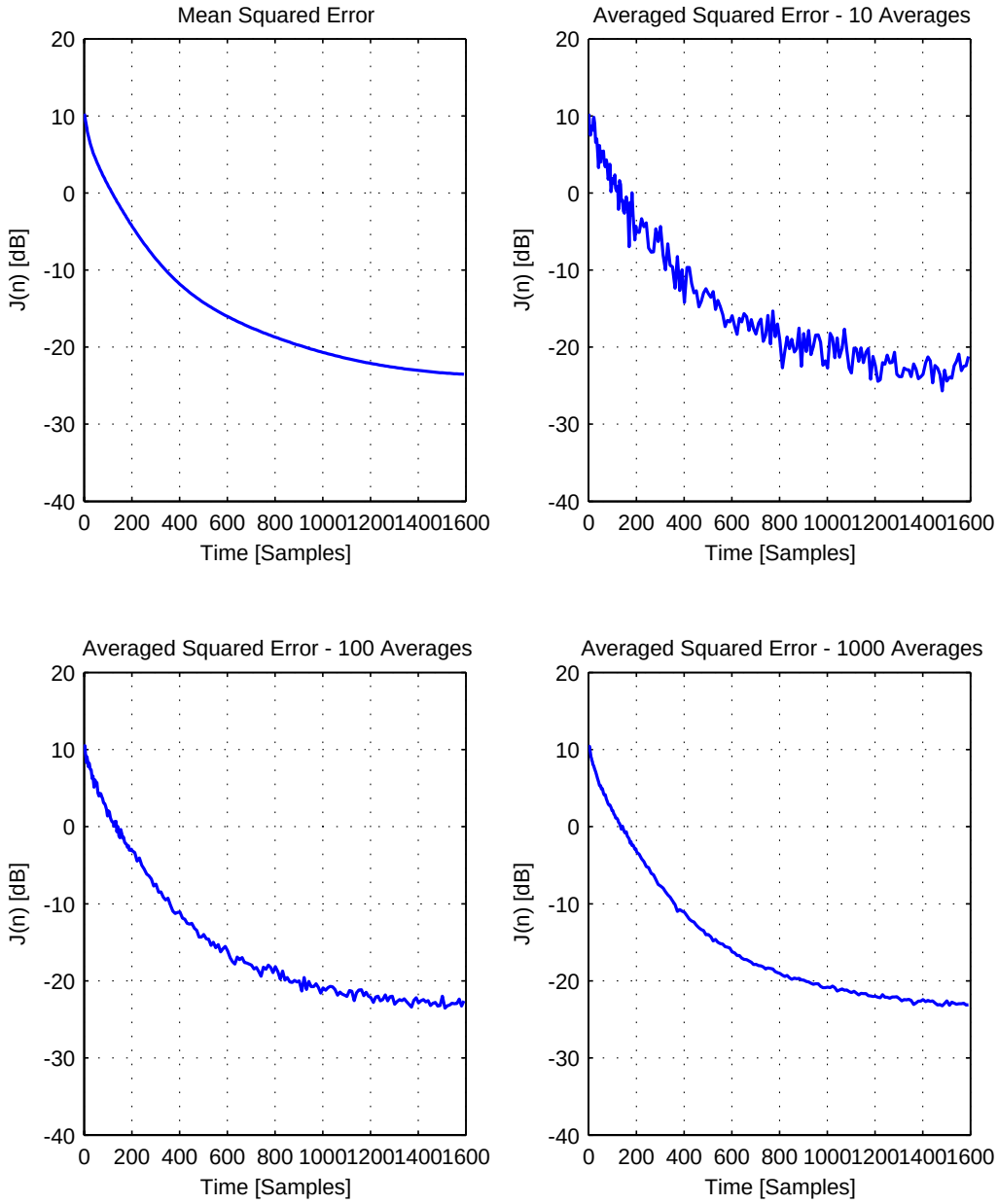

Figure 2.9: *Mean Square Error $J(n)$ for the open loop delayless subband adaptive filter.*

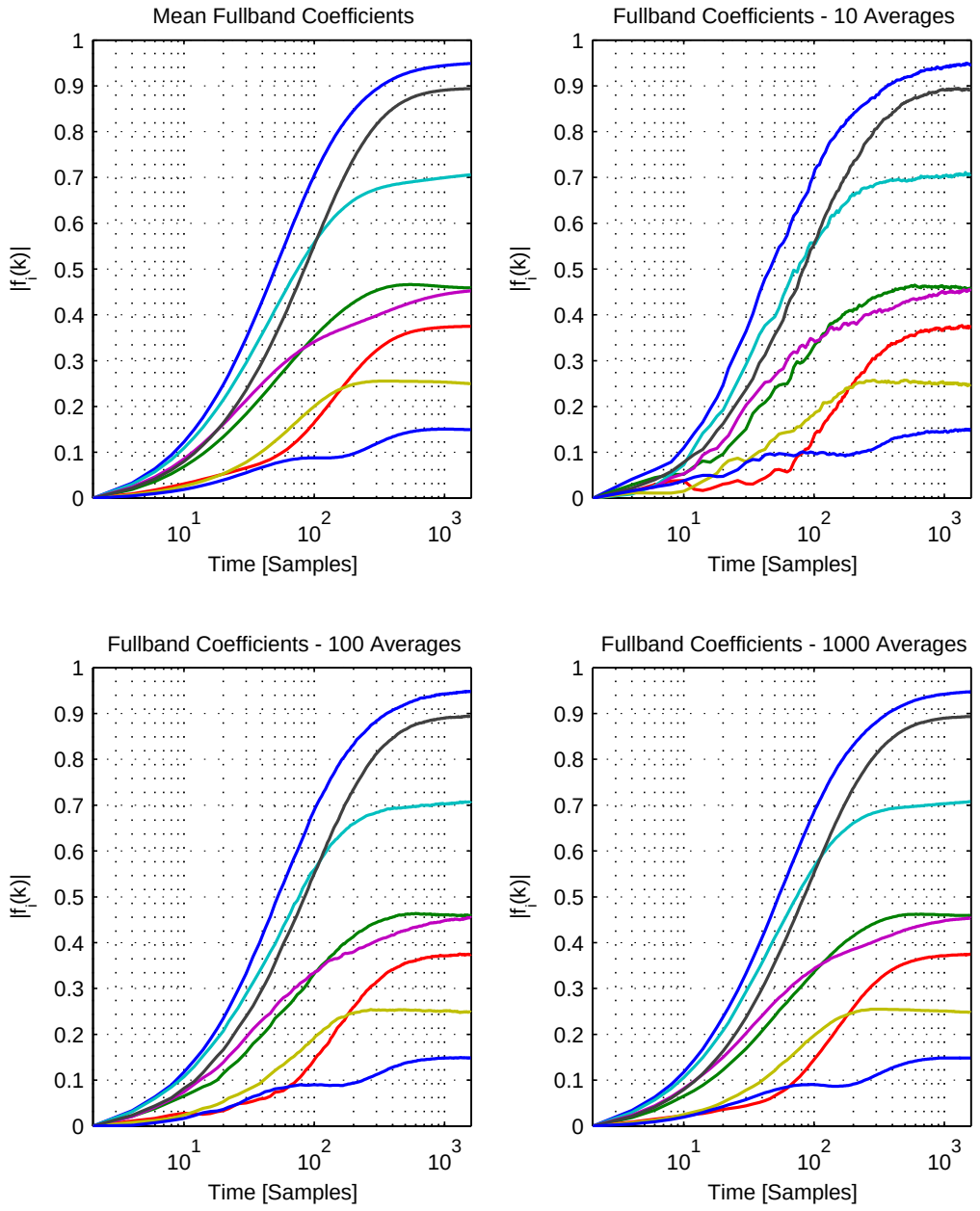

Figure 2.10: *Magnitude of the fullband filter coefficients* $|\overline{f_i}(k)|$ *for the open loop delayless subband adaptive filter.*

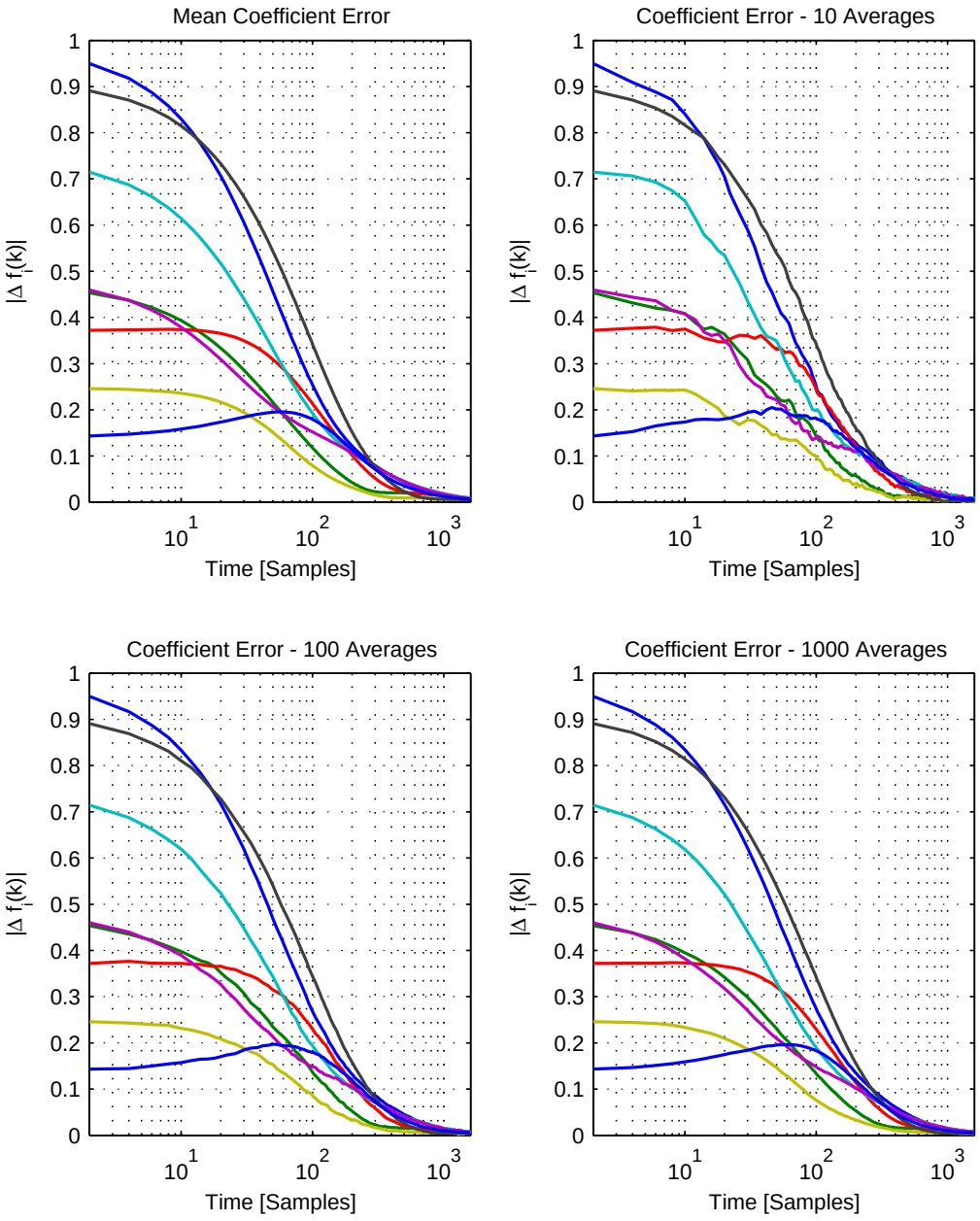

Figure 2.11: *Magnitude of the coefficient errors* $|\Delta\overline{f_i}(k)|$ *for the open loop delayless subband adaptive filter.*

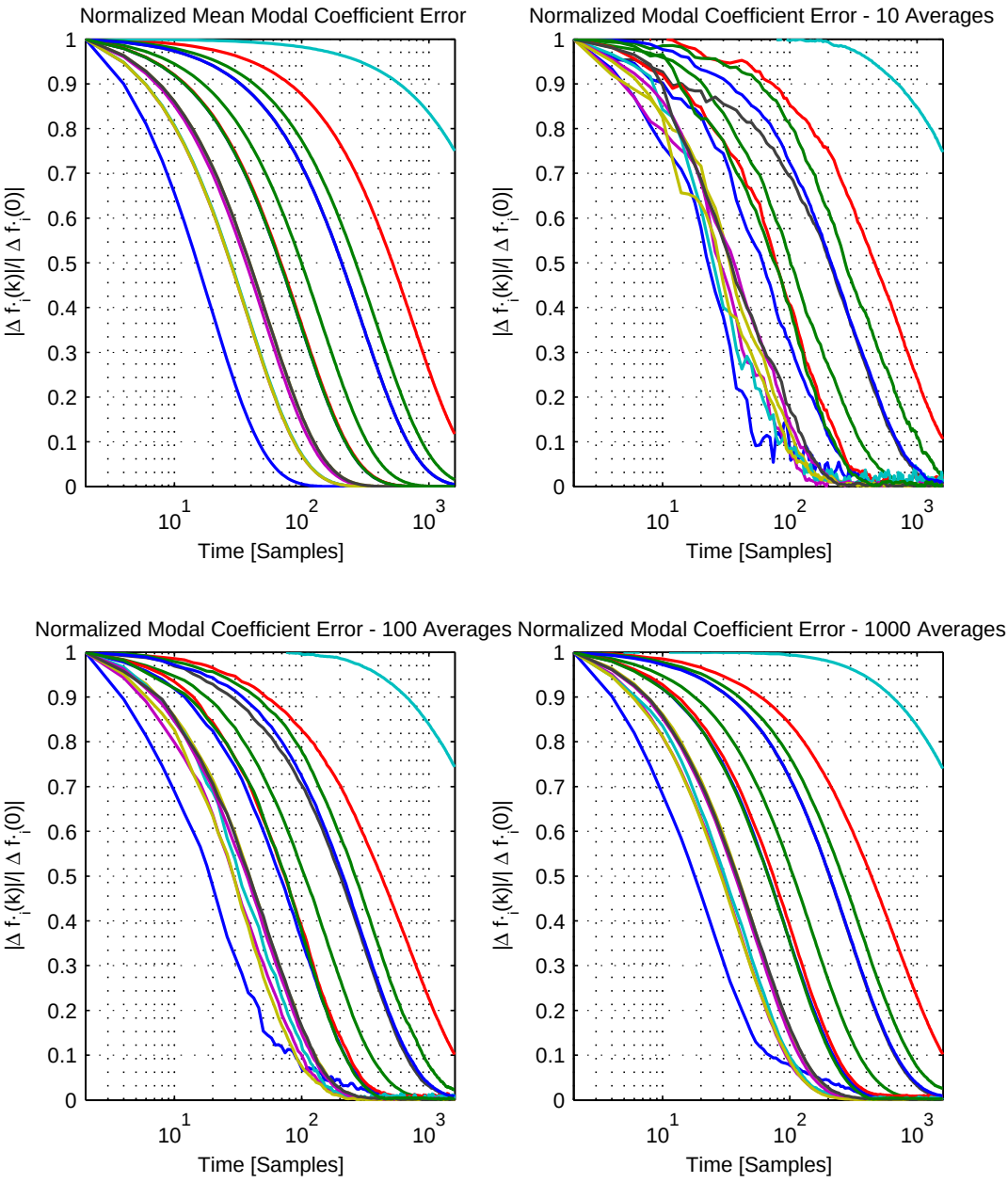

Figure 2.12: *Normalized magnitude of the modal coefficient errors* $|\Delta\overline{f_i}'(k)|/|\Delta f_i'(0)|$ *for the open loop delayless subband adaptive filter.*

2.4.2 Closed Loop Delayless Subband Adaptive Filter

In this section the convergence properties of a closed loop delayless subband adaptive filter is studied. The scenario is the same as in Chapter 2.4.1. The closed loop delayless subband adaptive filter has $L_f = 8$ fullband coefficients, uniform-DFT analysis filter banks with $M = 4$ subbands, decimation rate $D = 2$ and filter length $L = 2M$. The prototype filter is designed using the method described in Chapter 2.2.3. The coefficient transform is DFT-2. The step size is set at $\mu = 0.05 \cdot 2/|\lambda_{max}|$.

Fig. 2.13 shows the evolution of the MSE as a function of time. The evolution of the MSE is shown theoretically according to the coefficient update in the mean Eq. (2.99) and by averaging of multiple simulations with the adaptive algorithm according to Eq. (2.7). It can be seen that the simulation results correspond to the theoretical results. The following consecutive figures, Figs. 2.14, 2.15 and 2.16 show the evolution of the coefficients, the coefficient errors and the modal coefficient errors. From Fig. 2.15 it can be seen that the coefficient errors decay to zero.

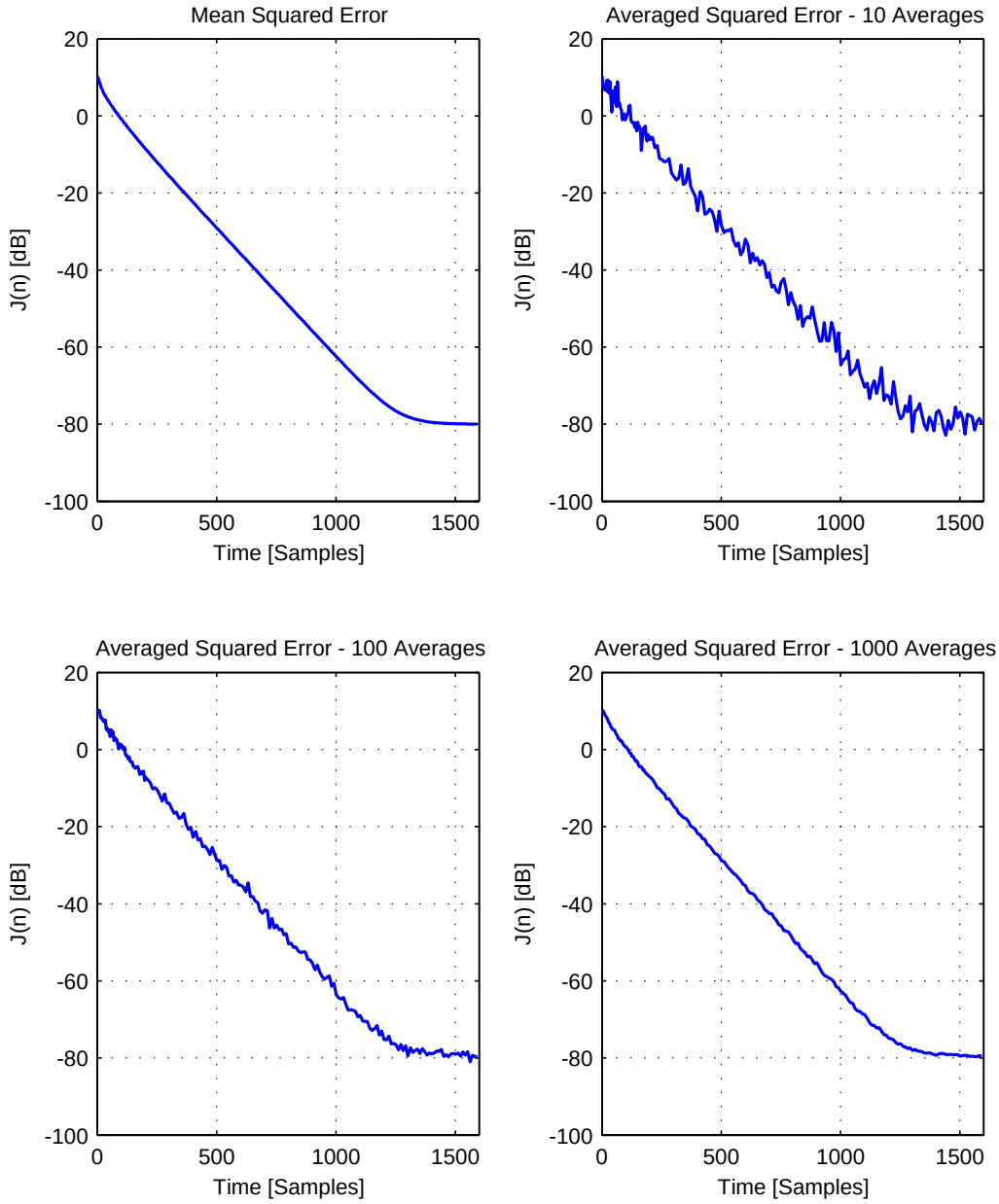

Figure 2.13: *Mean Square Error $J(n)$ for the closed loop delayless subband adaptive filter.*

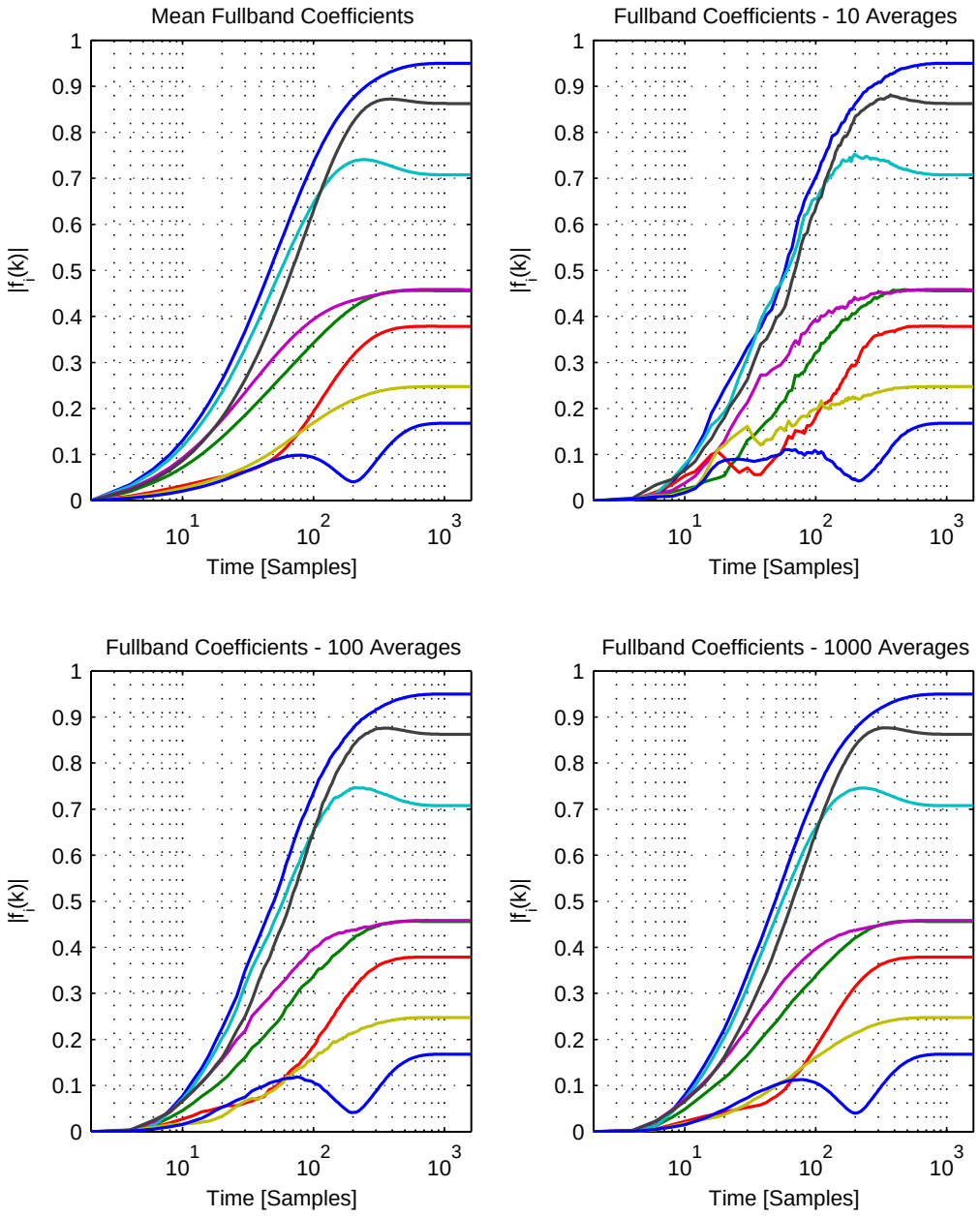

Figure 2.14: *Magnitude of the fullband filter coefficients* $|\overline{f_i}(k)|$ *for the closed loop delayless subband adaptive filter.*

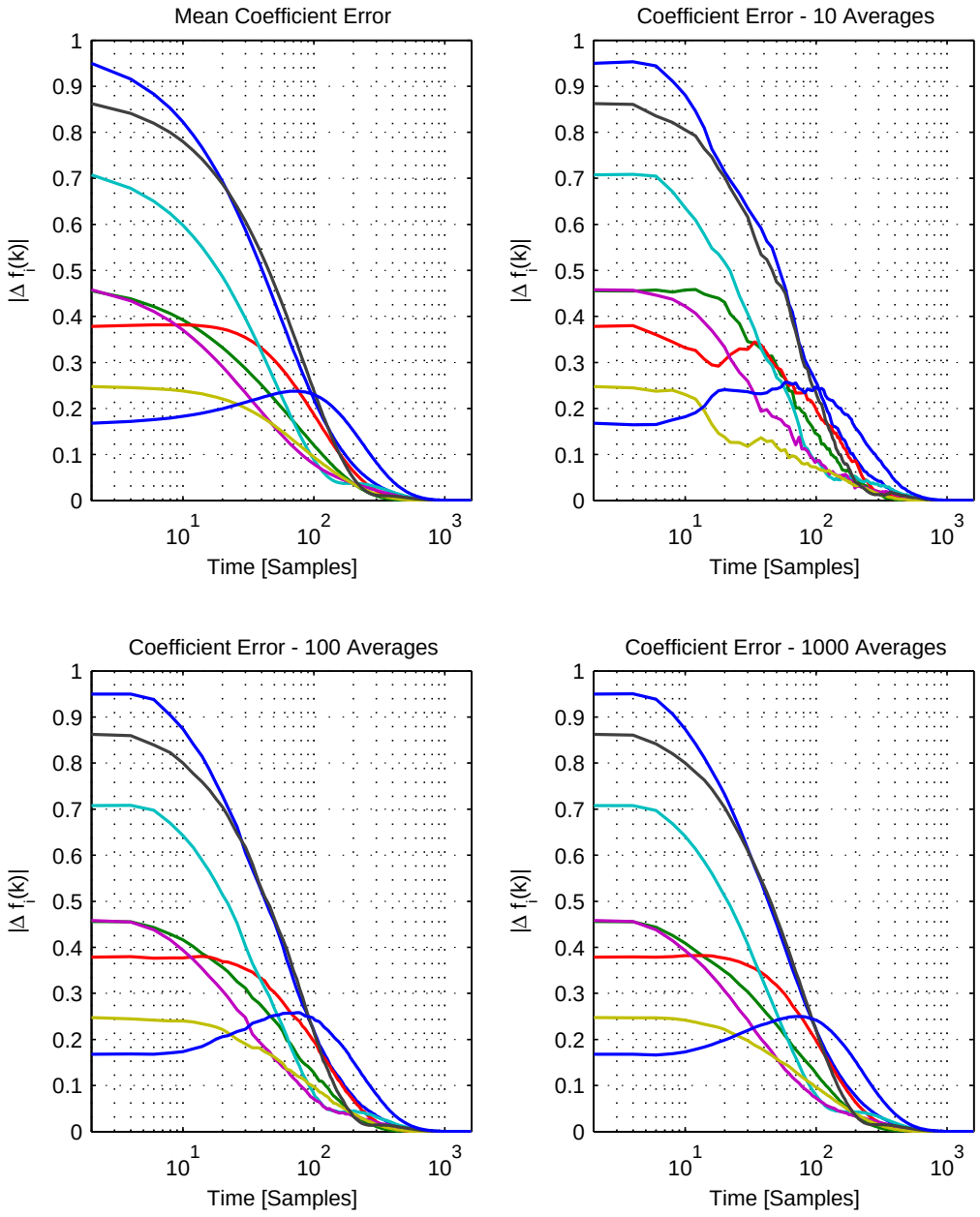

Figure 2.15: *Magnitude of the coefficient errors* $|\Delta\overline{f_i}(k)|$ *for the closed loop delayless subband adaptive filter.*

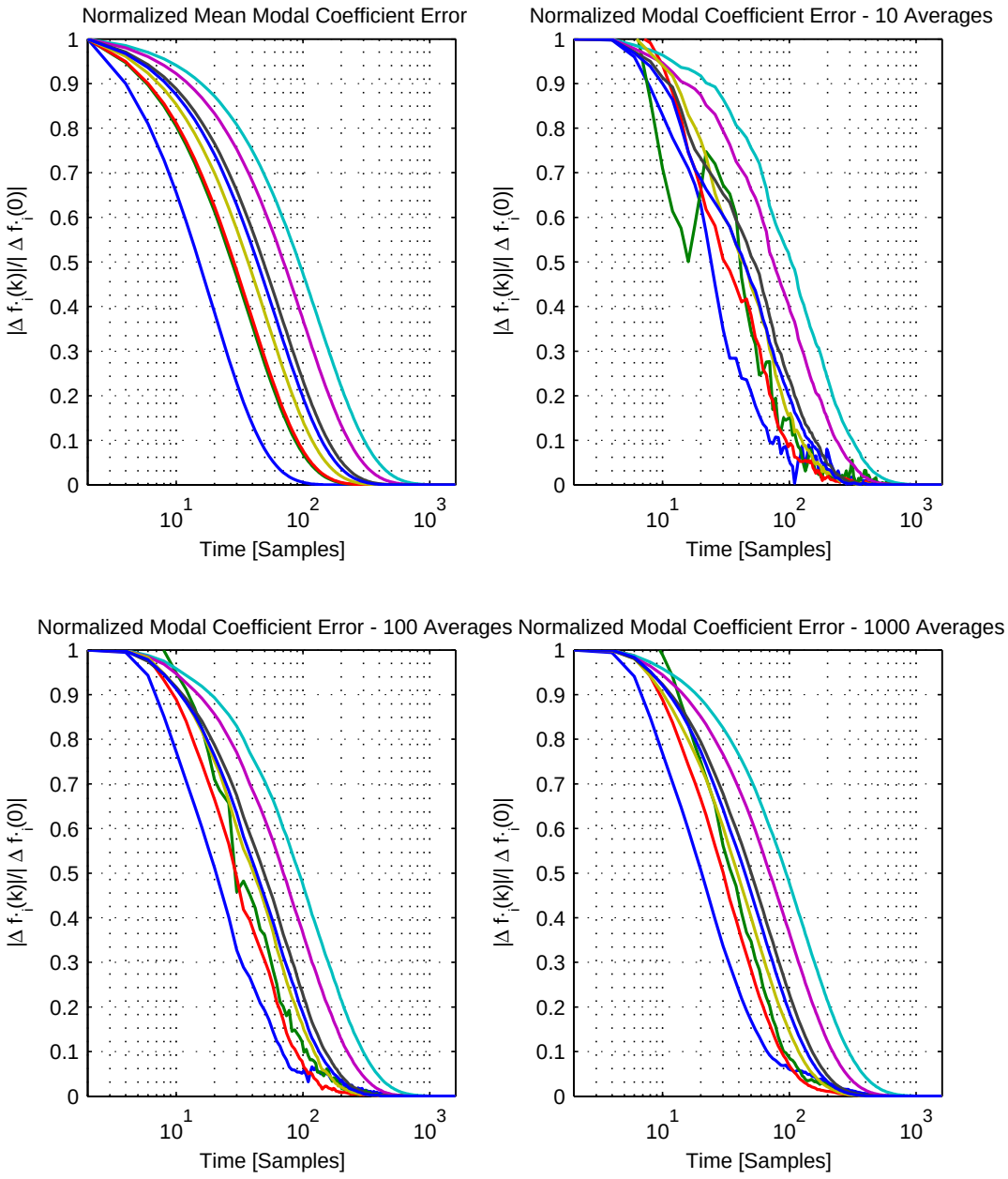

Figure 2.16: *Normalized magnitude of the modal coefficient errors* $|\Delta\overline{f_i}'(k)|/|\Delta f_i'(0)|$ *for the closed loop delayless subband adaptive filter.*

Chapter 3

Optimal Subband-to-Fullband Transform

3.1 Optimal Transform for Closed Loop Configuration

In Chapter 2.3.2 it was shown that the convergence speed of the closed loop delayless subband adaptive filter depends on the coefficient transform. It was also shown that uniform convergence is obtained when the following relationship is fulfilled

$$\mathbf{Q} = \mathbf{I}, \tag{3.1}$$

where $\mathbf{Q} = \mathbf{T}\mathbf{P}^{-1}\tilde{\mathbf{R}}$. When the input signal correlation is known, then the correlation matrix $\tilde{\mathbf{R}}$ is known and the coefficient transform can be obtained by finding the inverse matrix to $\mathbf{P}^{-1}\tilde{\mathbf{R}}$. However, since $\mathbf{P}^{-1}\tilde{\mathbf{R}}$ is a non-quadratic matrix, the inverse does not exist. Provided that $\tilde{\mathbf{R}}^H\mathbf{P}^{-2}\tilde{\mathbf{R}}$ is non-singular, a solution to Eq. (3.1) is given by the pseudo-inverse of $\mathbf{P}^{-1}\tilde{\mathbf{R}}$

$$\mathbf{T} = \left(\mathbf{P}^{-1}\tilde{\mathbf{R}}\right)^{+} = \left(\tilde{\mathbf{R}}^H\mathbf{P}^{-2}\tilde{\mathbf{R}}\right)^{-1}\tilde{\mathbf{R}}^H\mathbf{P}^{-H} \tag{3.2}$$

Using the pseudo-inverse of $\mathbf{P}^{-1}\tilde{\mathbf{R}}$ as the subband-to-fullband transform, diagonalizes the matrix $\mathbf{Q}$ that governs the convergence performance so that one coefficient in the fullband filter controls one and only one mode of the adaptive filter and normalizes the eigenvalues so that the modes converge uniformly, i.e. with the same speed.

3.2 Simulation Results

3.2.1 Optimal/Uniform-DFT Closed Loop Configuration

In this section, the theoretical results of Chapters 2.3.2 and 3.1 are compared with the practical implementation of a closed-loop delayless subband adaptive filter, where the subband-to-fullband transform is the optimal transform. For the sake of comparison the settings are the same as for the example in Chapter 2.4.2. Fig. 3.1 shows the evolution of the MSE as a function of time. The MSE evolution is shown theoretically according to the coefficient update in the mean Eq. (2.99) and by averaging of multiple simulations with the adaptive algorithm according to Eq. (2.7). It can be observed that the adaptive algorithm has a larger excess mean square error compared with the algorithm in Chapter 2.4.2. The following consecutive figures, Figs. 3.2, 3.3 and 3.4 show the evolution of the coefficients, the coefficient errors and the modal coefficient errors. Clearly from Fig. 3.3 it can be seen that the coefficient errors decay to zero.

In Fig. 3.4 it can be seen that modes decay uniformly due to the decorrelation and normalization effect of the transformation matrix.

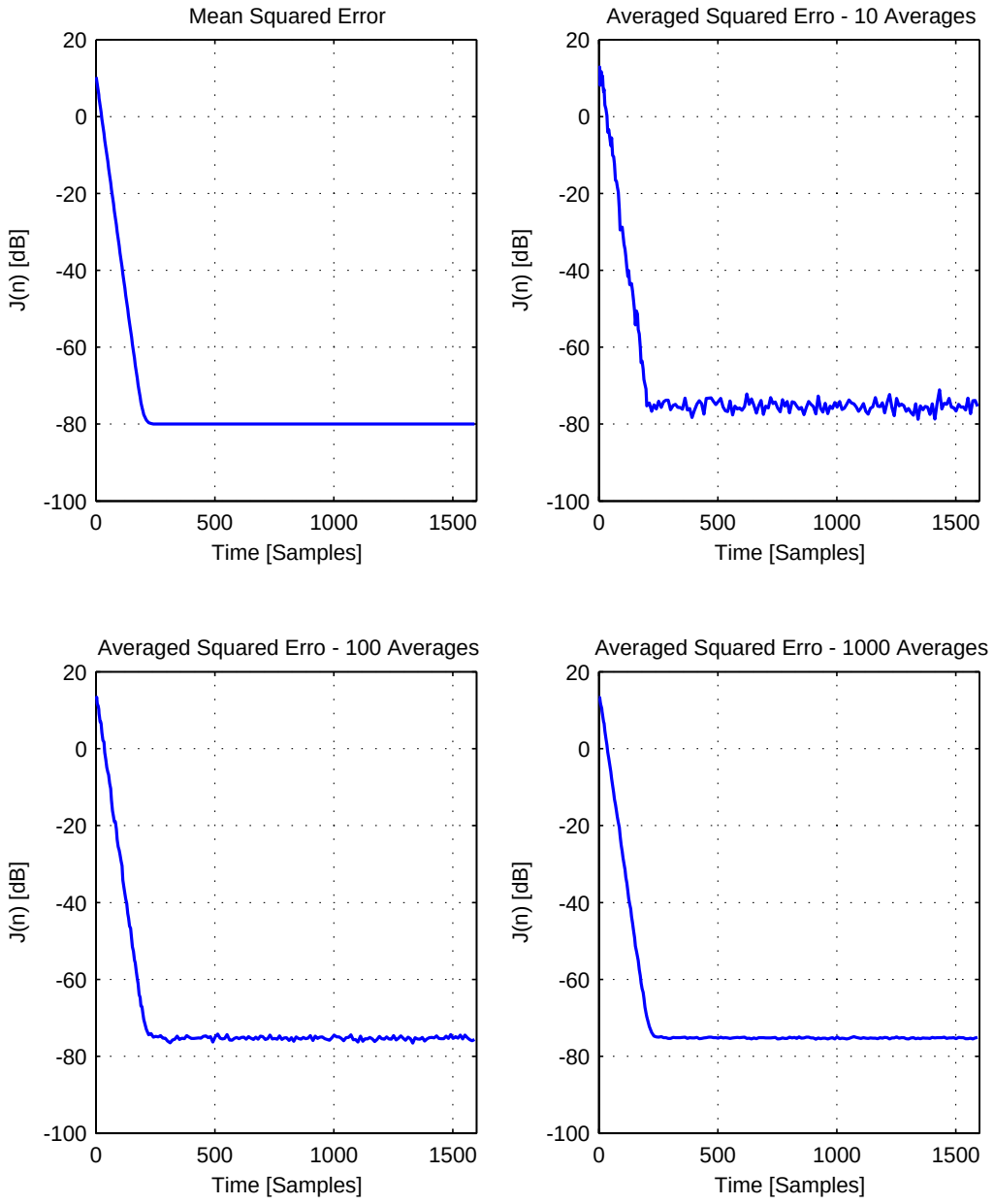

Figure 3.1: *Mean Square Error $J(n)$ for the closed loop delayless subband adaptive filter with the optimal transform.*

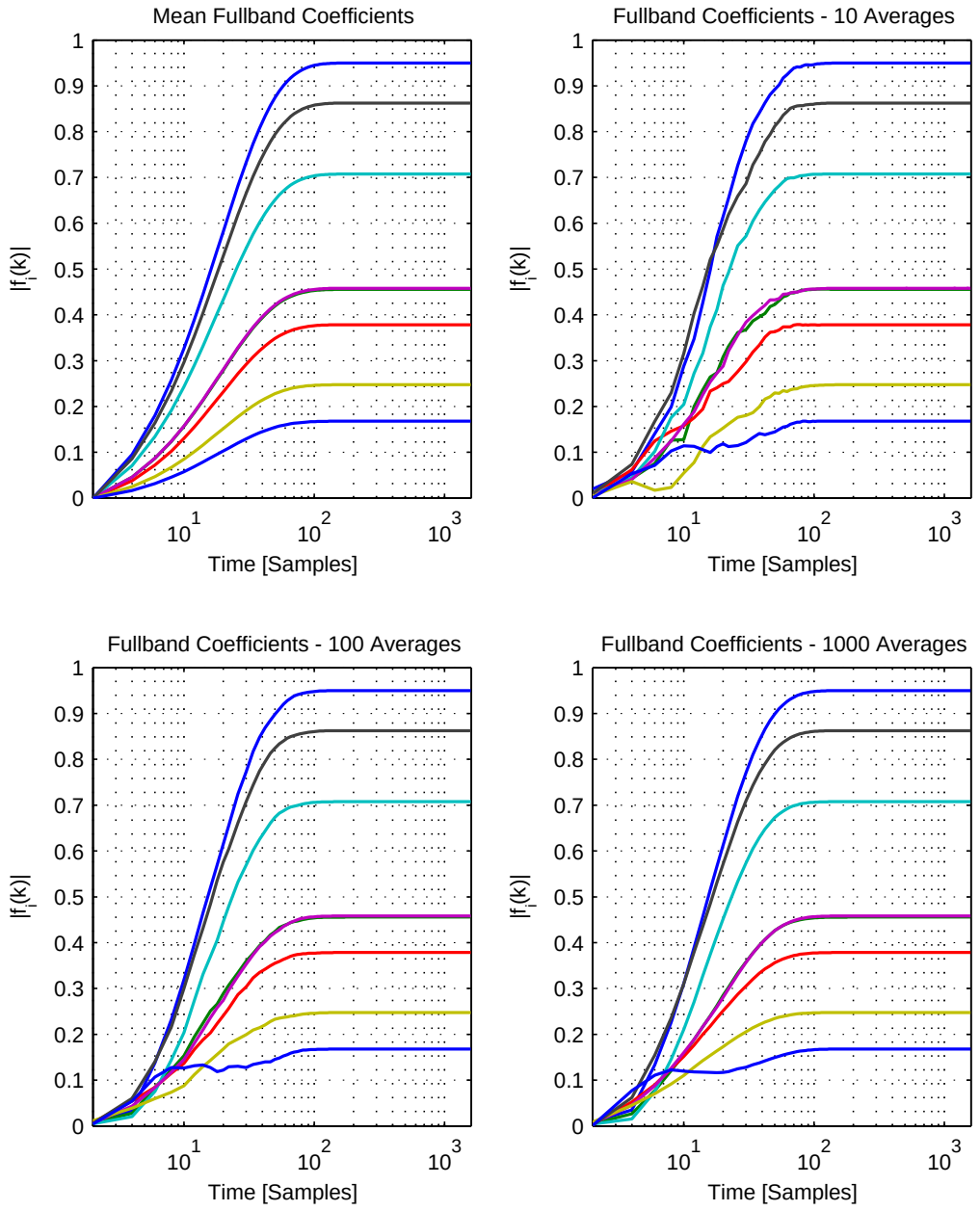

Figure 3.2: *Magnitude of the fullband filter coefficients* $|\overline{f_i}(k)|$ *for the closed loop delayless subband adaptive filter with the optimal transform.*

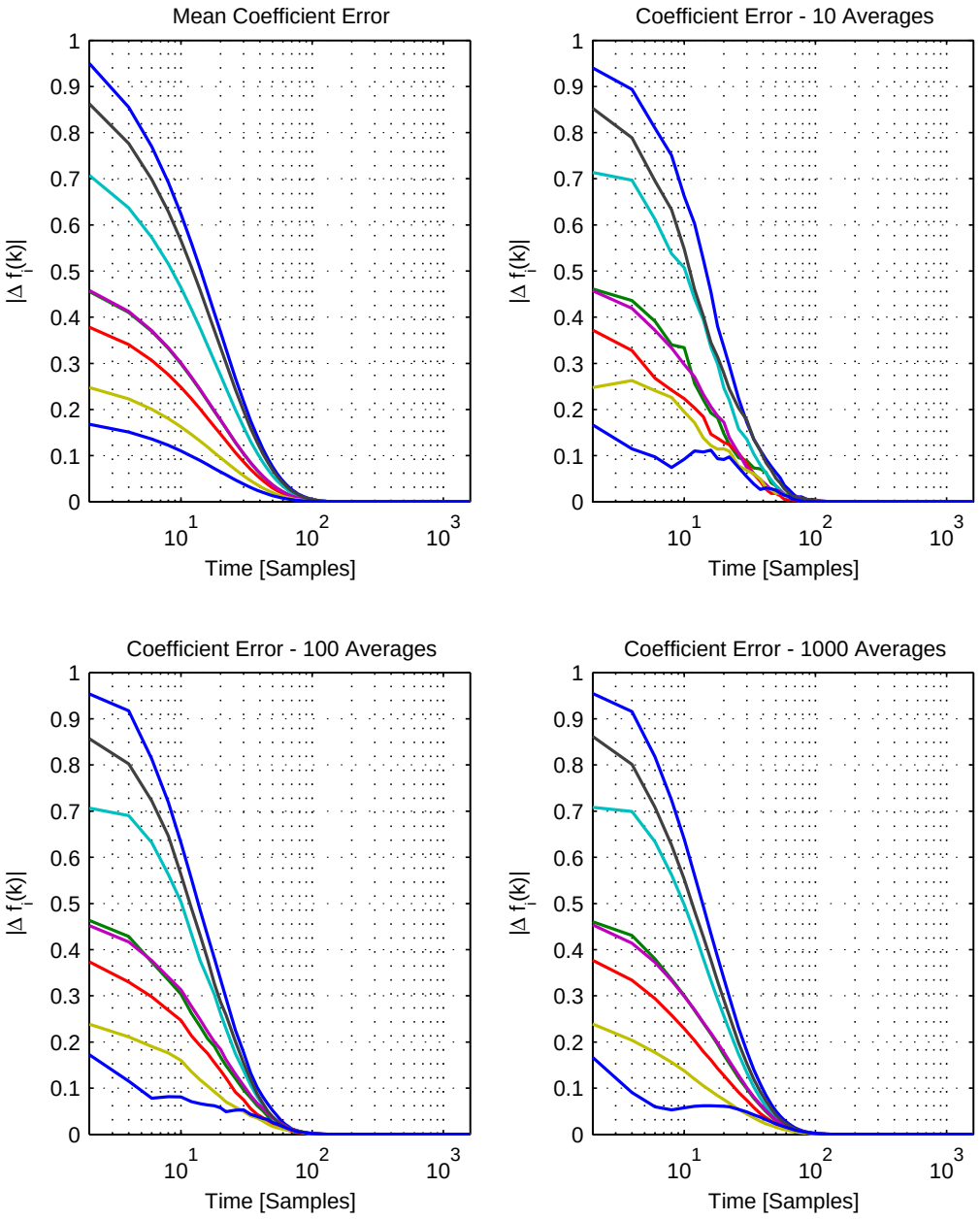

Figure 3.3: *Magnitude of the coefficient errors* $|\Delta\overline{f}_i(k)|$ *for the closed loop delayless subband adaptive filter with the optimal transform.*

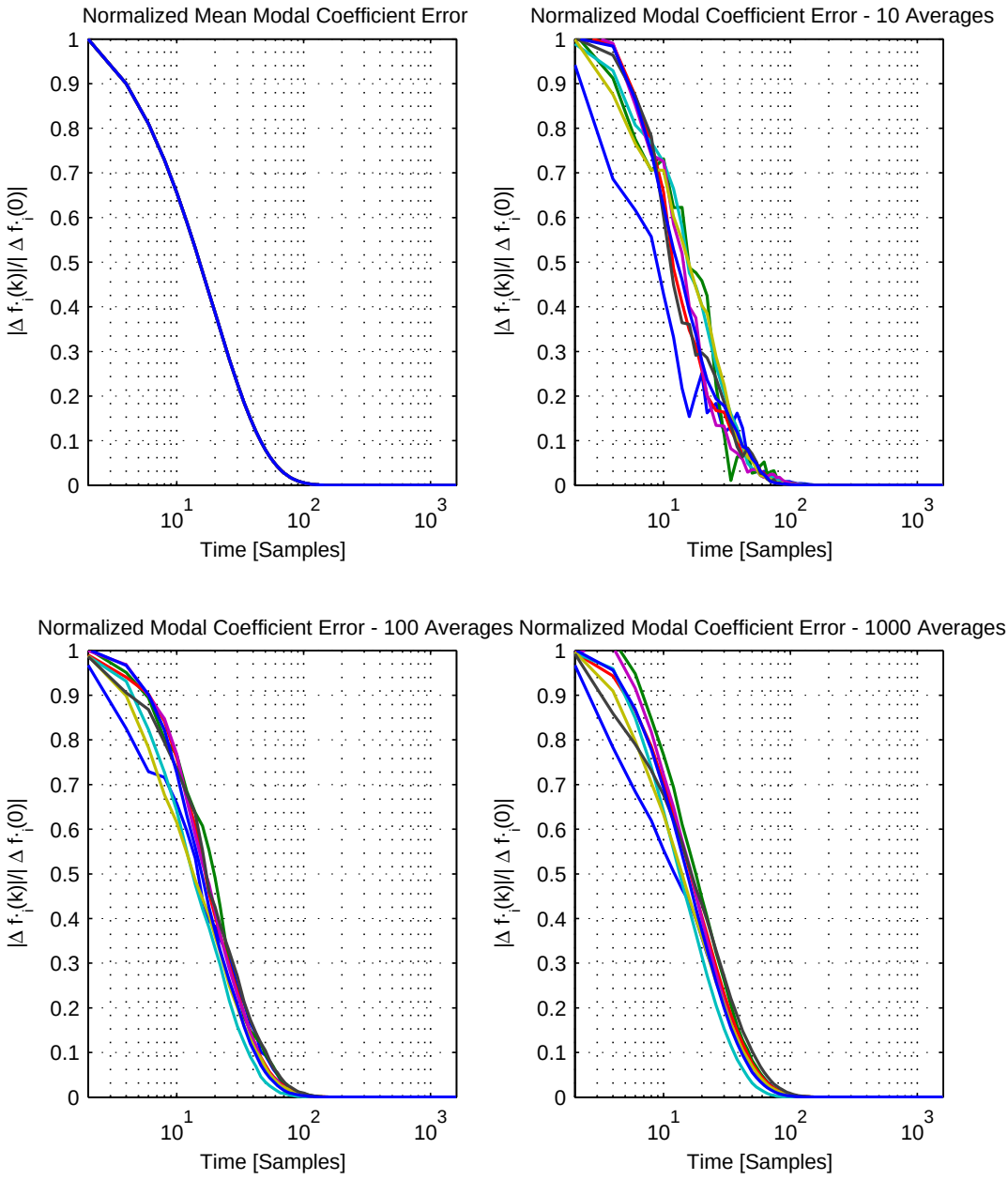

Figure 3.4: *Magnitude of the modal coefficient errors* $|\Delta \overline{f_i}'(k)|/|\Delta f_i'(0)|$ *for the closed loop delayless subband adaptive filter with the optimal transform.*

Chapter 4

Delayless Subband Adaptive Filter without Subband-to-Fullband Transform

4.1 Description of the Subband Adaptive Filter

In this chapter a new delayless subband adaptive filter is presented using the approach of polyphase filter adaptation, which was previously presented for subband adaptive filtering in [6]. Consider the input signal $x(n)$ and the desired signal $d(n)$. As in conventional delayless subband adaptive filtering, The output signal $y(n)$ is obtained by filtering $x(n)$ with the fullband filter $\mathbf{f}(k)$

$$y(n) = \mathbf{f}^T \left(\lfloor \tfrac{n}{D} \rfloor \right) \mathbf{x}(n), \tag{4.1}$$

where $\mathbf{f}(k) = [f_0(k), \ldots, f_{L_f-1}(k)]^T$ is a vector with fullband filter coefficients $f_i(k)$, where i is the coefficient index and n the time index corresponding to the input signal sample rate. The filter coefficients are updated at a lower sampling rate with time index $k = \lfloor \frac{n}{D} \rfloor$. The fullband filter length is denoted with L_f. The output signal $y(n)$ can be decomposed into decimated subband signals according to

$$y_m(k) = \mathbf{h}_m^T \mathbf{y}(kD), \quad m = 0, \ldots, M-1, \tag{4.2}$$

where $\mathbf{h}_m$ is a vector with analysis filter coefficients. The filter length of the analysis filters is L_h. Eq. (4.1) and Eq. (4.2) are illustrated in Fig. 4.1.

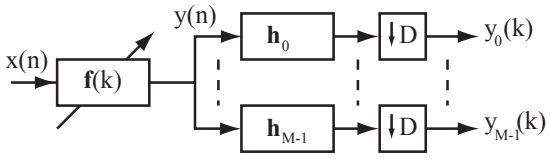

Figure 4.1: *Adaptive filtering and subband decomposition, Eq.* (4.1) *combined with Eq.* (4.2).

Assuming the open loop configuration for the delayless subband adaptive filter (see the final structure in Fig. 4.4), the desired signal $d(n)$ is also decomposed into decimated subband signals

$$d_m(k) = \mathbf{h}_m^T \mathbf{d}(kD), \quad m = 0, \ldots, M-1. \tag{4.3}$$

Subband error signals are obtained by

$$e_m(k) = d_m(k) - y_m(k), \quad m = 0, \ldots, M-1. \tag{4.4}$$

Inserting in Eq. (4.1) into in Eq. (4.2) yields

$$y_m(k) = \mathbf{f}^T(k)\tilde{\mathbf{H}}_m\mathbf{x}(kD) = \mathbf{f}^T(n)\tilde{\mathbf{x}}_m(kD), \tag{4.5}$$

where $\tilde{\mathbf{H}}_m$ denotes the conventional (non-decimated) convolution matrix with analysis filter coefficients. This means that the adaptive filter and the subband decomposition have traded place. Eq. (4.5) is illustrated in Fig. 4.2.

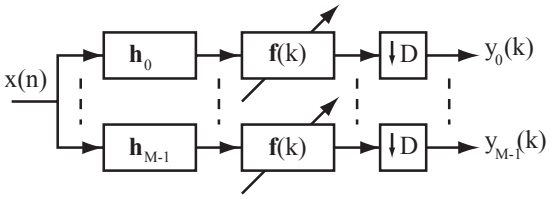

Figure 4.2: *Subband decomposition prior to adaptive filtering, Eq.* (4.5)*. This system is equivalent to the system in Fig. 4.1.*

A polyphase decomposition of the fullband filter into D components is given by

$$f_{d,l}(k) = f_{lD+d}(k), \quad d = 0, \ldots, D-1 \tag{4.6}$$

where $f_{d,l}(k)$ denotes the l-th coefficient of the d-th polyphase component of $\mathbf{f}(k)$ at time instant k. Since the polyphase components operate on the polyphase components of the input subband signal, they operate at the lower sample rate and are also updated by the adaptive algorithm at this rate. This explains the use of time index k. It is assumed that the fullband filter length L_f is a multiple of D. The polyphase decomposition of the non-decimated input subband signals $\tilde{x}_m(n)$ is

$$\tilde{x}_{m,d}(k) = \tilde{x}_m(kD - d), \quad d = 0, \ldots, D-1 \tag{4.7}$$

The output subband signals $y_m(k)$ in Eq. (4.5) can be expressed in terms of polyphase components as

$$y_m(k) = \sum_{d=0}^{D-1} \mathbf{f}_d^T(k)\tilde{\mathbf{x}}_{m,d}(k), \tag{4.8}$$

where

$$\mathbf{f}_d(k) = [f_d(k), f_{D+d}(k), \ldots, f_{L_f-D+d}(k)]^T, \tag{4.9}$$

and

$$\tilde{\mathbf{x}}_{m,d}(k) = [\tilde{x}_m(kD+d), \tilde{x}_m(kD-D+d), \ldots, \tilde{x}_m(kD-L_f+D-d)]^T. \tag{4.10}$$

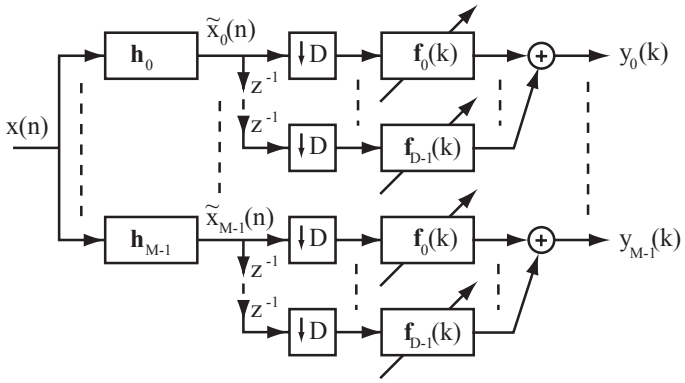

Figure 4.3: *Illustration of the polyphase implementation of the adaptive filters, Eq.* (4.8) *This system is equivalent to the system in Figs. 4.2 and 4.3.*

The calculation of the output subband signals according to Eq. (4.8) is illustrated in Fig. 4.3.

The subband error signal $e_m(k)$ in the open loop case is given by

$$e_m(k) = d_m(k) - \sum_{d=0}^{D-1} \mathbf{f}_d^T \tilde{\mathbf{x}}_{m,d}(k). \tag{4.11}$$

In the closed loop configuration, the error signals are not computed in the subband domain, but they are obtained by transforming the fullband error signal to the subband domain according to

$$e_m(k) = \mathbf{h}_m^T \mathbf{e}(kD). \tag{4.12}$$

By using the closed loop configuration, the computational savings are apparent since the filtering in the subband domain is omitted. An adaptive algorithm is now developed, which updates the fullband coefficients directly without the use of a coefficient transform. The delayless polyphase adaptive filter is illustrated in Fig. 4.4.

In both configurations, the fullband filter coefficients are updated to minimize the instantaneous cost function proposed in [6]

$$J(k) = \sum_{m=0}^{M-1} P_m^{-1} |e_m(k)|^2. \tag{4.13}$$

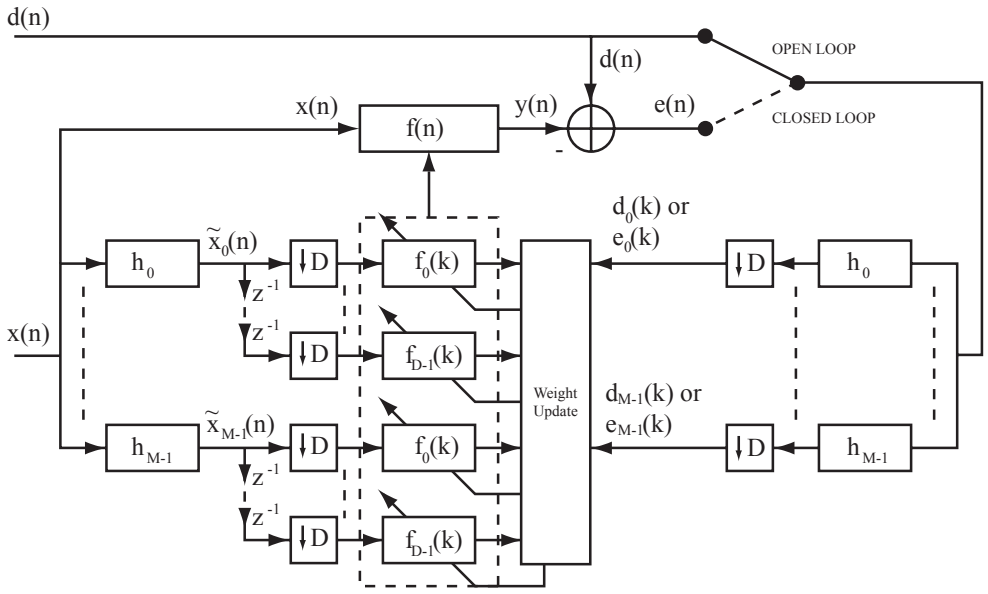

Figure 4.4: *Delayless Subband Adaptive Filter with Adaptive Polyphase Filters. Note that the polyphase filters have the same coefficients in all subbands and that there is no subband-to-fullband transformation of the coefficients, i.e. the subband coefficients are immediately applied in the fullband filtering.*

Based on the subband error definition of the open loop configuration, the gradient vector is given by

$$\boldsymbol{\nabla}(k) = 2\frac{\partial J(k)}{\partial \mathbf{f}_d^*(k)} = 2\sum_{m=0}^{M-1} P_m^{-1} e_m(k) \frac{\partial}{\partial \mathbf{f}_d^*(k)} e_m^*(k) \tag{4.14}$$

$$= -2\sum_{m=0}^{M-1} P_m^{-1} \tilde{\mathbf{x}}_{m,d}^*(k) e_m(k) \tag{4.15}$$

A Least Mean Square update equation for the polyphase components $\mathbf{f}_d(k)$ is given by

$$\begin{aligned} \mathbf{f}_d(k+1) &= \mathbf{f}_d(k) - \frac{1}{2}\mu\boldsymbol{\nabla}(k) \\ &= \mathbf{f}_d(k) + \mu\sum_{m=0}^{M-1} P_m^{-1}\tilde{\mathbf{x}}_{m,d}^*(k) e_m(k), \quad d = 0,\ldots,D-1 \end{aligned} \tag{4.16}$$

Combining the update equations for the polyphase components, a composite update equation for the whole fullband filter can be obtained as

$$\mathbf{f}(k+1) = \mathbf{f}(k) + \mu\sum_{m=0}^{M-1} P_m^{-1}\tilde{\mathbf{x}}_m^*(kD) e_m(k). \tag{4.17}$$

For non-stationary input, the subband signal powers P_m have to be estimated, for example using the estimate in Eq. (2.9) or by using exponential averaging

$$\hat{P}_m(k) = \alpha \hat{P}_m(k-1) + (1-\alpha)|x_m(k)|^2 \tag{4.18}$$

where the constant α is a forgetting factor.

4.2 Convergence Analysis

The mean coefficient update equation for both configurations is

$$\overline{\mathbf{f}}(k+1) = \overline{\mathbf{f}}(k) - \tfrac{1}{2}\mu \sum_{m=0}^{M-1} P_m^{-1} \overline{\boldsymbol{\nabla}}_m(k). \tag{4.19}$$

where the mean subband gradient vector is

$$\overline{\boldsymbol{\nabla}}_m(k) = -2E\{\tilde{\mathbf{x}}_m^*(kD) e_m(k)\} \tag{4.20}$$

4.2.1 Convergence Analysis of Open Loop Configuration

In the open loop configuration, the error signals are computed from the subband signals, hence the mean subband gradient vector is

$$\overline{\boldsymbol{\nabla}}_m(k) = -2E\{\tilde{\mathbf{x}}_m^*(kD)[d_m(k) - y_m(k)]\} \tag{4.21}$$

Assuming that the adaptive coefficients and the input subband signals are statistically independent, Eq. (4.21) can be rewritten as

$$\overline{\boldsymbol{\nabla}}_m(k) = -2E\{\tilde{\mathbf{x}}_m^*(kD) d_m(k)\} + 2E\{\tilde{\mathbf{x}}_m^*(kD)\tilde{\mathbf{x}}_m^T(kD)\}\overline{\mathbf{f}}(k). \tag{4.22}$$

A subband cross-correlation vector is defined, based on the non-decimated subband input signal $\tilde{x}_m(n)$ and desired subband signal $d_m(k)$ according to

$$\tilde{\mathbf{r}}_m = E\{\tilde{\mathbf{x}}_m^*(kD) d_m(k)\} = \tilde{\mathbf{H}}_m^H \mathbf{R}_{xd} \mathbf{h}_m, \tag{4.23}$$

and corresponding auto-correlation matrix

$$\tilde{\tilde{\mathbf{R}}}_m = E\{\tilde{\mathbf{x}}_m^*(kD)\tilde{\mathbf{x}}_m^T(kD)\} = \tilde{\mathbf{H}}_m^H \mathbf{R}_{xx} \tilde{\mathbf{H}}_m \tag{4.24}$$

With the definitions in Eqs. (4.23) and (4.24) the mean subband gradient vector $\overline{\boldsymbol{\nabla}}_m(k)$ becomes

$$\overline{\boldsymbol{\nabla}}_m(k) = -2\tilde{\mathbf{r}}_m + 2\tilde{\tilde{\mathbf{R}}}_m \overline{\mathbf{f}}(k) \tag{4.25}$$

Using the matrix and vector definitions

$$\mathbf{R} = \sum_{m=0}^{M-1} P_m^{-1} \tilde{\tilde{\mathbf{R}}}_m, \qquad \mathbf{r} = \sum_{m=0}^{M-1} P_m^{-1} \tilde{\mathbf{r}}_m, \tag{4.26}$$

the weighted sum of the mean subband gradient vectors in Eq. (4.19) becomes

$$\sum_{m=0}^{M-1} P_m^{-1} \overline{\boldsymbol{\nabla}}_m(k) = \sum_{m=0}^{M-1} P_m^{-1} \left(-2\tilde{\mathbf{r}}_m + 2\tilde{\tilde{\mathbf{R}}}_m \overline{\mathbf{f}}(k) \right) = -2\mathbf{r} + 2\mathbf{R}\overline{\mathbf{f}}(k) \tag{4.27}$$

The filter coefficients converge when the sum in Eq. (4.27) approaches zero. Denoting the converged weights with $\mathbf{f}_{\text{conv}} = \lim_{k\to\infty} \overline{\mathbf{f}}(k)$, this leads to the following system of equations

$$\mathbf{R}\mathbf{f}_{\text{conv}} = \mathbf{r}. \tag{4.28}$$

Hence, the filter coefficients converge in the mean to

$$\mathbf{f}_{\text{conv}} = \mathbf{R}^{-1}\mathbf{r}. \tag{4.29}$$

The sequel of the analysis is similar to that of the LMS adaptive filter in the Appendix. The main difference is that the rate of the coefficient update is D times lower than the full rate. The coefficient vector update equation in the mean is given by

$$\overline{\mathbf{f}}(k+1) = (\mathbf{I} - \mu\mathbf{R})\overline{\mathbf{f}}(k) + \mu\mathbf{R}\mathbf{f}_{\text{conv}} \tag{4.30}$$

The coefficient error $\Delta\overline{\mathbf{f}}(k)$ is defined as

$$\Delta\overline{\mathbf{f}}(k) = \overline{\mathbf{f}}(k) - \mathbf{f}_{\text{conv}} \tag{4.31}$$

Inserting Eq. (4.30) into Eq. (4.31) gives

$$\begin{aligned} \Delta\overline{\mathbf{f}}(k) &= (\mathbf{I} - \mu\mathbf{R})\overline{\mathbf{f}}(k-1) + \mu\mathbf{R}\mathbf{f}_{\text{conv}} - \mathbf{f}_{\text{conv}} && (4.32)\\ &= (\mathbf{I} - \mu\mathbf{R})(\overline{\mathbf{f}}(k-1) - \mathbf{f}_{\text{conv}}) && (4.33)\\ &= (\mathbf{I} - \mu\mathbf{R})\Delta\overline{\mathbf{f}}(k-1) && (4.34) \end{aligned}$$

Since $\mathbf{R} = \mathbf{R}^H$, the matrix is hermitian and can be factorized using the eigenvalue decomposition $\mathbf{R}_{xx} = \mathbf{V}\boldsymbol{\Lambda}\mathbf{V}^H$ (the spectral theorem) with orthogonal eigenvector matrix $\mathbf{V}$ and diagonal matrix $\boldsymbol{\Lambda}$ with real eigenvalues on the main diagonal. Using the eigenvalue decomposition and the fact that $\mathbf{V}\mathbf{V}^H = \mathbf{I}$, yields

$$\begin{aligned} \Delta\overline{\mathbf{f}}(k) &= (\mathbf{V}\mathbf{V}^H - \mu\mathbf{V}\boldsymbol{\Lambda}\mathbf{V}^H)\Delta\overline{\mathbf{f}}(k-1) && (4.35)\\ &= \mathbf{V}(\mathbf{I} - \mu\boldsymbol{\Lambda})\mathbf{V}^H\Delta\overline{\mathbf{f}}(k-1) && (4.36) \end{aligned}$$

A modal coefficient error vector is introduced $\Delta\overline{\mathbf{f}}'(n) = \mathbf{V}^H\Delta\overline{\mathbf{f}}(n)$ which yields

$$\Delta\overline{\mathbf{f}}'(k) = (\mathbf{I} - \mu\boldsymbol{\Lambda})\Delta\overline{\mathbf{f}}'(k-1) \tag{4.37}$$

With an initial modal coefficient error vector $\Delta\mathbf{f}'(0)$

$$\Delta\overline{\mathbf{f}}'(k) = (\mathbf{I} - \mu\boldsymbol{\Lambda})^k\Delta\mathbf{f}'(0) \tag{4.38}$$

Since $(\mathbf{I} - \mu\mathbf{\Lambda})$ is a diagonal matrix, the elements of $\Delta\overline{\mathbf{f}}'(k)$ can be expressed as

$$\Delta\overline{f}_i'(n) = (1 - \mu\lambda_i)^k \Delta f_i(0), \quad i = 0, \ldots, L_f - 1. \tag{4.39}$$

In order for $\overline{\mathbf{f}}(n)$ to converge to $\mathbf{f}_{\text{conv}}$, $\Delta\overline{\mathbf{f}}(n)$ should converge to zero and therefore $\Delta\overline{\mathbf{f}}'(n)$ should converge to zero. This will occur if and only if

$$|1 - \mu\lambda_i| < 1, \quad \forall i. \tag{4.40}$$

Therefore the step-size is restricted by

$$0 < \mu < \frac{2}{\lambda_{\text{max}}} \tag{4.41}$$

and λ_{max} is the maximum eigenvalue of matrix $\mathbf{R}$ in Eq. (4.26).

4.2.2 Convergence Analysis of the Closed Loop Configuration

For the closed loop configuration, the mean subband gradient vectors are given by

$$\overline{\boldsymbol{\nabla}}_m(k) = -2E\{\tilde{\mathbf{x}}_m^*(kD)\mathbf{e}^T(kD)\}\mathbf{h}_m \tag{4.42}$$

Inserting the fullband error signal vector $\mathbf{e}(n) = \mathbf{d}(n) - \mathbf{y}(n)$ yields

$$\begin{aligned} \overline{\boldsymbol{\nabla}}_m(k) &= -2E\{\tilde{\mathbf{x}}_m^*(kD)(\mathbf{d}^T(kD) - \mathbf{y}^T(kD))\}\mathbf{h}_m & (4.43)\\ &= -2E\{\tilde{\mathbf{x}}_m^*(kD)\mathbf{d}^T(kD)\}\mathbf{h}_m + 2E\{\tilde{\mathbf{x}}_m^*(kD)\mathbf{y}^T(kD)\}\mathbf{h}_m & (4.44) \end{aligned}$$

Using $\mathbf{d}^T(kD)\mathbf{h}_m = d_m(k)$ from Eq. (2.88) and $\mathbf{y}^T(kD)\mathbf{h}_m = \tilde{\mathbf{x}}_m^T(kD)\mathbf{f}(k)$ from Eq. (2.87), and assuming that the adaptive filter coefficients $\mathbf{f}(k)$ and the input signal samples from $\tilde{x}(k)$ are statistically independent yields

$$\overline{\boldsymbol{\nabla}}_m(k) = -2E\{\tilde{\mathbf{x}}_m^*(kD)d_m(k)\} + 2E\{\tilde{\mathbf{x}}_m^*(kD)\tilde{\mathbf{x}}_m^T(kD)\}\overline{\mathbf{f}}(k). \tag{4.45}$$

Inserting Eq. (4.23) and Eq. (4.24) leads to

$$\overline{\boldsymbol{\nabla}}_m(k) = -2\tilde{\mathbf{r}}_m + 2\tilde{\tilde{\mathbf{R}}}_m\overline{\mathbf{f}}(k). \tag{4.46}$$

When comparing Eq. (4.46) with Eq. (4.25), it can be concluded that the convergence behavior for the open loop and closed loop configurations is the same.

4.3 Simulation Results

4.3.1 Open Loop Delayless Polyphase Subband Adaptive Filter

In this section the convergence in the mean of a simple open loop delayless polyphase subband adaptive filter is studied and compared with averages of real simulations. All

settings are the same as in Chapter 2.4.1.

Fig. 4.5 shows the evolution of the MSE as a function of time. The MSE is found by using the coefficient update in Eq. (4.30). Also averages of the squared error over 10, 100 and 1000 runs are plotted using the coefficient update according to Eq. (4.16) with simulated signals. It can be seen that the adaptive algorithm has a larger excess mean square error compared with the algorithm in Chapter 2.4.2. The following consecutive figures, Figs. 4.6, 4.7 and 4.8 show the corresponding evolution of the coefficients, the coefficient errors and the modal coefficient errors. Clearly from Fig. 4.7 it can be seen that the coefficient errors decay to zero.

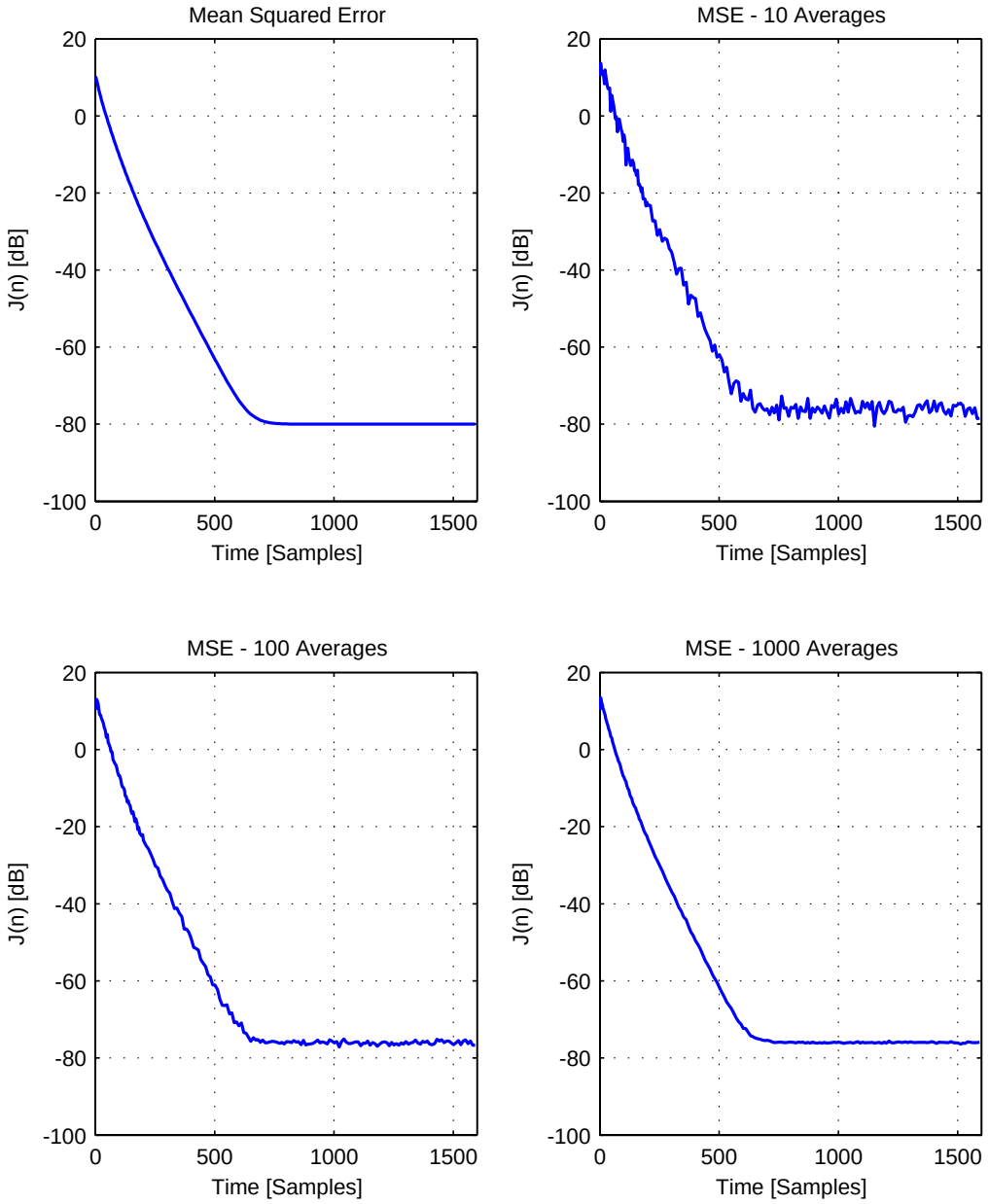

Figure 4.5: *Decay of the mean square error $J(k)$ for the open loop delayless polyphase subband adaptive filter.*

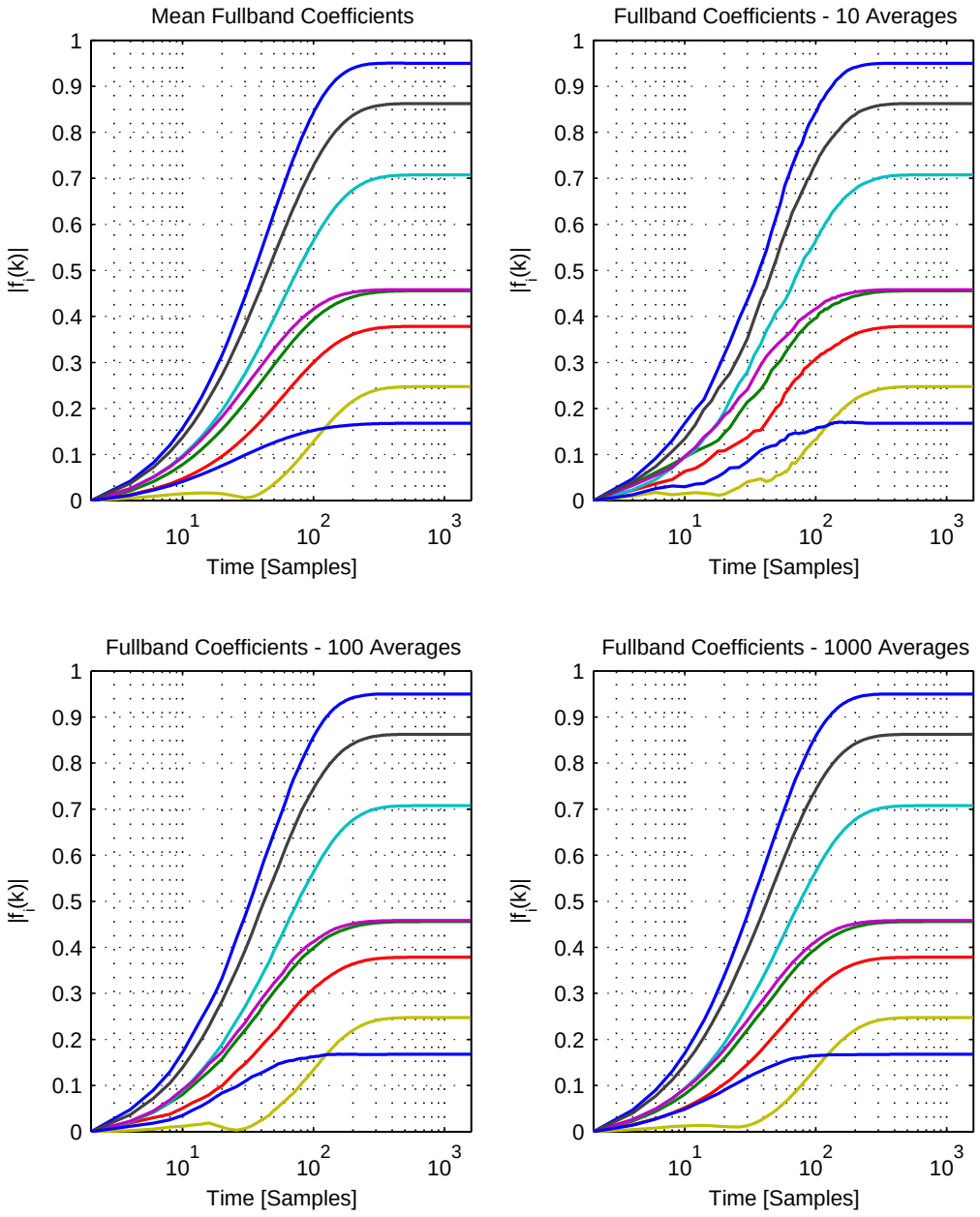

Figure 4.6: *Magnitude of the fullband filter coefficients* $|\overline{f_i}(k)|$ *for the open loop delayless polyphase subband adaptive filter.*

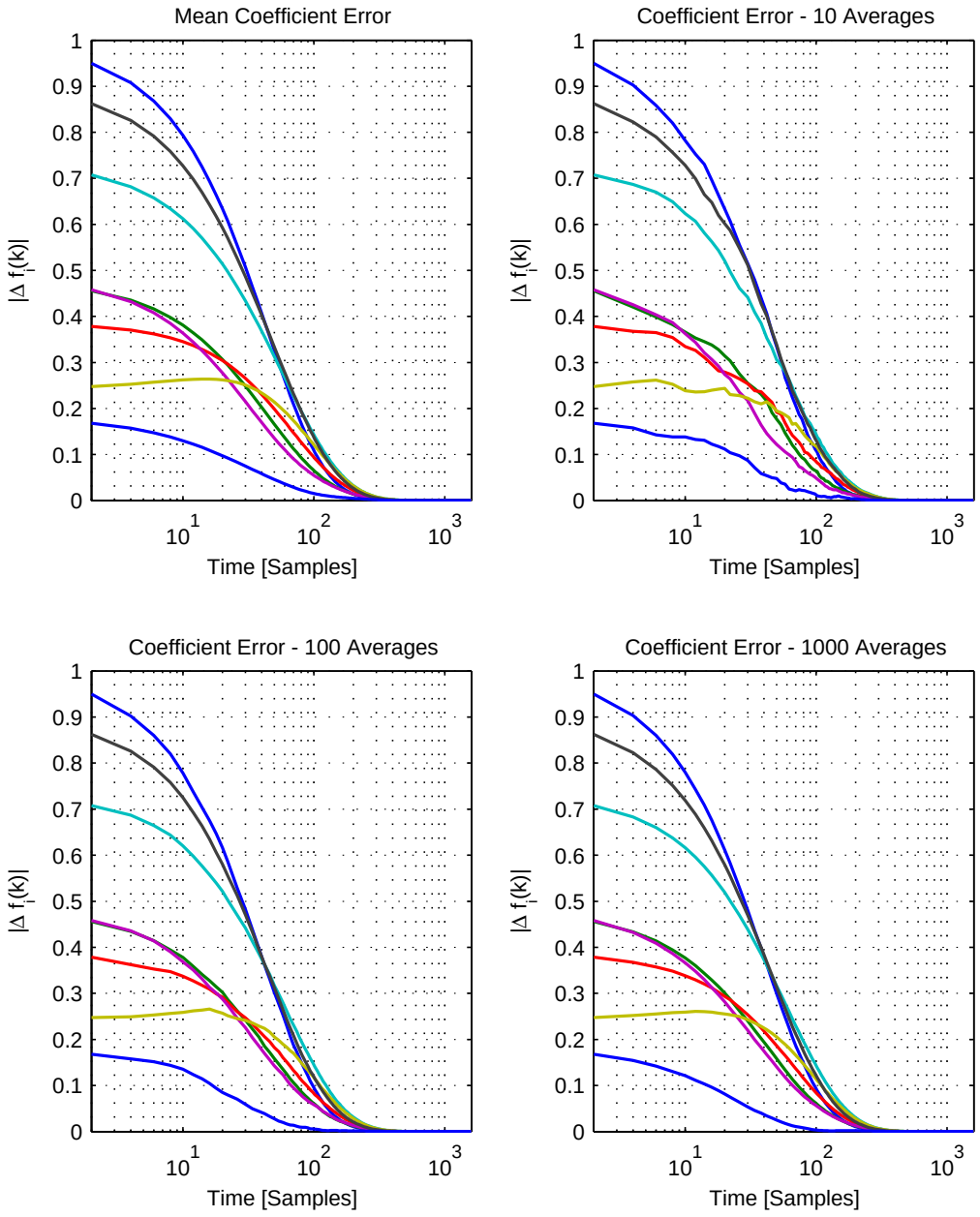

Figure 4.7: *Magnitude of the coefficient errors* $|\Delta\overline{f}_i(k)|$ *for the open loop delayless polyphase subband adaptive filter.*

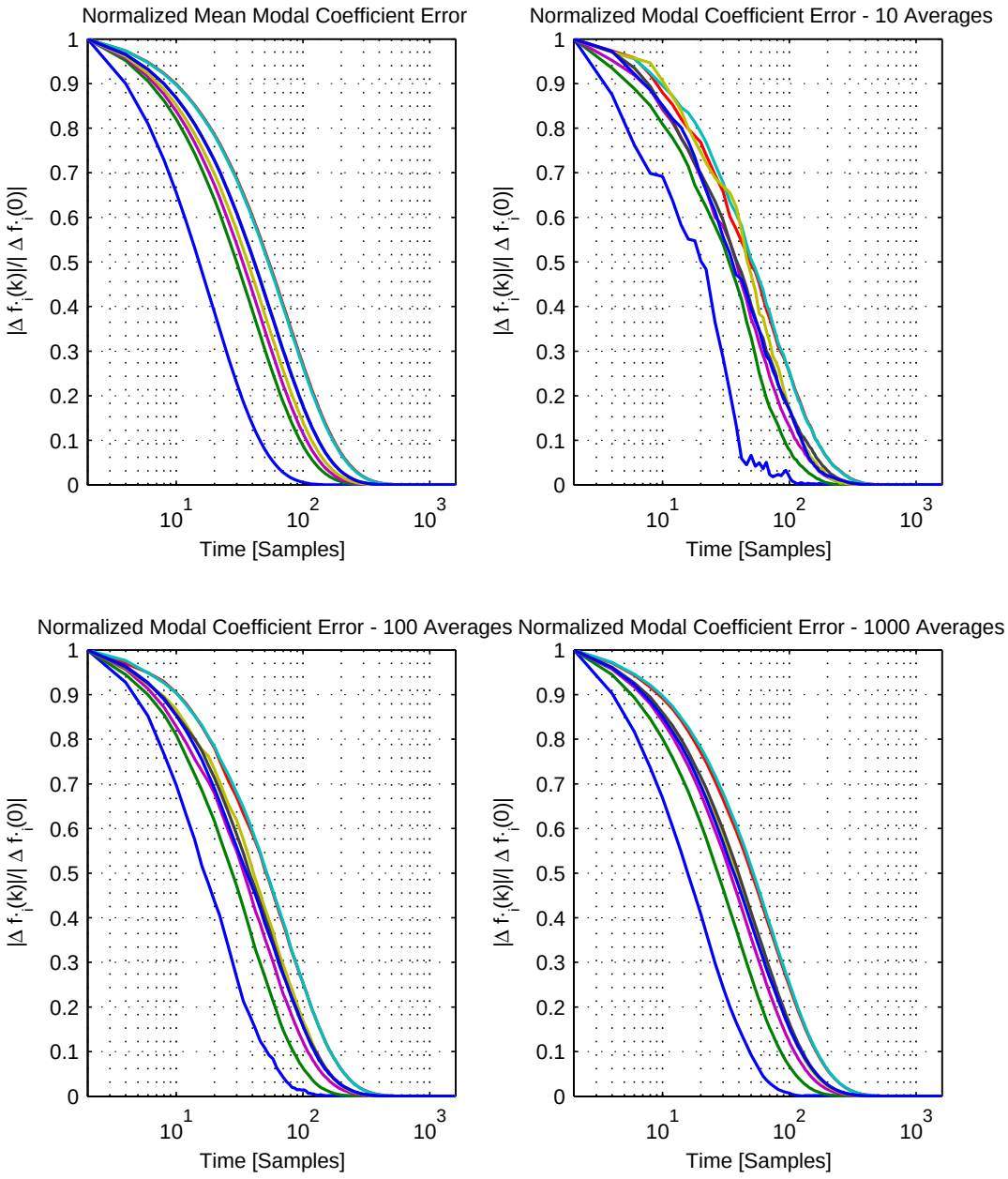

Figure 4.8: *Magnitude of the modal coefficient errors* $|\Delta \overline{f_i}'(k)|/|\Delta f_i'(0)|$ *for the open loop delayless polyphase subband adaptive filter.*

4.3.2 Closed Loop Delayless Polyphase Subband Adaptive Filter

In this section the convergence in the mean of a simple closed loop delayless polyphase subband adaptive filter is studied and compared with averages of real simulations. It is verified that the convergence properties in the mean of the open loop delayless polyphase subband adaptive filter and the closed loop delayless polyphase subband adaptive filter are the same. The parameter settings are the same as in Chapter 2.4.1.

Fig. 4.5 shows the evolution of the MSE as a function of time. The MSE is found by using the coefficient update in Eq. (4.30). Also averages of the squared error over 10, 100 and 1000 runs are plotted using the coefficient update according Eq. (4.16) with simulated signals. Also in this case, it can be observed that the adaptive algorithm has a larger excess mean square error compared with the algorithm in Chapter 2.4.2. The following consecutive figures, Figs. 4.10, 4.11 and 4.12 show the corresponding evolution of the coefficients, the coefficient errors and the modal coefficient errors. Comparing the figures from this scenario with Figs. 4.5, 4.6, 4.7 and 4.8, for the open loop configuration in Chapter 4.3.1, it is confirmed that the open loop and closed loop configurations have the same convergence properties.

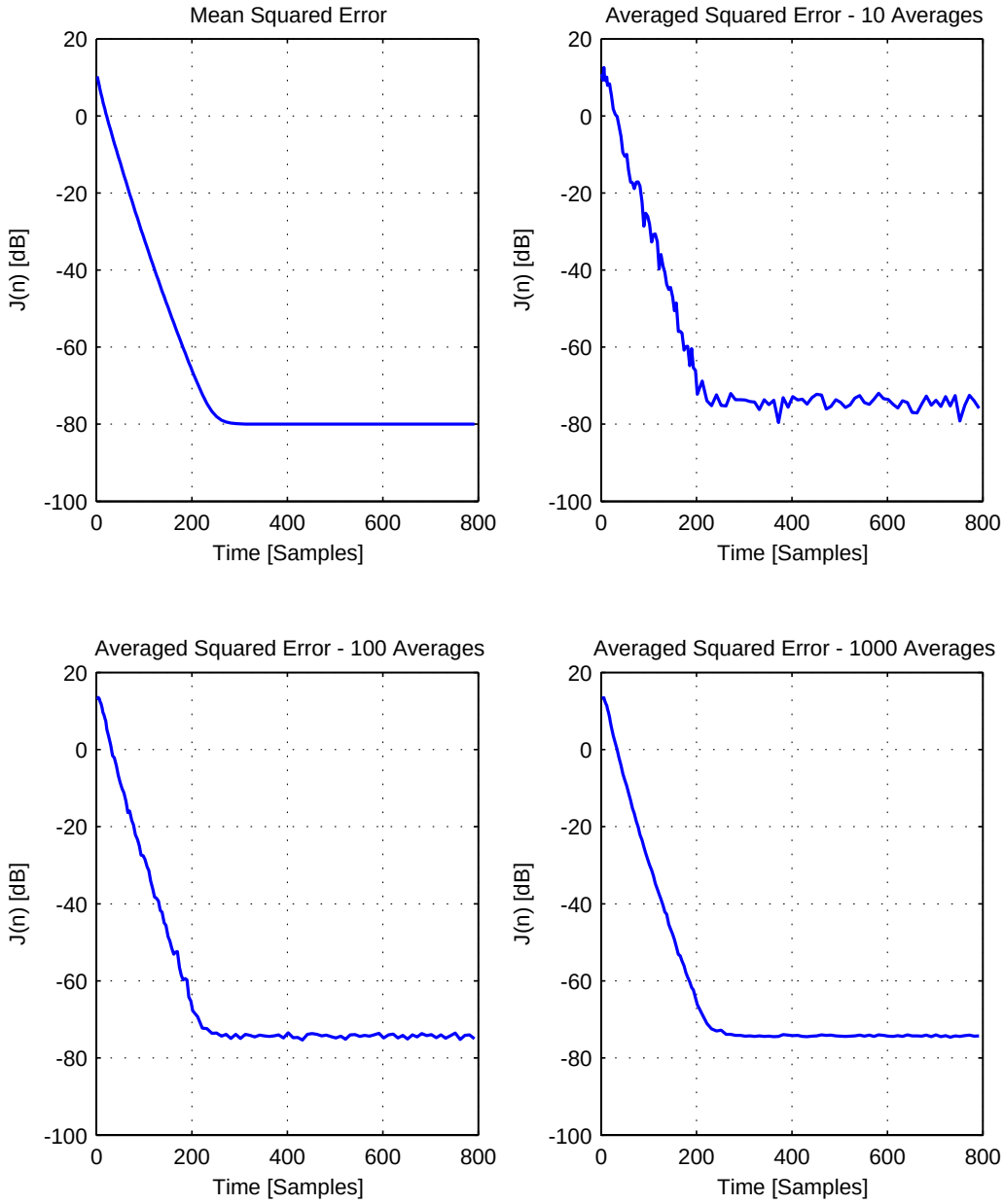

Figure 4.9: *Decay of the Mean Square Error $J(k)$ for the closed loop delayless sub-band adaptive filter.*

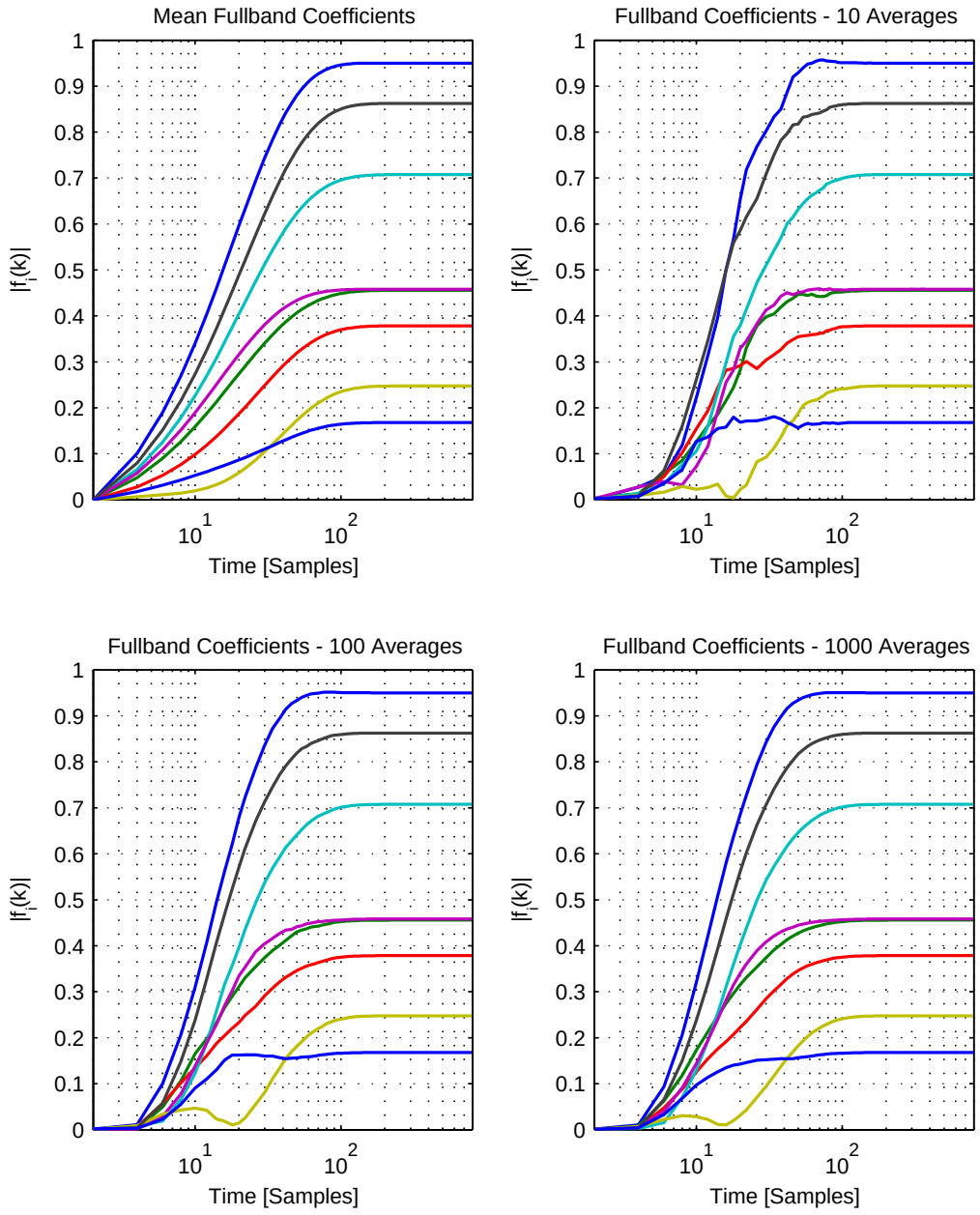

Figure 4.10: *Magnitude of the fullband filter coefficients* $|\overline{f_i}(k)|$ *for the closed loop delayless subband adaptive filter.*

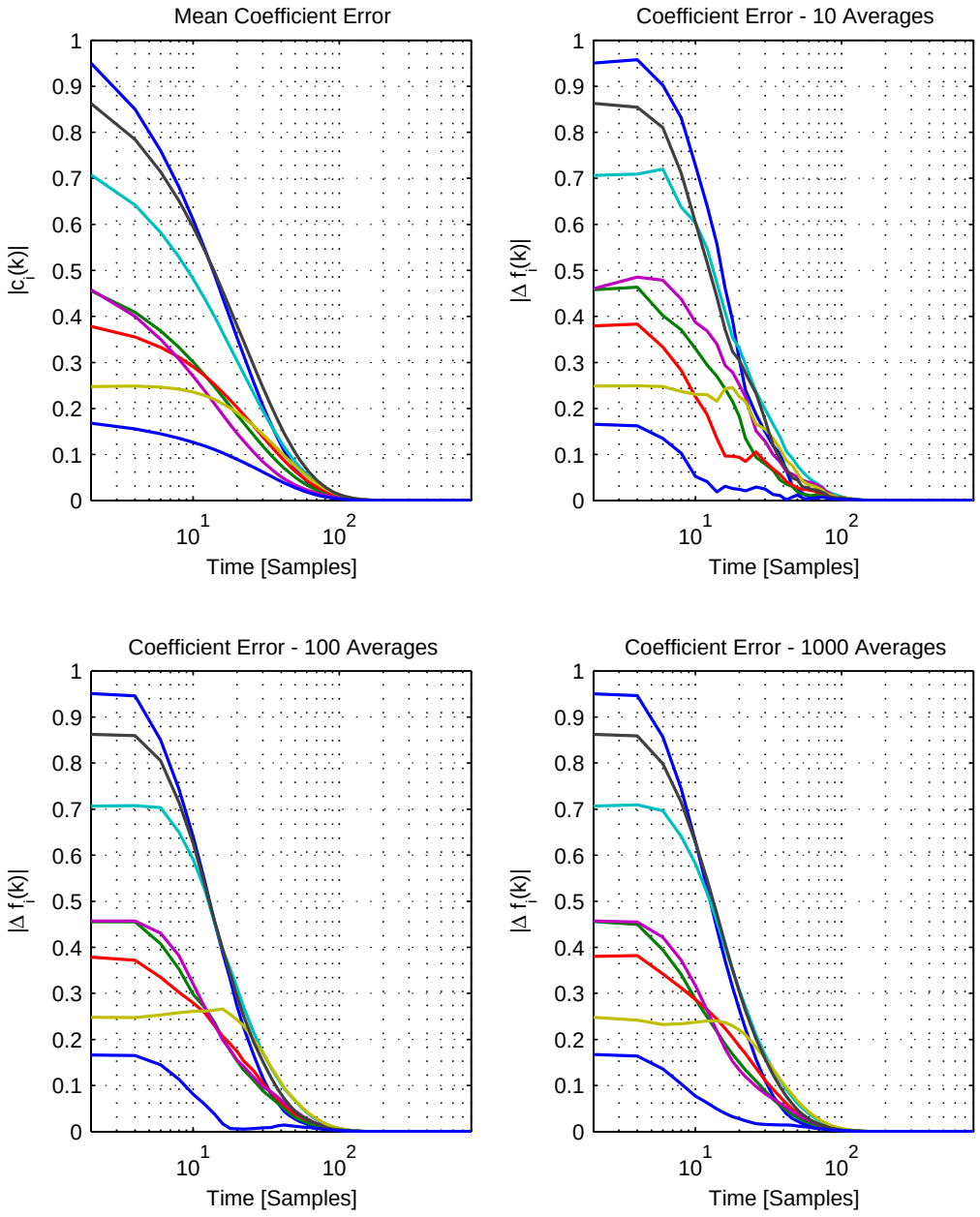

Figure 4.11: *Magnitude of the coefficient errors* $|\Delta\overline{f_i}(k)|$ *for the closed loop delayless subband adaptive filter.*

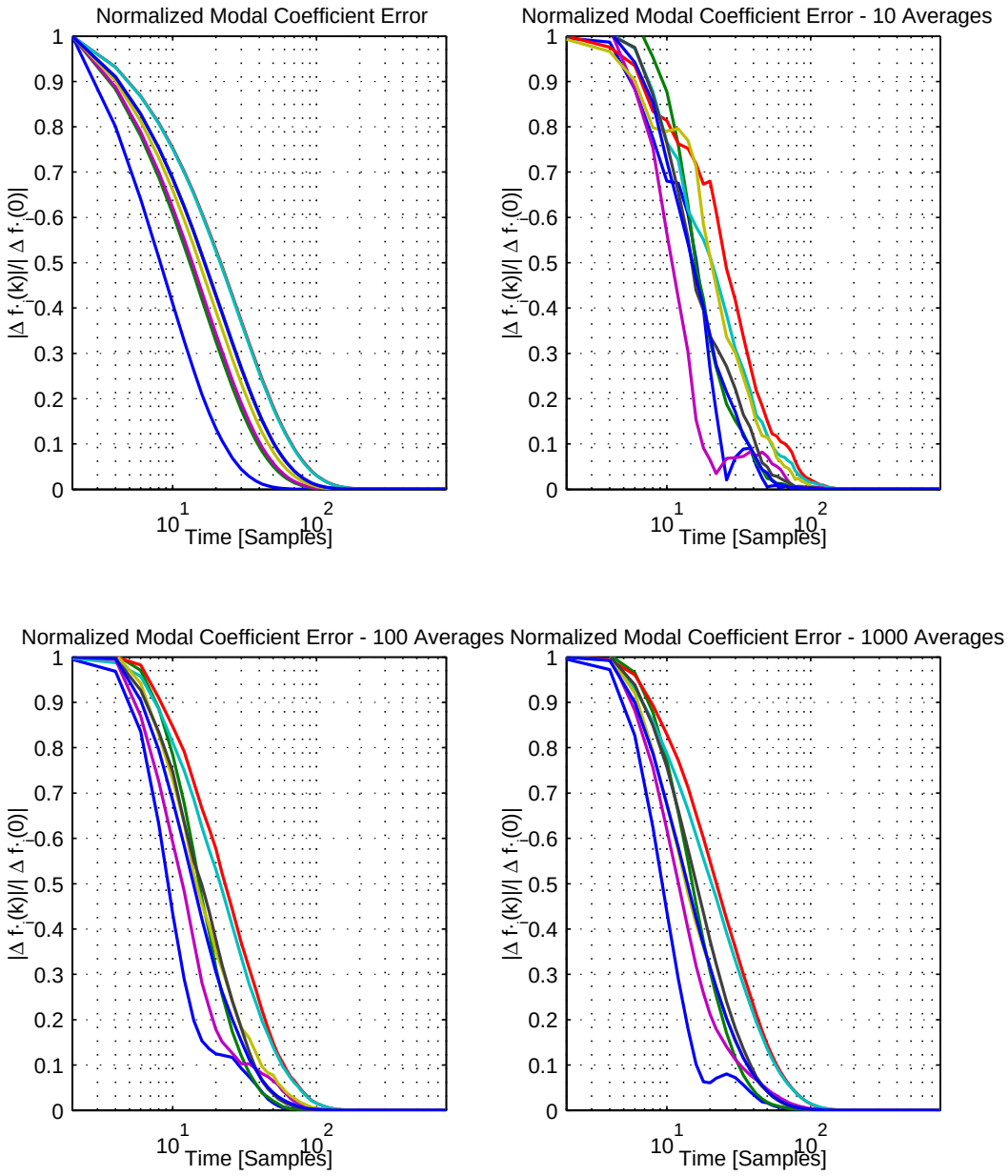

Figure 4.12: *Magnitude of the modal coefficient errors* $|\Delta\overline{f_i}'(k)|/|\Delta f_i'(0)|$ *for the closed loop delayless subband adaptive filter.*

Chapter 5

Convergence Speed Comparison

In this section, the convergence speed of all delayless subband adaptive filtering algorithms is compared. The convergence time can be measured by calculating a time constant based on the eigenvalues from the convergence analysis. The time constant τ_i is the time required for the k-th natural mode to reach $1/e$ of its value

$$(1 - \mu\lambda_i)^{\tau_i} = 1/e \tag{5.1}$$

Taking the natural logarithm on both sides yields

$$\tau_i = \frac{-1}{\ln(1 - \mu\lambda_i)}. \tag{5.2}$$

since μ is set such that $|1 - \mu\lambda_k| < 1$, then the largest time constant τ_{max}, which is related to the slowest mode and therefore important for the overall convergence behavior, is due to the eigenvalue for which the quantity $|1 - \mu\lambda_i|$ is closest to unity. The maximum convergence speed is obtained when $\mu = 1/\lambda_{\text{max}}$. The corresponding time constant for the fastest mode is then equal to zero. The minimum eigenvalue corresponds to slowest converging mode. It should be noted that the time constant unit is related to the update rate of the adaptive coefficients and must be multiplied with D to relate it to the fullband sampling rate.

In this comparison, the largest time constant corresponding to slowest mode, is compared for different delayless subband adaptive filters with number of subbands $M = 4, 8, 16, 32$ and fullband filter length $L_f \leq 256$. The scenario is the system identification scenario as in the previous sections, see Chapter 2.4.1. A time constant ratio τ/τ_{LMS} relative to the LMS adaptive filter is calculated.

5.1 Open Loop Delayless Subband Adaptive Filter

The largest time constants and time constant ratios are plotted in Fig. 5.1. As concluded earlier, the coefficient transform does not influence these results. The step size is set at, $\mu = 1/\lambda_{\text{max}}$. It can be observed that for scenarios with a large number of fullband filter coefficients, the slowest mode of the LMS adaptive filter is slower than the slowest mode of the delayless subband adaptive filter. This is not necessarily the case with only few filter coefficients. It can also be seen that a distinct improvement is obtained when the number of subbands is increased towards $M = 32$. It should be noted that in the open loop case, the slowest mode does not necessarily influence the convergence in terms of the mean square error. It does influence the converge of the subband filter coefficients.

5.2 Closed Loop Delayless Subband Adaptive Filter

The largest time constants for different transform configurations is compared. Also in this comparison, the step size is set at, $\mu = 1/\lambda_{\text{max}}$. The subband-to-fullband transform is the DFT-2 transform. The time constants and time constant ratios are plotted in Fig. 5.2. It can be observed that the closed loop delayless adaptive filter converges faster than the LMS. It can also be observed that the delayless subband adaptive filter with $M = 32$ does not give better performance than the scenario with $M = 16$.

5.3 Open/Closed Loop Delayless Polyphase Subband Adaptive Filter

The largest time constants and time constant ratios for the open/closed loop delayless polyphase subband adaptive filter are plotted in Fig. 5.3. It can be observed that the adaptive filter converges much faster than the conventional closed loop delayless adaptive filters. It can also be observed that an increased number of subbands does not lead to a corresponding improvement of the convergence speed.

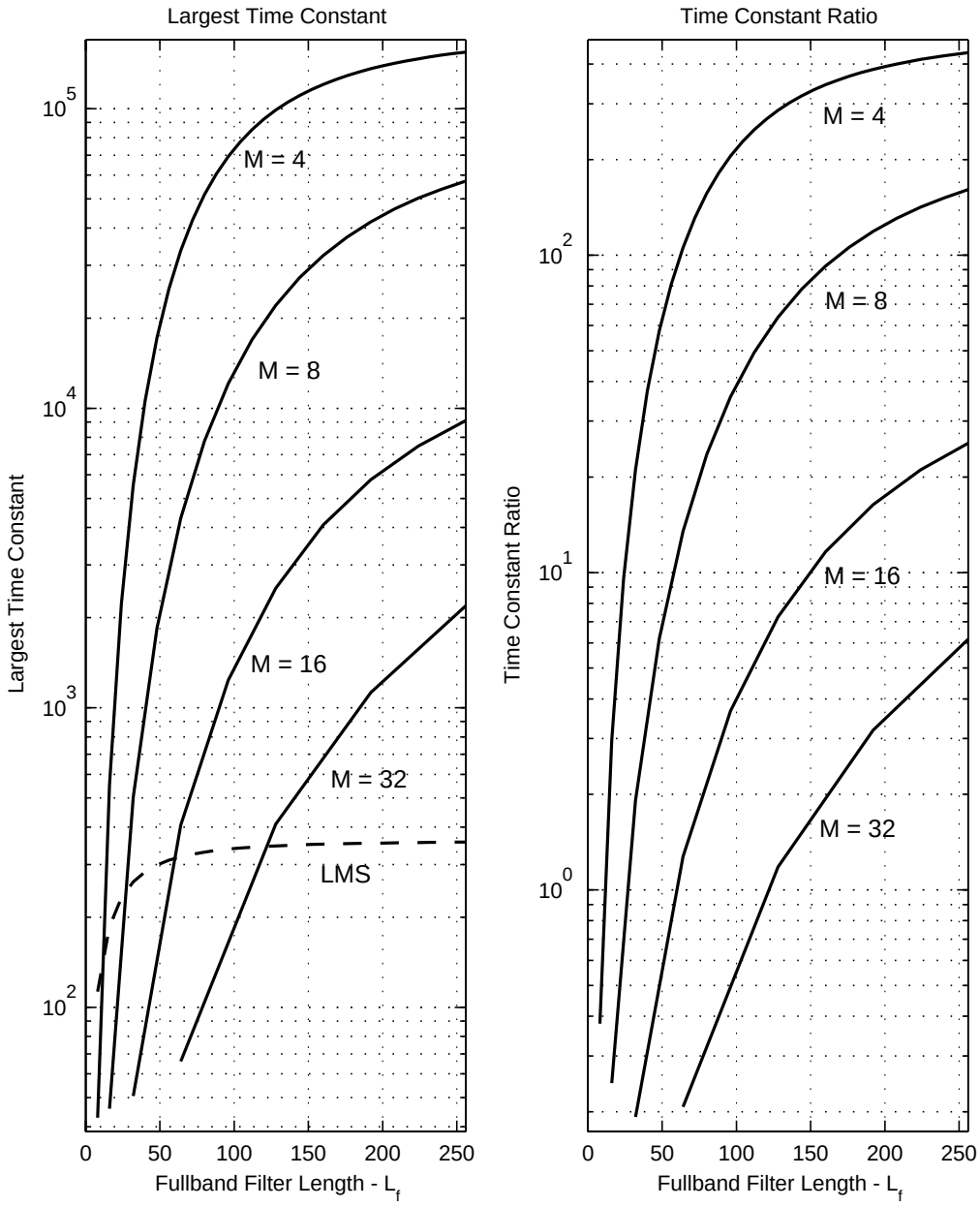

Figure 5.1: *Largest time constant and time constant ratios for an open loop delayless subband adaptive filter as a function of the fullband filter length for different number of subbands.*

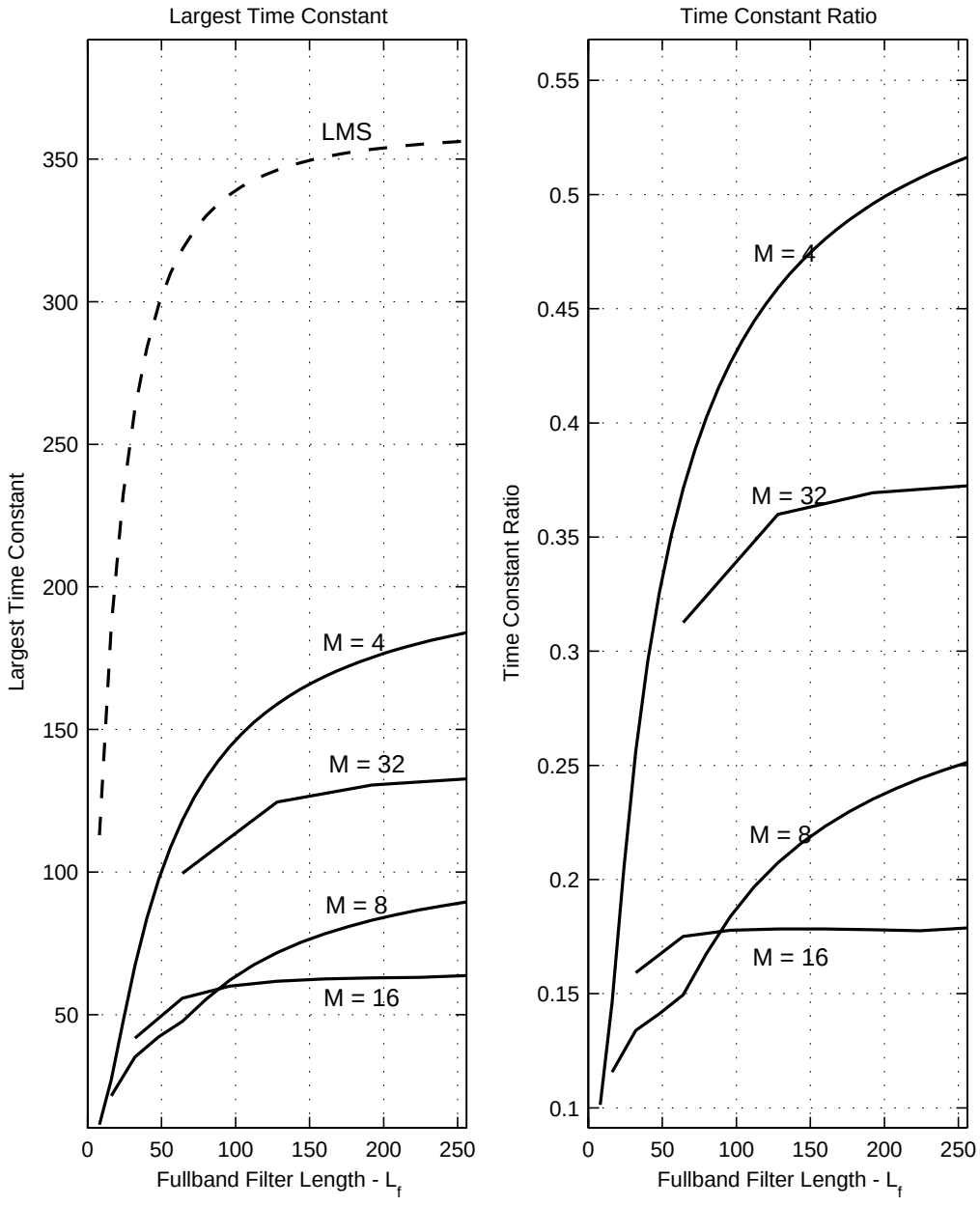

Figure 5.2: *Largest time constant and time constant ratios for an Closed Loop Delayless Subband Adaptive Filter with the DFT-2 transform as a function of the fullband filter length for different number of subbands.*

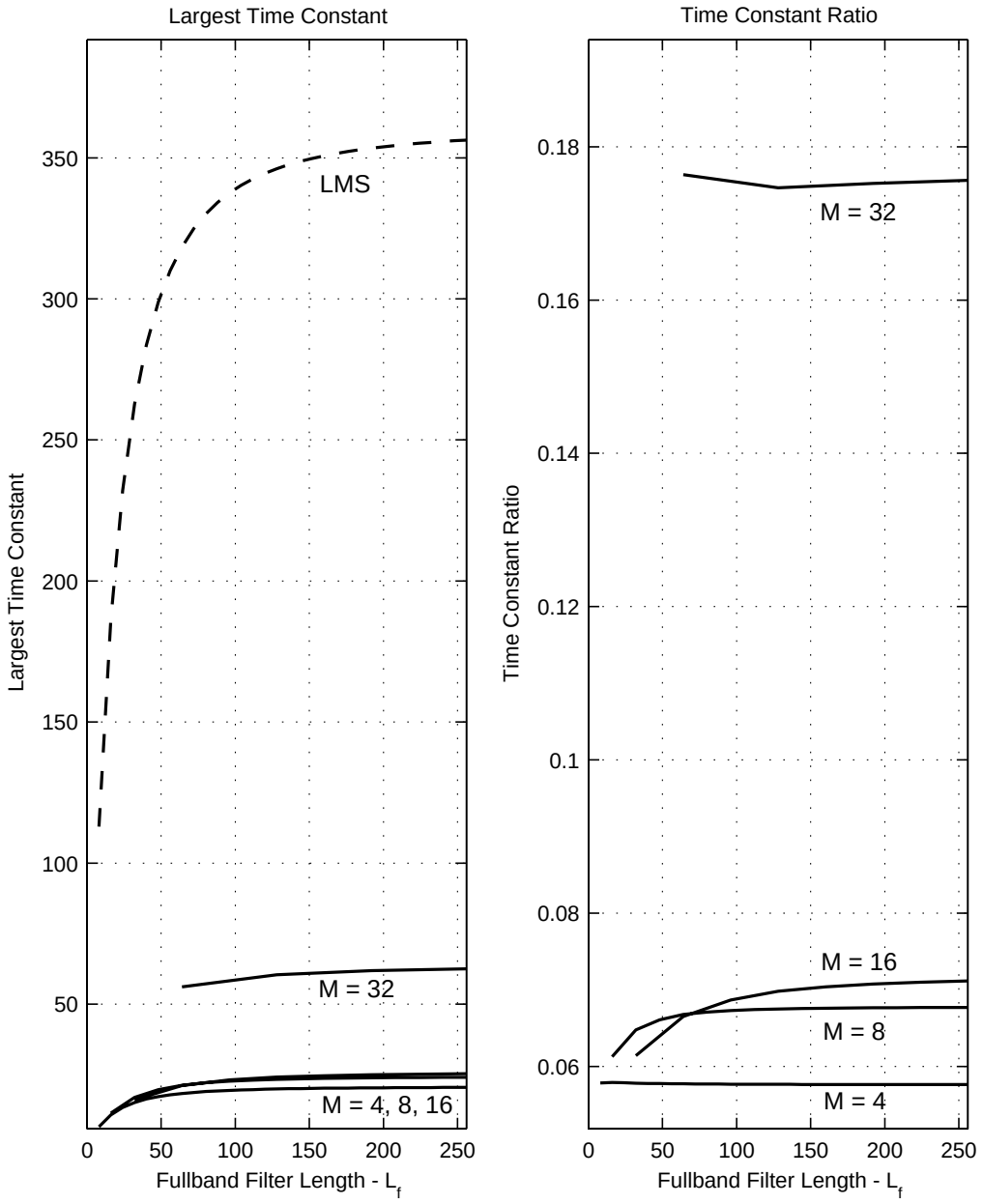

Figure 5.3: *Largest time constant and time constant ratios for an Open Loop/Closed Loop Delayless Polyphase Subband Adaptive Filter as a function of the fullband filter length for different number of subbands.*

Chapter 6

Complexity Comparison

In this section a comparison of the computational complexity of the different algorithms is given. Different implementations of signal processing algorithms require different definitions of ”computational cost”. For the sake of simplicity the computational complexity comparison is given in terms of the number of multiplications.

6.1 Efficient Fullband Filter Implementation

The fullband filter $\mathbf{f}(k)$ can be implemented efficiently using a delayless partitioned block frequency domain implementation. In this implementation, the fullband filter $\mathbf{f}(k)$ is partitioned into B sub-filters of length $K = L_f/B$,

$$f_i^{(b)}(k) = f_{i+bK}(k),\ i = 0, \ldots, K-1,\ b = 0, \ldots, B-1, \tag{6.1}$$

where i is a coefficient index and b is a block index. See Fig. 6.1 a). The sub-filters $f^{(b)}$, $b = 1, \ldots, B-1$ are implemented using efficient *overlap-add* or *overlap-save* block-wise filtering, which is depicted in Fig. 6.1 c).

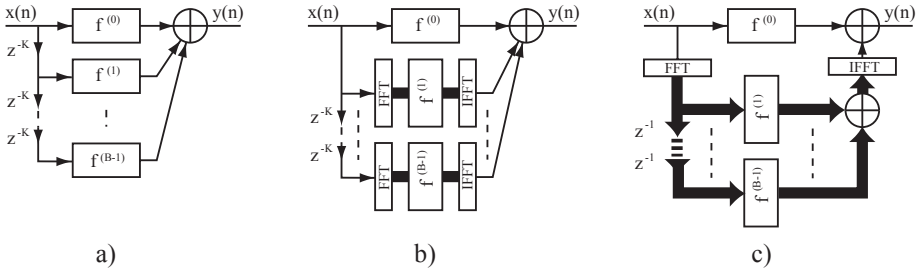

Figure 6.1: *Efficient Partitioned Block Filtering Implementation.* **a)** *Partitioned filtering with B sub-filters of length K.* **b)** *Partitioned filtering using overlap-save or overlap-add frequency domain block filtering for all but the first sub-filter.* **c)** *same as b) but now reduced in complexity by computing the FFT and IFFT only once for all sub-filters.*

The first sub-filter $f^{(0)}$ is still implemented in the time-domain to ensure delayless filtering. The size of the FFT and IFFT is $2K$ and the update rate of the coefficients is K lower than the full rate. Note that the coefficients need to be transformed to the FFT domain from the fullband domain. Hence the block size needs to be set at $K = D$ to ensure that the performance of the adaptive filter is not affected.

The complexity of the first sub-filter is K multiplications per sample. The complexity

of the FFT and IFFT is $4\log_2(2K)$ multiplications per sample since they are performed at once every K-th sample. The other $B-1$ sub-filters require $2(B-1)$ multiplications per sample. The FFT transforms, which are necessary to calculate the FFT coefficients, give an additional cost of $2(B-1)\log_2(2K)$. Hence the total cost for the filtering operation is

$$\begin{aligned} \mathcal{C}_{\text{FBF}}(L_f, B) &= L_f/B + (2+2B)\log_2(2L_f/B) + 2(B-1) && (6.2)\\ &= L_f/B + (2+2B)\log_2(L_f/B) + 4B && (6.3)\end{aligned}$$

With $K = D$, this yields

$$\mathcal{C}_{\text{FBF}}(L_f, B) = D + (2 + 2L_f/D)\log_2(D) + 4L_f/D. \tag{6.4}$$

With a cost of L_f multiplications per sample for the fullband filter implemented in direct-form, the cost improvement (ratio) of the efficient filtering scheme is

$$\mathcal{R}(L_f, B) = L_f/\mathcal{C}(L_f, B) \tag{6.5}$$

6.2 Filter Bank Complexity

6.2.1 Uniform-DFT Filter Banks

The non-decimated filter bank requires L_h multiplications per sample for the polyphase components and $M\log_2 M$ for the IFFT.

$$\mathcal{C}_{\text{UFB}}(L_h, M) = L_h + M\log_2 M. \tag{6.6}$$

The complexity for oversampled analysis uniform-DFT filter banks is L_h/D multiplications per sample in the subband domain for the polyphase components and $\frac{M}{D}\log_2 M$ for the IFFT. Hence the total complexity is

$$\mathcal{C}_{\text{UFBD}}(L_h, M) = L_h/D + (M\log_2 M)/D \tag{6.7}$$

6.2.2 Tree Structured Filter Banks

Using a polyphase implementation of the individual two-channel filter banks, the first filter bank requires L/D multiplications per sample. The filter banks in the next level require L/D^2 multiplications per sample. Continuing with subsequent levels and assuming critical sampling $D = M$, the total cost can be calculated as

$$\mathcal{C}_{\text{TFB}}(L_h, M) = \frac{L_h}{M} + 2\frac{L_h}{M^2} + 4\frac{L_h}{M^4} + \ldots = \sum_{i=0}^{\log_2 M} 2^i \frac{L_h}{M^{2^i}} \tag{6.8}$$

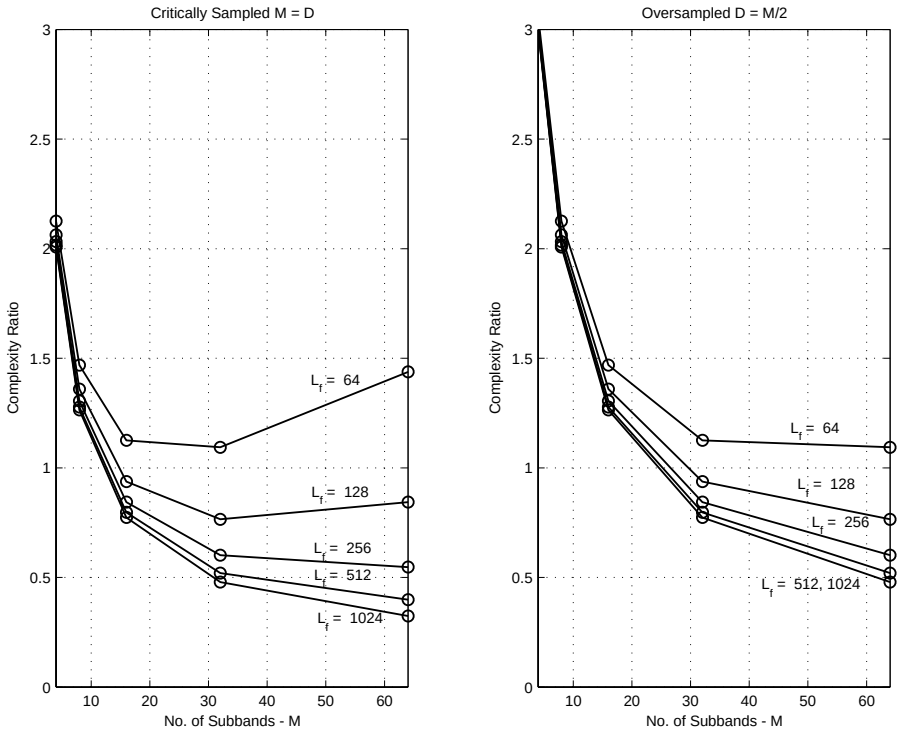

Figure 6.2: *Improvement in computational complexity with the efficient implementation of the fullband filter. The curves show the complexity improvement for fullband filter length* $L_f = 64, 128, 256, 512$ *and* 1024*, with increasing improvement. The left plot shows the improvement when critically sampled filter banks* $K = D = M$ *are used, and the right plot shows the improvement when oversampled filter banks* $K = D = M/2$ *are used.*

6.3 Subband-to-fullband Transform complexity

6.3.1 DFT-1 Transform

The computational complexity for the DFT-1 transform, see Fig. 2.3, is $ML_w \log_2 L_w$ for the FFTs and $L_f \log_2 L_f$ for the IFFT. Since the transform is used only each D-th sample, and $L_w = L_f/D$, the total cost per sample for the DFT-1 transform is given by

$$\mathcal{C}_{\text{DFT-1}} = \frac{ML_f}{D^2} \log_2 \frac{L_f}{D} + \frac{L_f}{D} \log_2 L_f. \tag{6.9}$$

With the oversampled uniform DFT filter bank, where $D = M/2$, the complexity becomes expressed in terms of the fullband filter length L_f and the number of subbands M

$$\mathcal{C}_{\text{DFT-1}} = 4\frac{L_f}{M} \log_2 \frac{2L_f}{M} + 2\frac{L_f}{M} \log_2 L_f. \tag{6.10}$$

6.3.2 DFT-2 Transform

The computational complexity is $2ML_w \log_2(2L_w)$ for the FFTs and $2L_f \log_2(2L_f)$ for the IFFT. The total cost per sample is, the total cost for the DFT-2 transform is given by

$$\mathcal{C}_{\text{DFT-2}} = \frac{2ML_f}{D^2} \log_2 \frac{2L_f}{D} + \frac{2L_f}{D} \log_2 2L_f. \tag{6.11}$$

With the oversampled uniform DFT filter bank, where $D = M/2$, the complexity becomes expressed in terms of the fullband filter length L_f and the number of subbands M

$$\mathcal{C}_{\text{DFT-2}} = 8\frac{L_f}{M} \log_2 \frac{4L_f}{M} + 4\frac{L_f}{M} \log_2 2L_f. \tag{6.12}$$

6.3.3 Hadamard Transform

The total cost for the Hadamard transform in terms of multiplications per sample is zero, although the transforms still require additions. For the sake of simplicity, the cost of additions are neglected in this study.

6.4 Total Algorithm Cost

6.4.1 Open Loop Delayless Subband Adaptive Filter

The computational cost of the open loop delayless subband adaptive filter is based on the cost of two analysis filter banks, the fullband filter, the subband-to-fullband transform, the filtering operations in the subband domain and the subband adaptive algorithm. The adaptive filters require ML_w/D multiplications per sample. The adaptive algorithm also requires ML_w/D multiplications per sample. The time-varying step size with recursively implemented power estimation requires $2M/D$ multiplications per sample. An overview of all computational costs is given in Table. 6.4.1.

Part	DFT-1	DFT-2	Hadamard
Analysis Filter Bank for $x_m(k)$	$\mathcal{C}_{\text{UFBD}}(L, M)$	$\mathcal{C}_{\text{UFBD}}(L, M)$	$\mathcal{C}_{\text{TFB}}(L, M)$
Analysis Filter Bank for $d_m(k)$	$\mathcal{C}_{\text{UFBD}}(L, M)$	$\mathcal{C}_{\text{UFBD}}(L, M)$	$\mathcal{C}_{\text{TFB}}(L, M)$
Adaptive Filters $\mathbf{w}_m$	ML_w/D	ML_w/D	ML_w/D
Adaptive Algorithm $\mathbf{w}_m$	ML_w/D	ML_w/D	ML_w/D
Subband-Fullband Transform $\mathbf{T}$	$\mathcal{C}_{\text{DFT-1}}(M, L_f)$	$\mathcal{C}_{\text{DFT-2}}(M, L_f)$	0
Fullband Filter $\mathbf{f}$	$D + (2 + 2L_f/D)\log_2(D) + 4L_f/D$		
Time Varying Step Size $\mu_m(k)$	4	4	2

Table 6.1: *Computational cost in terms of multiplications per sample for all parts of the open loop delayless subband adaptive filter.*

6.4.2 Closed Loop Delayless Subband Adaptive Filter

The computational cost of the closed loop delayless subband adaptive filter is based on the cost of two analysis filter banks, the fullband filter, the subband-to-fullband transform and the subband adaptive algorithm. The adaptive filtering requires ML_w/D multiplications per sample. The time-varying step size with recursively implemented power estimation requires $2M/D$ multiplications per sample. An overview of all computational costs is given in Table. 6.4.2.

Part	DFT-1	DFT-2	Hadamard
Analysis Filter Bank for $x_m(k)$	$\mathcal{C}_{\text{UFBD}}(L, M)$	$\mathcal{C}_{\text{UFBD}}(L, M)$	$\mathcal{C}_{\text{TFB}}(L, M)$
Analysis Filter Bank for $e_m(k)$	$\mathcal{C}_{\text{UFBD}}(L, M)$	$\mathcal{C}_{\text{UFBD}}(L, M)$	$\mathcal{C}_{\text{TFB}}(L, M)$
Adaptive Algorithm $\mathbf{w}_m$	ML_w/D	ML_w/D	ML_w/D
Subband-Fullband Transform $\mathbf{T}$	$\mathcal{C}_{\text{DFT-1}}(M, L_f)$	$\mathcal{C}_{\text{DFT-2}}(M, L_f)$	0
Fullband Filter $\mathbf{f}$	$D + (2 + 2L_f/D)\log_2(D) + 4L_f/D$		
Time Varying Step Size $\mu_m(k)$	4	4	2

Table 6.2: *Computational cost in terms of multiplications per sample for all parts of the closed loop delayless subband adaptive filter.*

6.4.3 Discussion on Complexity of Conventional Delayless Subband Adaptive Filters

A comparison of computational costs for the conventional delayless subband adaptive filter is given in Fig. 6.3 and Fig. 6.4. Comparing both figures, it can be seen that the open loop case is more costly, due to the filtering operations in the subband domain.

Comparing the cost for different configurations, it can be seen that for the DFT-1 and DFT-2 configurations, the complexity ratio is increasing as the fullband filter length is increased. This is not the case for the Hadamard configuration, where it is decreasing as the fullband filter length is increased. It can also be seen that a low number of subbands gives more cost than the LMS for the DFT-1/2 configurations. The Hadamard configurations with $M = 4$ is approximately as costly as the LMS. Increasing the number of subbands in all cases yields lower cost.

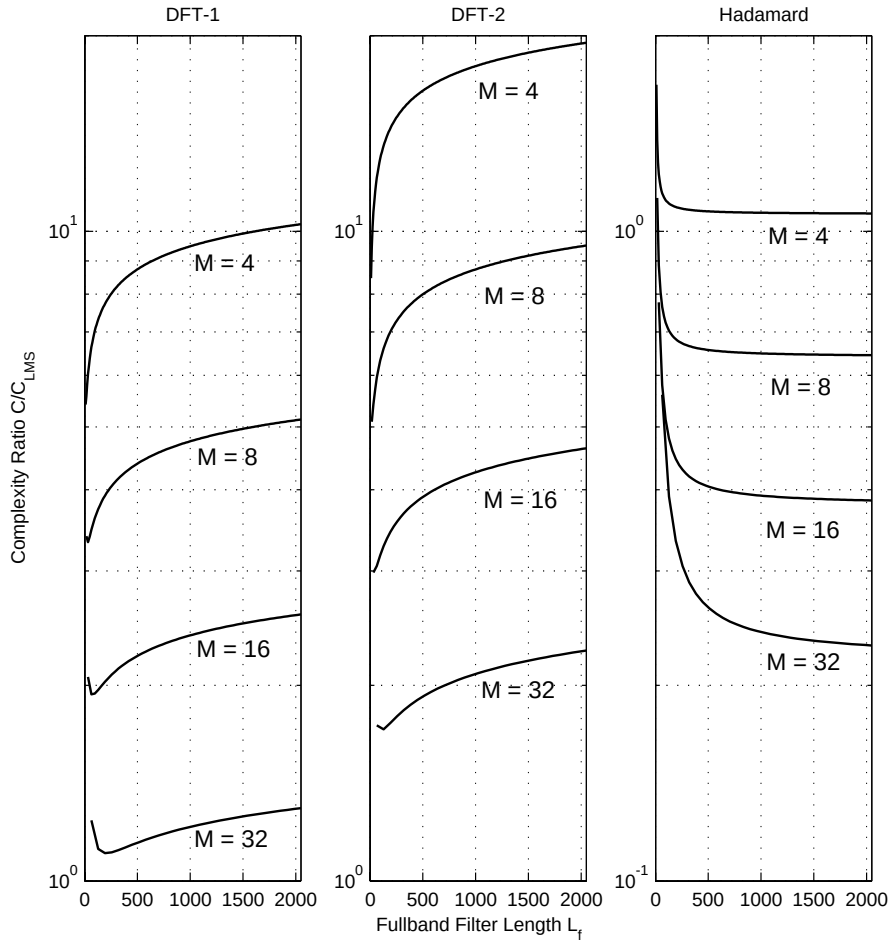

Figure 6.3: *Complexity ratio for open loop delayless subband adaptive filters. From left to right: DFT-1, DFT-2 and Hadamard*

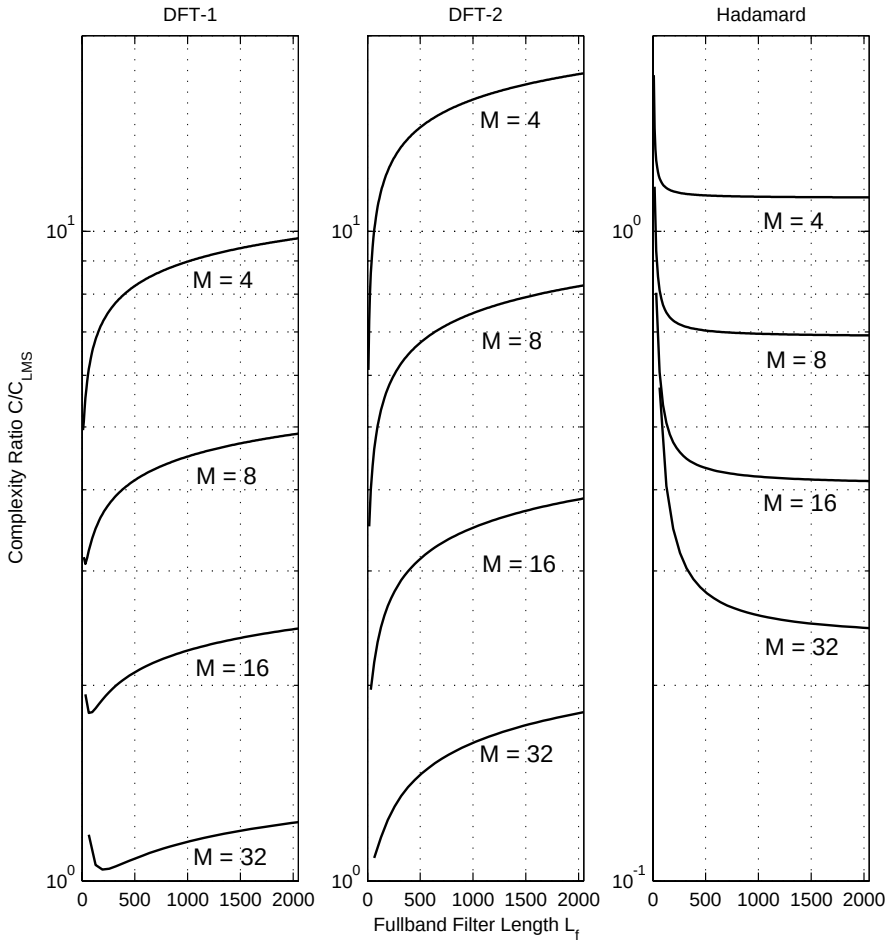

Figure 6.4: *Complexity ratio for closed loop delayless subband adaptive filters. From left to right: DFT-1, DFT-2 and Hadamard*

6.4.4 Open Loop Delayless Polyphase Subband Adaptive Filter

The computational cost of the closed loop delayless subband adaptive filter is based on the cost of two analysis filter banks (of which one is non-decimated), the fullband filter, the subband-to-fullband transform and the subband adaptive algorithm. The adaptive filtering requires ML_w/D multiplications per sample. The time-varying step size with recursively implemented power estimation requires $2M/D$ multiplications per sample.

Part	Open loop delayless polyphase subband adaptive filter
Analysis Filter Bank for $x_m(k)$	$\mathcal{C}_{\text{UFB}}(L_h, M)$
Analysis Filter Bank for $d_m(k)$	$\mathcal{C}_{\text{UFBD}}(L_h, M)$
Adaptive Filters $\mathbf{w}_m$	ML_w/D
Adaptive Algorithm $\mathbf{w}_m$	ML_w/D
Fullband Filter $\mathbf{f}$	$D + (2 + 2L_f/D)\log_2(D) + 4L_f/D$
Time Varying Step Size $\mu_m(k)$	$2M/D$

Table 6.3: *Computational cost in terms of multiplications per sample for all parts of the open loop delayless polyphase subband adaptive filter.*

6.4.5 Closed Loop Delayless Polyphase Subband Adaptive Filter

The computational cost of the closed loop delayless subband adaptive filter is based on the cost of two analysis filter banks (of which one is non-decimated), the fullband filter, the subband-to-fullband transform and the subband adaptive algorithm. The adaptive filtering requires ML_w/D multiplications per sample. The time-varying step size with recursively implemented power estimation requires $2M/D$ multiplications per sample.

Part	Closed loop delayless polyphase subband adaptive filter
Analysis Filter Bank for $x_m(k)$	$\mathcal{C}_{\text{UFB}}(L_h, M)$
Analysis Filter Bank for $e_m(k)$	$\mathcal{C}_{\text{UFBD}}(L_h, M)$
Adaptive Algorithm $\mathbf{w}_m$	ML_w/D
Fullband Filter $\mathbf{f}$	$D + (2 + 2L_f/D)\log_2(D) + 4L_f/D$
Time Varying Step Size $\mu_m(k)$	$2M/D$

Table 6.4: *Computational cost in terms of multiplications per sample for all parts of the closed loop delayless polyphase subband adaptive filter.*

6.4.6 Discussion on Complexity of Delayless Polyphase Subband Adaptive Filters

A comparison of computational costs for the open loop and closed loop configurations of the delayless polyphase subband adaptive filter is given in Fig. 6.5. Comparing both

configurations, it can be seen that the open loop case is more costly, due to the filtering operations in the subband domain. The complexity is decreasing as the fullband filter length is decreased, similar to the conventional approach with the Hadamard configuration. Further, increasing the number of subbands yields lower cost.

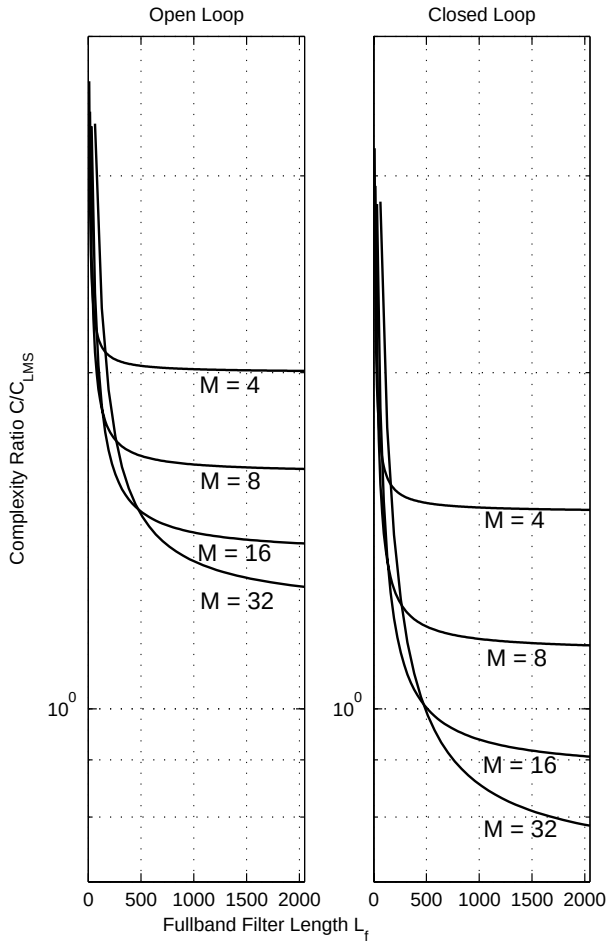

Figure 6.5: *Complexity ratio for open loop and closed loop delayless polyphase subband adaptive filters.*

Chapter 7

Conclusions and Future Research

In this paper, the convergence behavior of the open loop and closed loop configurations of the delayless subband adaptive filters is studied. It is shown that the subband-to-fullband transform greatly affects the performance in terms of the fullband mean square error for the open loop configuration and in terms of the convergence speed for the closed loop configuration. It is shown that based on the results for the closed loop case, a transform with optimal convergence performance can be derived. A novel delayless subband adaptive filter is presented, which employs polyphase adaptive filters.

The convergence and complexity analysis in this report give the following results

- The conventional open loop delayless subband adaptive filter has limited performance in terms of the fullband mean square error. However, the performance may be sufficient for the application at hand and the convergence speed may be high.
- The conventional closed loop delayless subband adaptive filter may reach the same mean square error as the LMS algorithm but may have limited performance in terms of the convergence speed, due to a non-optimal transform. A theoretical expression for the optimal transform is derived. Sub-optimal transforms may be derived using a-priori knowledge about the input signal.
- An open loop delayless polyphase subband adaptive filter can converge with high speed, using only few subbands. For a certain scenario it is shown that an adaptive filter with approximately 1000 taps can be adapted using 16 subbands with slightly lower complexity than the LMS algorithm while the convergence speed is higher than the speed of the LMS and the conventional delayless subband adaptive filters.
- The closed loop delayless polyphase subband adaptive filter has the same performance and convergence behavior as the open loop configuration. Since the closed loop configurations does not require filtering operations in the subband domain, the computational cost is lower.

The convergence analysis requires further study in terms of the mean square error and the excess mean square error. This is especially the case for the conventional open loop delayless adaptive filter. It is of importance to study how the different natural modes and their magnitudes influence the decay of the mean square error. As further research, the convergence aspects in practical application will be studied, such as system identification and inverse filtering. The impact of the results will be verified in applications with real signals, such as acoustic echo cancellation and channel equalization in digital communications.

Appendix

Least Mean Square Algorithm

One of the most well-known control algorithm for adaptive filters is the Least Mean Square algorithm [17]. The LMS algorithm can in short be summarized using the equations

$$\begin{aligned} y(n) &= \mathbf{f}^T(n)\mathbf{x}(n) && (7.1)\\ e(n) &= d(n) - y(n) && (7.2)\\ \mathbf{f}(n+1) &= \mathbf{f}(n) + \mu\mathbf{x}^*(n)e(n), && (7.3) \end{aligned}$$

where $\mathbf{f}(n) = [f_0(n), \ldots, f_{L_f-1}(n)]^T$ is a vector with the filter coefficients at time instant n, and L_f denotes the number of filter coefficients. The vector $\mathbf{x}(n) = [x(n), \ldots, x(n-L_f+1)]^T$ is an input signal vector at time instant n, which holds L_f input samples starting with $x(n)$.

The LMS adaptive filter is an adaptive solution to the FIR Wiener filter design problem. The FIR Wiener filter is an optimal filter, which minimizes the Mean-Square Error

$$J = E\{|e(n)|^2\}, \tag{7.4}$$

where $E\{.\}$ is the expectation operator. The Minimum Mean-Square Error and corresponding optimal coefficients found by taking the gradient with respect to the filter coefficients and setting it to zero

$$\nabla E\{|e(n)|^2\} = E\{e(n)\nabla e^*(n)\} = -2E\{e(n)\mathbf{x}^*(n)\} \tag{7.5}$$

Inserting Eqs. (7.1) and (7.2) and setting the gradient to zero yields the system of equations

$$-2E\{d(n)\mathbf{x}^*(n)\} + 2E\{\mathbf{x}^*(n)\mathbf{x}^T(n)\}\mathbf{f} = -2\mathbf{r}_{dx} + 2\mathbf{R}_{xx}\mathbf{f} = \mathbf{0} \tag{7.6}$$

where matrix $\mathbf{R}_{xx} = E\{\mathbf{x}^*(n)\mathbf{x}^T(n)\}$ is the input signal autocorrelation matrix, vector $\mathbf{r}_{dx} = E\{d(n)\mathbf{x}^*(n)\}$ is a cross-correlation vector. Solving Eq. (7.6) leads to the optimal Wiener filter

$$\mathbf{f}_{\text{Wiener}} = \mathbf{R}_{xx}^{-1}\mathbf{r}_{dx} \tag{7.7}$$

The coefficients of the adaptive LMS algorithm are updated using an instantaneous estimate of the gradient.

Convergence in the Mean

In this section, the theoretic analysis of the convergence of the adaptive LMS filter in the mean is briefly described. It is shown that the convergence speed of the adaptive filter is dependent on the properties of the input correlation matrix [17]. Substituting Eqs. (7.1) and (7.2) into Eq. (7.3) gives

$$\mathbf{f}(n+1) = \mathbf{f}(n) + \mu \left[d(n) - \mathbf{f}^T(n)\mathbf{x}(n) \right] \mathbf{x}^*(n), \tag{7.8}$$

Taking the expected value,

$$\overline{\mathbf{f}}(n+1) = \overline{\mathbf{f}}(n) + \mu E\left\{ d(n)\mathbf{x}^*(n) \right\} - \mu E\left\{ \mathbf{x}^*(n)\mathbf{x}^T(n)\mathbf{f}(n) \right\}, \tag{7.9}$$

Under the assumption that the data $\mathbf{x}(n)$ and the LMS coefficient vector $\mathbf{f}(n)$ are statistically independent Eq. (7.9) can be rewritten as

$$\begin{aligned} \overline{\mathbf{f}}(n+1) &= \overline{\mathbf{f}}(n) + \mu E\left\{ d(n)\mathbf{x}^*(n) \right\} - \mu E\left\{ \mathbf{x}^*(n)\mathbf{x}^T(n) \right\} \overline{\mathbf{f}}(n) && (7.10) \\ &= (\mathbf{I} - \mu \mathbf{R}_{xx})\overline{\mathbf{f}}(n) + \mu \mathbf{r}_{dx} && (7.11) \end{aligned}$$

Replacing $\mathbf{r}_{dx}$ by $\mathbf{R}_{xx}\mathbf{f}_{\text{Wiener}}$, where $\mathbf{f}_{\text{Wiener}}$ is the optimal Wiener filter, yields

$$\overline{\mathbf{f}}(n+1) = (\mathbf{I} - \mu \mathbf{R}_{xx})\overline{\mathbf{f}}(n) + \mu \mathbf{R}_{xx}\mathbf{f}_{\text{Wiener}} \tag{7.12}$$

The coefficient error $\Delta\overline{\mathbf{f}}(n)$ is defined as

$$\Delta\overline{\mathbf{f}}(n) = \overline{\mathbf{f}}(n) - \mathbf{f}_{\text{Wiener}}. \tag{7.13}$$

Inserting Eq. (7.12) into Eq. (7.13) gives

$$\begin{aligned} \Delta\overline{\mathbf{f}}(n) &= (\mathbf{I} - \mu \mathbf{R}_{xx})\overline{\mathbf{f}}(n-1) + \mu \mathbf{R}_{xx}\mathbf{f}_{\text{Wiener}} - \mathbf{f}_{\text{Wiener}} && (7.14) \\ &= (\mathbf{I} - \mu \mathbf{R}_{xx})(\overline{\mathbf{f}}(n-1) - \mathbf{f}_{\text{Wiener}}) && (7.15) \\ &= (\mathbf{I} - \mu \mathbf{R}_{xx})\Delta\overline{\mathbf{f}}(n-1) && (7.16) \end{aligned}$$

Since the correlation matrix is hermitian, i.e. $\mathbf{R}_{xx} = \mathbf{R}_{xx}^H$, the matrix can be factorized using the eigenvalue decomposition $\mathbf{R}_{xx} = \mathbf{V}\mathbf{\Lambda}\mathbf{V}^H$ (the spectral theorem) with orthogonal eigenvector matrix $\mathbf{V}$ and diagonal matrix $\mathbf{\Lambda}$ with real eigenvalues on the main diagonal [24]. Using the eigenvalue decomposition and the fact that $\mathbf{V}\mathbf{V}^H = \mathbf{I}$, yields

$$\begin{aligned} \Delta\overline{\mathbf{f}}(n) &= (\mathbf{V}\mathbf{V}^H - \mu \mathbf{V}\mathbf{\Lambda}\mathbf{V}^H)\Delta\overline{\mathbf{f}}(n-1) && (7.17) \\ &= \mathbf{V}(\mathbf{I} - \mu\mathbf{\Lambda})\mathbf{V}^H\Delta\overline{\mathbf{f}}(n-1) && (7.18) \end{aligned}$$

A modal coefficient error vector is introduced as $\Delta\overline{\mathbf{f}}'(n) = \mathbf{V}^H \Delta\overline{\mathbf{f}}(n)$ and evolves as a function of time according to

$$\Delta\overline{\mathbf{f}}'(n) = (\mathbf{I} - \mu\mathbf{\Lambda})\Delta\overline{\mathbf{f}}'(n-1) \tag{7.19}$$

With an initial vector $\Delta\mathbf{f}'(0)$, Eq. (7.19) can be rewritten as

$$\Delta\overline{\mathbf{f}}'(n) = (\mathbf{I} - \mu\mathbf{\Lambda})^n \Delta\mathbf{f}'(0) \tag{7.20}$$

Since $(\mathbf{I} - \mu\mathbf{\Lambda})$ is a diagonal matrix, the elements of $\Delta\overline{\mathbf{f}}'(n)$ can be expressed as

$$\Delta\overline{f_i}'(n) = (1 - \mu\lambda_k)^n \Delta f_i'(0), \tag{7.21}$$

which are referred to as the *natural modes* of the adaptive filter [17]. The time constant τ_i is the time required for the k-th mode to reach $1/e$ of its value

$$(1 - \mu\lambda_i)^{\tau_i} = 1/e \tag{7.22}$$

Taking logarithms yields

$$\tau_i = \frac{-1}{\ln(1 - \mu\lambda_i)} \tag{7.23}$$

In order for $\overline{\mathbf{f}}(n)$ to converge to $\mathbf{f}_{\text{Wiener}}$, $\Delta\overline{\mathbf{f}}(n)$ should converge to zero and therefore $\Delta\overline{\mathbf{f}}'(n)$ should converge to zero. This will occur if and only if

$$|1 - \mu\lambda_i| < 1, \quad \forall i. \tag{7.24}$$

The decay for each mode is dependent on the magnitude of $|1 - \mu\lambda_i|$ and is thus dependent on both μ and λ_i. Therefore the step-size is restricted by

$$0 < \mu < \frac{2}{\max\limits_i \lambda_i} \tag{7.25}$$

This however is in practise not restrictive enough, therefore the following restriction is more commonly used

$$0 < \mu < \frac{2}{\beta} \tag{7.26}$$

where

$$\beta = \sum_i \lambda_i = tr\{\mathbf{R}_{xx}\} = L_f \cdot r_{xx}(0) = L_f \cdot E\{|x(n)|^2\} \tag{7.27}$$

Eq. (7.16) shows that the convergence of the coefficients is dependent on the correlation matrix. If $x(n)$ is white noise, the correlation matrix is diagonal and all eigenvalues are the same. In this case, the modes will converge in a uniform manner. However, when the input is correlated and the eigenvalues are not the same, some modes will converge more quickly than others.

Simulation Results

In this section the theoretical results are compared to results based on averages from practical simulations. The settings are the same as in Chapter 2.4.1. Fig. 7.1 shows the evolution of the MSE as a function of time. The MSE is found by using the coefficient update in Eq. (7.12). Also, averages of the squared error over 10, 100 and 1000 simulations runs are plotted using the coefficient update according Eq. (7.3) with simulated signals. The following consecutive figures, Figs. 7.2, 7.3 and 7.4 show the corresponding evolution of the coefficients, the coefficient errors and the modal coefficient errors. Clearly from Fig. 7.3 it can be seen that the coefficient errors decay to zero. However, in Fig. 7.4 it can be seen that modes decay at different rates depending on the eigenvalue spread.

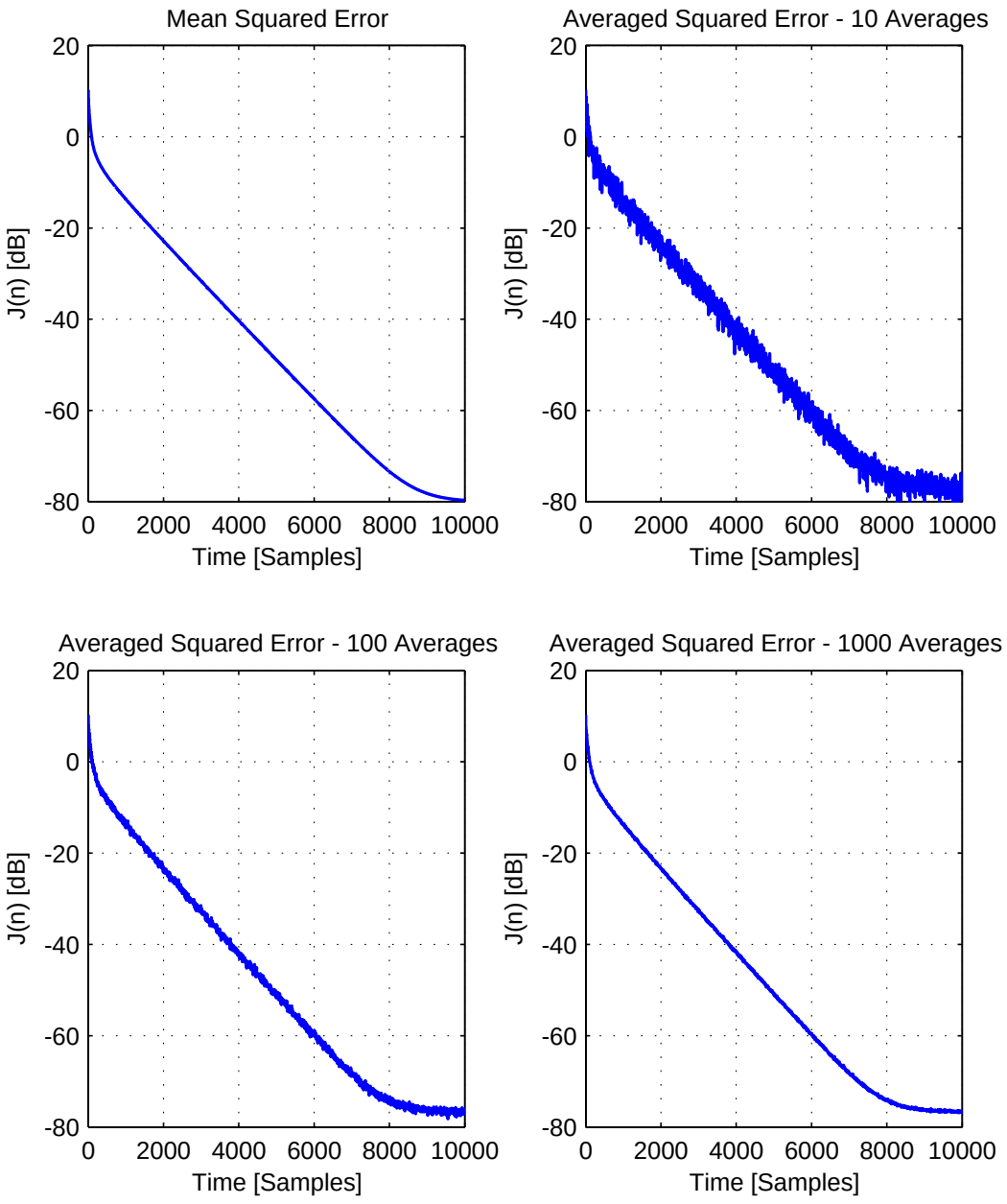

Figure 7.1: *Mean square error $J(n)$ for the LMS adaptive filter.*

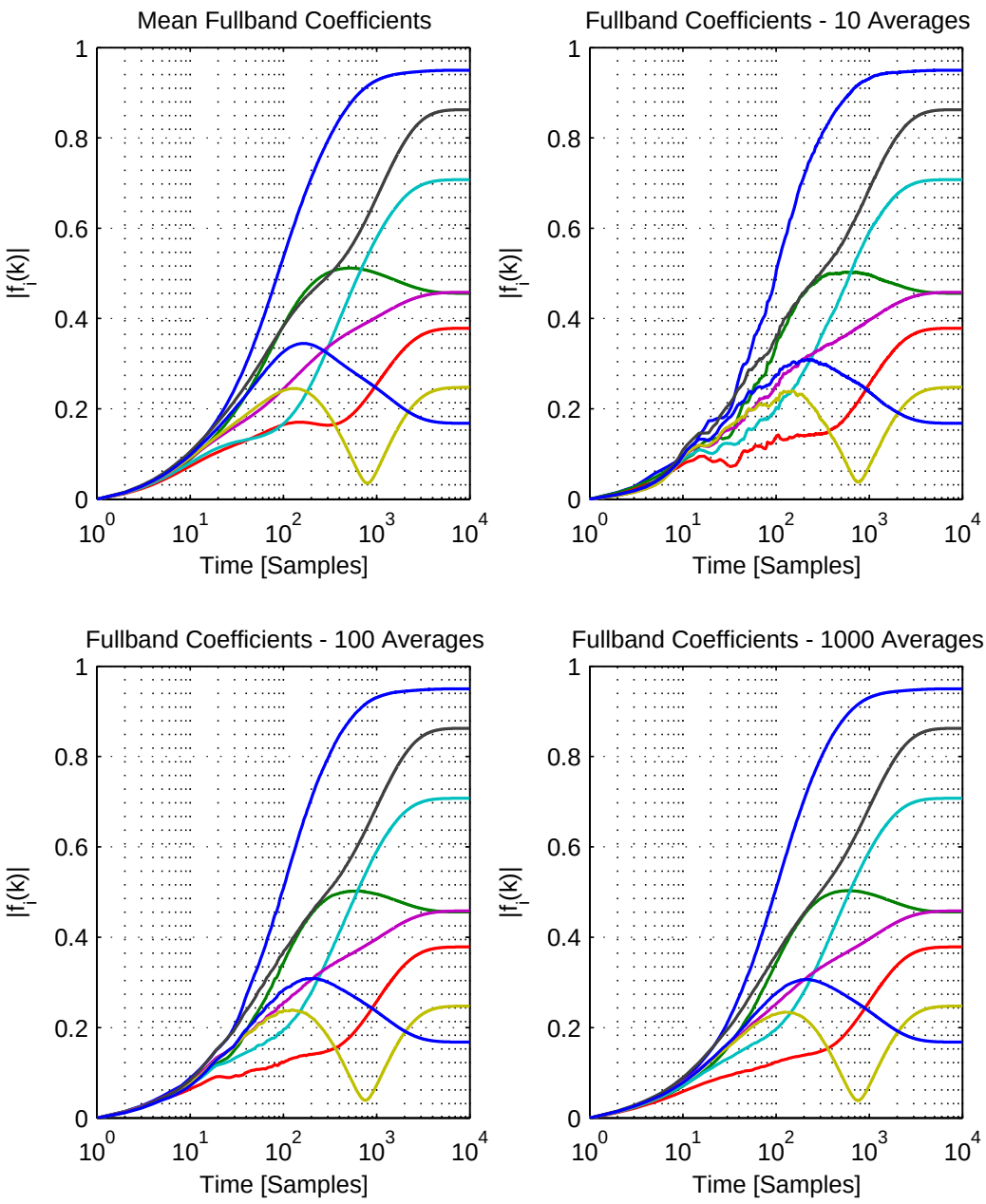

Figure 7.2: *Magnitude of the fullband filter coefficients* $|\overline{f_i}(n)|$ *for the LMS adaptive filter.*

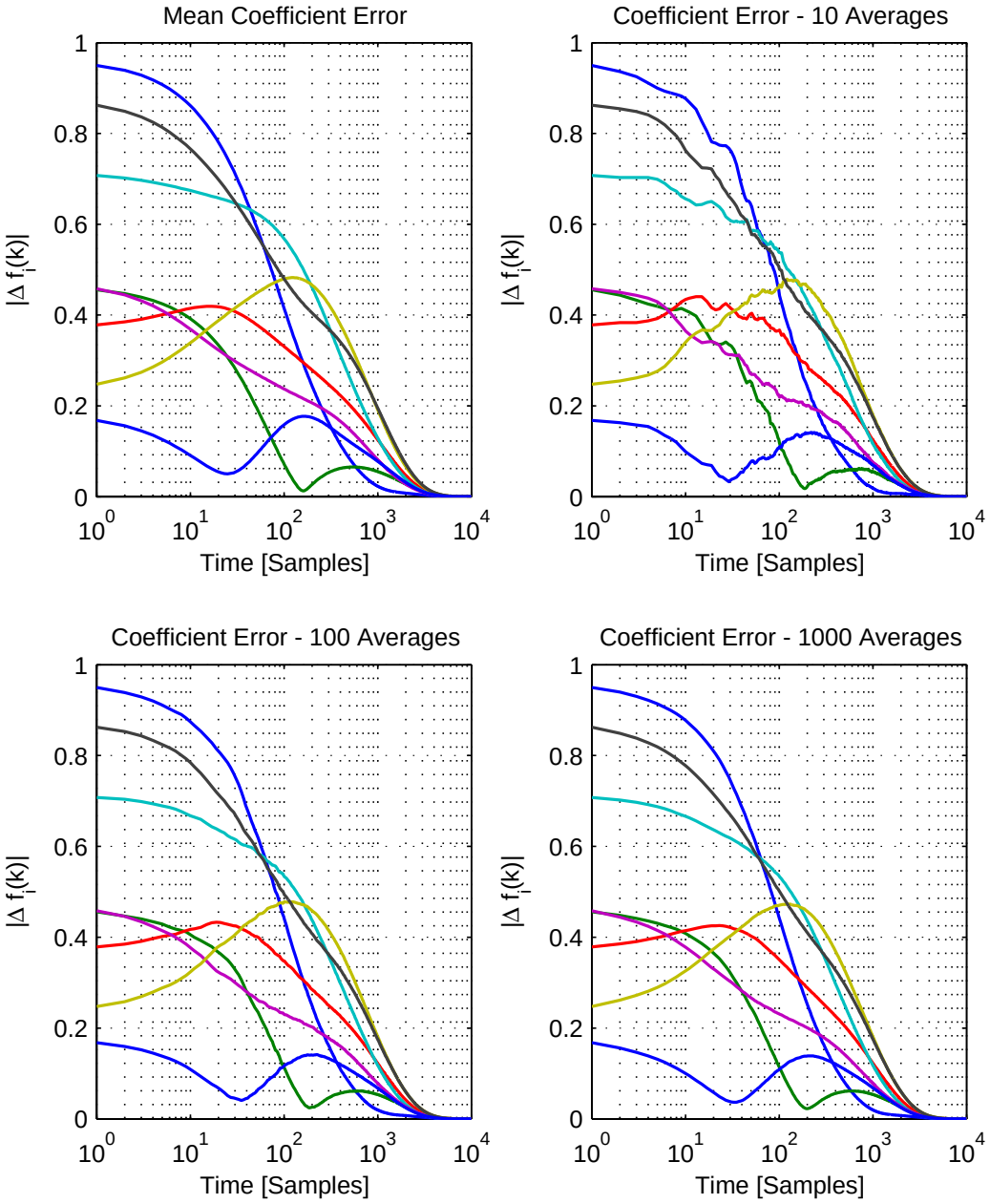

Figure 7.3: *Magnitude of the coefficient errors* $|\Delta\overline{f}_i(n)|$ *for the LMS adaptive filter.*

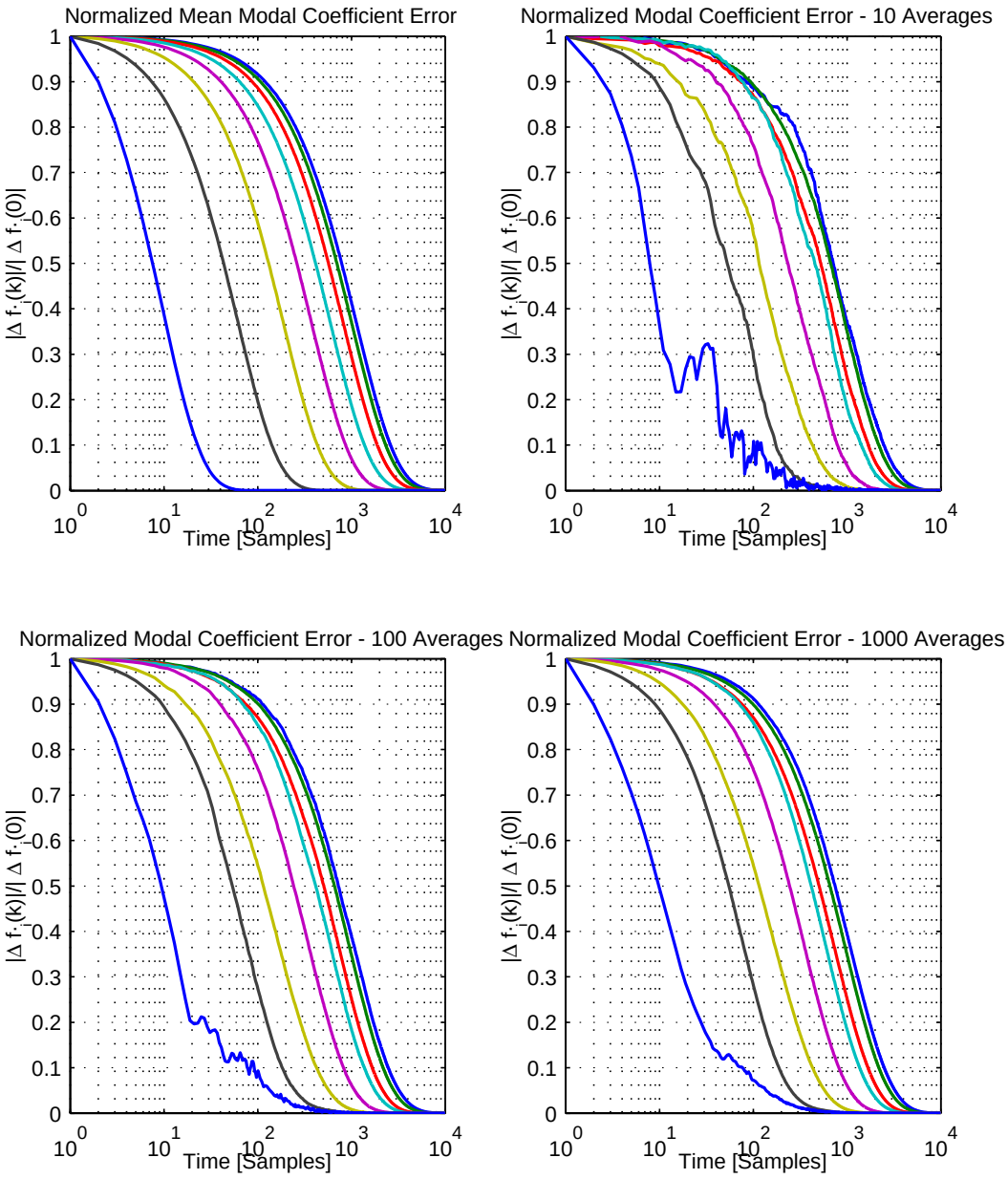

Figure 7.4: *Magnitude of the modal coefficient errors* $|\Delta\overline{f_i}'(k)|/|\Delta f_i'(0)|$ *for the LMS adaptive filter, normalized with the magnitude of the initial error.*

Bibliography

[1] M. Dentino, J. M. McCool, and B. Widrow, "Adaptive Filtering in the Frequency Domain," *Proceedings of the IEEE*, vol. 66, pp. 1658–1659, December 1978.

[2] S. S. Narayan and A. M. Peterson, "Frequency Domain LMS Algorithm," *Proceedings of the IEEE*, vol. 69, pp. 124–126, 1981.

[3] J. S. Soo and K. Pang, "Multidelay Block Frequency Domain Adaptive Filter," *IEEE Transactions on Acoustics, Speech and Audio Processing*, vol. 38, pp. 373–376, Fubruary 1990.

[4] A. Gilloire and M. Vetterli, "Adaptive Filtering in Subbands," in *IEEE International Conference on Acoustics, Speech and Signal Processing*, 1988, vol. 3, pp. 1572–1575.

[5] A. Gilloire and M. Vetterli, "Adaptive Filtering in Subbands with Critical Sampling: Analysis, Experiments, and Application to Acoustic Echo Cancellation," *IEEE Transactions on Signal Processing*, vol. 40, no. 8, pp. 1862–1875, August 1992.

[6] S. S. Pradhan and V. U. Reddy, "A New Approach to Subband Adaptive Filtering," *IEEE Transactions on Signal Processing*, vol. 47, pp. 655–664, March 1999.

[7] K. Eneman and M. Moonen, "Hybrid Subband/Frequency–Domain Adaptive Systems," *Elsevier Signal Processing*, pp. 117–136, 2001.

[8] S. L. Gay and J. Benesty (Eds), *Acoustic Signal Processing for Telecommunication*, Kluwer Academic Press, 2000.

[9] J. Nordberg, *Blind Subband Adaptive Equalization*, Blekinge Institute of Technology Research Report 2002/11, ISSN 1103-1571, 2002.

[10] P. A. Naylor, O. Tanrikulu, and A. G. Constantinidis, "Subband Adaptive Filtering for Acoustic Echo Control using Allpass Polyphase IIR Filter Banks," *IEEE Transactions on Speech and Audio Processing*, vol. 6, no. 2, pp. 143–155.

[11] D. R. Morgan and J. C. Thi, "A Delayless Subband Adaptive Filter Architecture," *IEEE Transactions on Signal Processing*, pp. 1819–1830, August 1995.

[12] J. Huo, S. Nordholm, and Z. Zang, "New Weight Transform Schemes for Delayless Adaptive Filtering," in *IEEE Global Telecommunications Conference*, 2001, pp. 197–201.

[13] N. Hirayama, H. Sakai, and S. Miyagi, "Delayless Subband Adaptive Filtering using the Hadamard Transform," *IEEE Transactions on Signal Processing*, vol. 47, no. 6, pp. 1731–1734, June 1999.

[14] L.-O. Larson, J.M. de Haan, and I. Claesson, "A New Subband Weight Transform for Delayless Subband Adaptive Filtering Structures," in *IEEE Digital Signal Processing Workshop 2002*, October 2002, pp. 201–206.

[15] R. Merched, P. S. R. Diniz, and M. R. Petraglia, "A New Delayless Subband Adaptive Filter Structure," *IEEE transactions on Signal Processing*, vol. 47, pp. 1580–1591, June 1999.

[16] Y. Bendel, D. Burshtein, O. Shalvi, and E. Weinstein, "Delayless Frequency Domain Acoustic Echo Cancellation," *IEEE transactions on Signal Processing*, vol. 49, pp. 589–597, July 2001.

[17] S. Haykin, *Adaptive Filter Theory*, Prentice-Hall, 2002.

[18] I. Claesson, S. Nordholm, and P. Eriksson, "Noise Cancelling Convergense Rates for the LMS Algorithm," *Academic Press - Mechanical Systems and Signal Processing*, vol. 5, pp. 375–388, 1991.

[19] P. P. Vaidyanathan, *Multirate Systems and Filter Banks*, Prentice-Hall, 1993.

[20] N. J. Fliege, *Multirate Digital Signal Processing – Multirate Systems, Filter Banks, Wavelets*, John Wiley and Sons, 1999.

[21] N. Hirayama and H. Sakai, "Analysis of a Delayless Subband Adaptive Filter," in *IEEE International Conference on Acoustics, Speech and Signal Processing*, 1997, vol. 3, pp. 2329–2332.

[22] T. W. Parks and C. S. Burrus, *Digital Filter Design*, John Wiley and Sons, 1987.

[23] R. M. Gray, "On the Asymptotic Eigenvalue Distribution of Toeplitz Matrices," *IEEE transactions on Information Theory*, vol. 16, pp. 725–730, 1972.

[24] G. Strang, *Linear Algebra and Its Applications*, Academic Press, 1980.

Convergence and Complexity Analysis of Delayless Subband Adaptive Filters
Jan Mark de Haan

ISSN 1103-1581
ISRN BTH-RES--04/04--SE

Printed by Kaserntryckeriet AB, Karlskrona 2004